UFRGS
UNIVERSIDADE FEDERAL
DO RIO GRANDE DO SUL

The rich population of jellyfish galaxies in the Abell 901/2 multi-cluster system at $z \sim 0.165$

A rica população de galáxias *jellyfish* no sistema multi-aglomerado Abell 901/2 em $z \sim 0.165$

Fernanda Roman de Oliveira

UFRGS
UNIVERSIDADE FEDERAL
DO RIO GRANDE DO SUL

The rich population of jellyfish galaxies in the Abell 901/2 multi-cluster system at $z \sim 0.165$

DISSERTATION

submitted in partial fulfillment of the
requirements for the degree of

MASTER OF SCIENCE
in
PHYSICS

Author : Fernanda Vitória Roman de Oliveira
Supervisor : Dr. Ana Chies Santos
Co-supervisor : Dr. Fabrício Ferrari

Porto Alegre, Brazil – March 13, 2020

To everyone who wonders about the unknown.

"The fact that we live at the bottom of a deep gravity well, on the surface of a gas covered planet going around a nuclear fireball 90 million miles away and think this to be normal is obviously some indication of how skewed our perspective tends to be."

— Douglas Adams

The rich population of jellyfish galaxies in the Abell 901/2 multi-cluster system at $z \sim 0.165$

Fernanda Vitória Roman de Oliveira

Departamento de Astronomia, Instituto de Física
Universidade Federal do Rio Grande do Sul

Campus do Vale, Avenida Bento Gonçalves, 9500, Agronomia, 90650-001
Porto Alegre, RS, Brazil

March 13, 2020

Abstract

The evolution of galaxies can be significantly altered in galaxy clusters as a result of interactions with other galaxies and the intracluster medium that surrounds them. Jellyfish galaxies are the most striking examples of galaxies undergoing ram pressure stripping – the removal of gas as a result of a hydrodynamic friction in dense environments. In this work, we present a morphometric follow-up study on 73 ram pressure stripping candidates in the Abell 901/2 multi-cluster system at $z \sim$0.165. This sample was selected by visually inspecting F606W/HST images for ram pressure stripping morphological features. We show that these galaxies have a systematic enhancement of their specific star formation rates and find no correlation between AGN activity and ram pressure stripping. By investigating the environment, we find that the merging regions in the A901/2 system may function as a trigger to the formation of ram pressure stripping events, being a possible origin for most of candidates in this sample. We use the algorithm MORFOMETRYKA as a tool to characterise the morphologies and structural parameters in search for patterns that can provide an insight as to the evolution of jellyfish galaxies. We show that the surface brightness profiles of jellyfish galaxies signalise a diffusing effect in the outskirt regions and we propose a robust and automatic way of characterising the apparent direction of motion of these galaxies.

Resumo

A evolução de galáxias pode ser significativamente alterada em aglomerados de galáxias em resultado das interações com outras galáxias e com o meio intra-aglomerado que as cerca. Galáxias água-viva, conhecidas como galáxias *jellyfish*, são os exemplos mais impressionantes de galáxias sofrendo o fenômeno de remoção de gás por pressão de arrasto, conhecido como *ram pressure stripping*. Isto é a remoção do gás interno da galáxia em consequência da fricção hidrodinâmica existente em ambientes densos. Neste trabalho, apresentamos um estudo morfométrico de 73 galáxias candidatas no sistema multi-aglomerado Abell 901/2 em $z \sim 0.165$. Esta amostra foi selecionada via inspeção visual de imagens F606W/HST observando características morfológicas que se assemelham a galáxias *jellyfish*. Nós mostramos que essas galáxias têm taxas de formação estelar específicas sistematicamente mais altas do que as outras galáxias e não encontramos correlação entre atividade AGN e *ram pressure stripping*. Investigando o ambiente, encontramos que regiões de fusão presentes no sistema A901/2 podem agir como um gatilho da formação de galáxias *jellyfish*, sendo uma possível origem da maioria das candidatas desta amostra. Nós usamos o algoritmo MORFOMETRYKA como ferramenta para caracterizar as morfologias e parâmetros estruturais presentes na amostra em busca de padrões que possam auxiliar no entendimento da evolução de galáxias *jellyfish*. Identificamos uma tendência de difusão na distribuição de luz nas partes externas das galáxias *jellyfish* e também propomos um método robusto e automático de caracterização da aparente direção de movimento dessas galáxias.

Press Release – Comunicado de imprensa

A maior parte das galáxias no Universo residem em aglomerados que contém de dezenas a milhares de galáxias unidas pela gravidade. Mas as suas vidas não são fáceis, o ambiente ao seu redor é muitas vezes hostil e acaba deformando e desnutrindo as galáxias que ali vivem. Apesar de sabermos que o meio em que as galáxias habitam tem muita influência em como elas crescem e se desenvolvem, ainda não entendemos em detalhe como os processos ambientais acabam alterando as suas propriedades. Esta pesquisa teve como objetivo entender como a pressão de arrasto, um processo ambiental presente em aglomerados, afeta a evolução de galáxias. A pressão de arraste acontece quando uma galáxia se movimenta em torno do aglomerado e sofre resistência do "ar" em sua volta. Similar a um ciclista sentindo resistência do ar ao pedalar. Esse processo remove o gás disponível dentro das galáxias que de outra forma poderia ser usado para formar estrelas. Enquanto a galáxia perde esse gás, a forma dela também é modificada de forma que ela se parece como uma água-viva cósmica, ou conhecida também como uma galáxia *jellyfish* como as da figura abaixo. Analisando as imagens de várias galáxias no rico aglomerado Abell 901/2, nós encontramos um grupo de 73 galáxias candidatas a *jellyfish*. Encontramos que durante esse processo elas criam muito mais estrelas do que as outras galáxias e que a formação desses objetos peculiares pode ser engatilhada em regiões de fusão de aglomerados de galáxias. Por fim, ao analisar as morfologias, ou seja, o formato das galáxias *jellyfish*, encontramos vestígios de que esse processo está difundindo a luz nas regiões externas.

Notation

A901/2 - Abell 901/2

AGN - Active Galactic Nucleus

GASP - GAs Stripping Phenomena in galaxies with MUSE

HST - Hubble Space Telescope

ICM - Intra-cluster Medium

ISM - Interstellar Medium

OMEGA - OSIRIS Mapping of Emission-line Galaxies in A901/2

RPS - Ram Pressure Stripping

SFR - Star Formation Rate

sSFR - specific Star Formation Rate

STAGES - the Space Telescope A901/2 Galaxy Evolution Survey

.

Contents

List of Figures

List of Tables

Chapter 1

Introduction

> ” In a spiral galaxy, the ratio of dark-to-light matter is about a factor of ten. That is probably a good number for the ratio of our ignorance-to-knowledge. We are out of kindergarten, but only in about third grade. ”
>
> *Vera Rubin*

1.1 Galaxies in the Local Universe

Galaxies are systems composed by stars and their remnants, dust, interstellar gas and dark matter (Sparke & Gallagher, 2000). It was just under a hundred years ago that we have been able to resolve these objects and understand they are not part of our own galaxy. Before that, they were known as *nebulae*, a class of faint and smooth-looking objects considered to be unresolved stellar systems residing in the Milky Way. In 1926, Edwin Hubble was the first to measure distances to these nebulae by looking at Cepheid stars and determined those were in fact extragalactic objects.

This groundbreaking discovery was accompanied by observations of unprecedented detail on the structure of galaxies. This allowed for the first time the attempt of classifying large number of galaxies based on their observed morphologies. The most important classification scheme was proposed by Hubble (1926) and it is known as the Hubble Tuning Fork or Hubble Sequence, represented in Figure 1.1. This diagram shows a sequence of galaxies which increases in structural complexity from 'early-type' galaxies to 'late-type' galaxies:

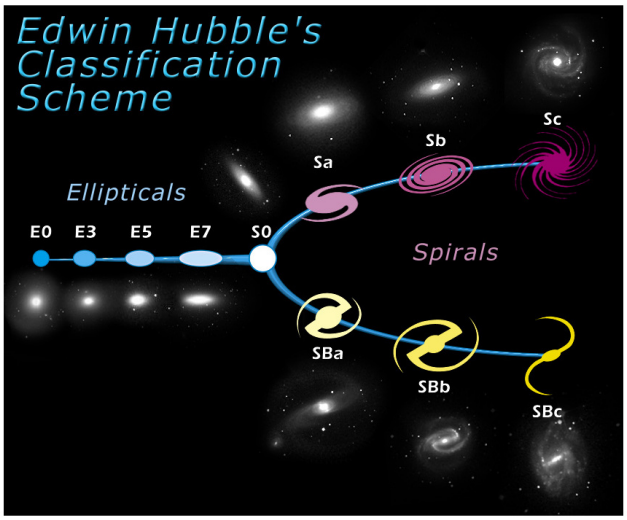

Figure 1.1: Hubble tuning fork: first attempt at classifying galaxies according to their different morphologies. Taken from Hubble Site, available at `https://hubblesite.org/contents/media/images/1999/34/890-Image.html`.

Early-type galaxies

- Ellipticals: smooth and spheroidal galaxies;
- Lenticulars (or S0s): large spheroidal component and smooth disc.

Late-type galaxies

- Spirals: disc dominated with spiral arms that can vary in number and shape; can be barred or not; can have a large bulge or not;
- Irregulars: do not have a regular structure.

It is important to note that, regardless of the use of words 'early' and 'late', this classification is entirely empirical and was not meant to imply a temporal evolution along the different morphological types in the sequence (Baldry, 2008). It was clear from these first observations that the Universe had a diverse population of galaxies with very different characteristics, however we are yet to understand how exactly their formation took place and how they have evolved to be so different from each other.

The broad population of galaxies is not only different in structure – there is a strong correlation between morphological types and colours (Buta et al., 1994). In Figure 1.2 we show the colour-magnitude diagram (CMD) for galaxies at low redshift taken from Baldry et al. (2004), in which

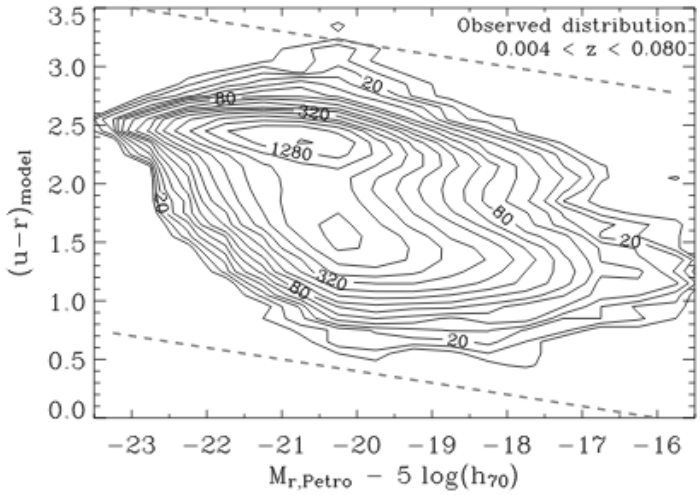

Figure 1.2: Colour bimodality in galaxies at low redshift: the population of galaxies is clearly dominated by a blue less massive group, known as the blue cloud, and a red more massive group, known as the red sequence. Taken from Baldry et al. (2004).

there is a clear bimodality in the colour distribution of galaxies. Therefore, in this diagram, the population of galaxies in the Local Universe shows a clear division in two major groups: the 'blue cloud' and the 'red sequence'. The blue cloud has a prevalence of late-type galaxies with spectra dominated by emission in the blue as a result of recent and/or ongoing star formation. On the other hand, the red sequence contains passive galaxies, i.e. which do not have significant star formation, and is dominated by early-type galaxies. The region in between these two groups is known as the green valley, which suggests a continuum in galaxy properties as their transition from star-forming to passivity, known as quenching (Wyder et al., 2007). However, as shown in Schawinski et al. (2014), galaxies may pass through the green valley stage differently, with late-type galaxies presenting a much longer (> 1 Gyr) quenching timescale than early-type galaxies (< 250 Myr). This finding suggests that late-type galaxy quenching is driven by secular and environmental processes while early-type galaxies quench rapidly through violent processes such as major mergers.

Dressler (1980) found that galaxies with different morphologies are distributed differently according to the environment, i.e. they follow a morphology-density relation. Reproduced in Figure 1.3, this relation shows that early-type galaxies tend to be found in denser environments, such as

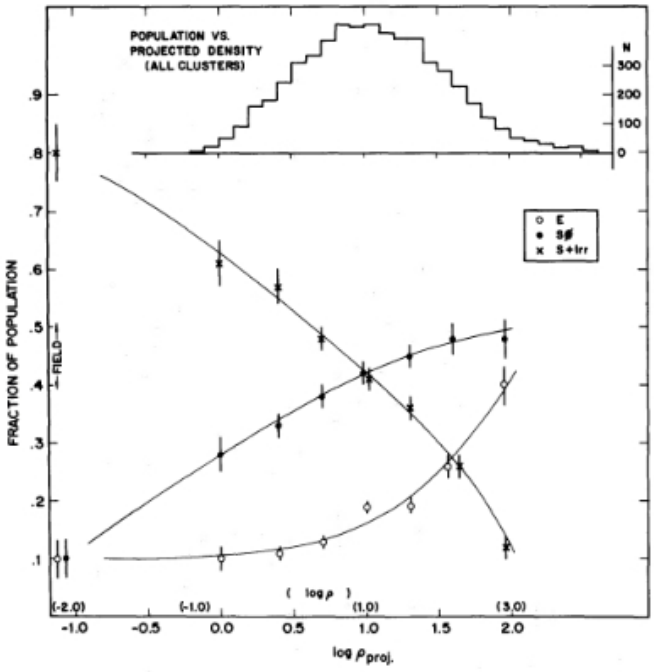

Figure 1.3: Morphology-density relation as seen from the fraction of different galaxy populations (Elliptical, Spirals plus Irregulars and S0s) across projected density. As the density increases, the fraction of late-type galaxies decreases and the fraction of early-type galaxies increases. This result suggests that the environment plays a role in the morphological evolution of galaxies from late-type to early-type galaxies in the densest regions such as the centre of clusters. Taken from Dressler (1980).

the centre of rich galaxy clusters, while late-type galaxies are more abundantly found in the outskirts of clusters and isolated in the field. This indicates that dense environments can play a major role shaping the evolution of galaxies by driving morphological transformation and accelerating the quenching process.

1.2 Drivers of galaxy evolution

In order to describe the rich and diverse evolutionary path of the population of galaxies found in the Local Universe, it is necessary to understand what drives galaxy evolution in different contexts. As discussed so far, galaxies are not isolated systems and their evolution is heavily affected by the environment they inhabit. This happens as a result of their interac-

tion with external elements, such as surrounding galaxies or gas. Moreover, star formation quenching can also be driven by their stellar masses (Haines et al., 2006) or internal processes such as mass-dependent feedback mechanisms (Bundy et al., 2006), AGN and supernovae feedback (Booth & Schaye, 2009, Newton & Kay, 2013). Here we focus on the external processes and how they can affect galaxies in different environments.

1.2.1 Gravitational Interactions

Mergers

Strong interaction at slow speed between two or more galaxies that results in a single object. More likely to happen in low-density environments where galaxies can be found at low-velocities. Mergers can be classified as wet or dry, depending on the richness of gas available in the galaxies, and as minor or major, depending on the mass ratio of the galaxies involved. Major mergers, encounters of galaxies of comparable masses, can result in the formation of an elliptical galaxy (Hopkins et al., 2008, Toomre, 1977). Minor mergers, when one galaxy is much more massive than the other, usually do not cause strong disturbances in the main galaxy. However, they have been suggested to be a possible mechanism in the transformation of spirals into S0s (Bekki, 1998, Tapia et al., 2014) and triggering of star formation episodes (Kaviraj, 2014).

Tidal Interactions and Harassment

Tidal interactions are slow encounters that do not result in a merger. They are very disturbing on the morphologies of the galaxies involved as they can strip gas and create extensive tidal tails (Eneev et al., 1973, Pettitt & Wadsley, 2018), in which structures can be formed and become progenitors to Tidal Dwarf Galaxies Bournaud et al. (2004).

Harassment is an intense encounter of galaxies at high speed in a short period of time. It can severely disturb the morphology and lead to truncation of star forming discs (Moore et al., 1996). More likely to happen in clusters where galaxy velocities are higher.

1.2.2 Hydrodynamic Interaction – Ram Pressure Stripping

Ram pressure stripping is a physical process that removes the interstellar medium (ISM) in gas-rich galaxies as they orbit dense clusters and encounter the intra-cluster medium (ICM) (Gunn & Gott, 1972). It happens through a hydrodynamic friction and is dependent on the ICM density

and the relative velocity between the galaxy and the surrounding ICM as described by:

$$P_{ram} = v_{rel}^2 \, \rho_{ICM} \tag{1.1}$$

Jellyfish galaxies

Jellyfish galaxy was a term first used in Bekki (2009) and describes the most extreme cases of galaxies undergoing ram pressure stripping. While the gas is removed it clumps into tail-like structures, the original stellar disc is mostly preserved, then resembling a jellyfish.

Through the past decade, ram pressure stripping has been a major topic within galaxy evolution in clusters. Many studies covered the main properties of a few jellyfish galaxies both observed and simulated (Bekki, 2009, 2014, Cortese et al., 2007, Rawle et al., 2014, Roediger et al., 2014, Smith et al., 2010) and there have been a few major systematic searches for jellyfish galaxy candidates throughout many different clusters at different redshifts (Ebeling et al., 2014, McPartland et al., 2016, Poggianti et al., 2016). A great contribution to the field has been made with the GASP survey (GAs Stripping Phenomena in galaxies with MUSE) (Poggianti et al., 2017b) that has analysed MUSE data cubes for more than 100 jellyfish galaxies at low redshift ($z = 0.04 - 0.07$) across many clusters as a follow-up to Poggianti et al. (2016). More recently, in Yun et al. (2019) a sample of more than 800 jellyfish galaxies is studied in the Illustris TNG.

1.3 Morphological transformation

The Hubble Sequence is still used to classify different morphological types qualitatively. Traditionally, the classification has been done by visual inspection on optical images, depending on multiple people to identify structural features. However, this method is not appropriate to the current large volume of data in astronomy as it is time consuming, prone to human error and highly subjective. Therefore, morphometry emerges as a reliable alternative to quantitatively define morphology. Morphometry can be either parametric, which models the light distribution assuming different components within the galaxy (e.g. bulge, disc) (Peng et al., 2002, Simard et al., 2002), or non-parametric, which directly measures the properties of the light distribution (e.g. asymmetry, concentration) (Abraham et al., 1996, Conselice et al., 2000).

Figure 1.4: Abell 901/2 multi-cluster system: composition of the HST imaging and a superposition in pink of the dark matter content as determined in (Heymans et al., 2008).

As discussed before, morphologies may encode information about the formation and subsequent evolutionary path of galaxies. In this work we pursue the challenge of characterising the morphologies of jellyfish galaxy candidates, highly irregular objects, to better understand the role of ram pressure stripping on the morphological evolution of galaxies. For that, we conduct a non-parametric morphometric analysis on the HST F606W band images with MORFOMETRYKA (Ferrari et al., 2015).

1.4 The A901/2 multi-cluster system

Abell 901/2, shown in Figure 1.4, is a multi-cluster system at z$\sim$0.165 composed by four main substructures: the clusters A901a, A901b and A902, and the southwest group (SW group). It covers a field of view of 0.5x0.5 deg^2 of the sky and is home to thousands of galaxies, making it an optimal laboratory for studying the impact of a broad range of environments on galaxy evolution.

It has been extensively studied by the Space Telescope A901/902 Galaxy Evolution Survey (STAGES) (Gray et al., 2009), a multi-wavelength survey which collected photometric redshifts, SEDs and stellar masses for 15000 galaxies in the system up to M_R=24. It includes data from the COMBO-17 photometric survey, HST images in the F606W band, Spitzer, XMM-

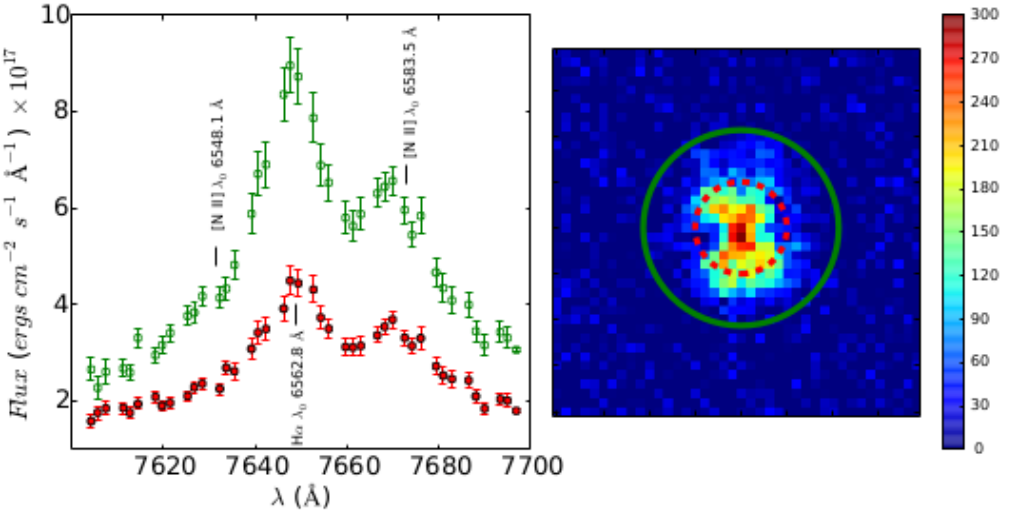

Figure 1.5: Left panel: flux-calibrated spectra showing the Hα and [NII] emission lines in the OMEGA survey for two apertures. Right Panel: PSF (red dashed line) and total (green solid line) apertures overlaid on the image of the galaxy at λ = 7646 Å. This is for the galaxy 42713 and is taken from Chies-Santos et al. (2015).

Newton, GALEX, GMRT and 2dF. More recently, the follow-up OSIRIS Mapping of Emission-line Galaxies in A901/2 (OMEGA) survey (Chies-Santos et al., 2015) has collected data regarding the Hα and [NII] emission lines in order to study the star formation and active galaxy nucleus (AGN) processes. The survey used the Optical System for Imaging and low-Intermediate-Resolution Integrated Spectroscopy (OSIRIS) instrument on Gran Telescopio Canarias on the tuneable-filter mode. Figure 1.5 shows how the mapped spectrum around the Hα, [NII]λ6548 and [NII]λ6583 for the inner and outer spatial regions being analysed.

The data acquisition and reduction is shown in Chies-Santos et al. (2015) as well as the first results. Following that, Rodríguez del Pino et al. (2017) presents the influence of the environment on star formation rates and AGN. Moreover, Weinzirl et al. (2017) studies galaxy properties in the projected phase space diagram, while Wolf et al. (2018) shows the effects of extinction in star formation estimators as a function of galaxy inclination. Finally, in Roman-Oliveira et al. (2019), presented in the Chapter 2 of this thesis, we show the selection of ram pressure stripping candidates and an analysis of the star formation rates, AGN activity and environment.

1.5 Outline of the thesis

In this thesis we show a comprehensive analysis of the rich population of ram pressure stripping candidates in the Abell 901/2 multi-cluster system in the attempt of addressing some of the outlined open problems regarding the influence of ram pressure stripping in the evolution of galaxies in dense systems. The outline of the chapters is as follows:

Chapter 2 – OMEGA V: The rich populations of jellyfish galaxies in the Abell 901/2 multi-cluster system

Roman-Oliveira et al. (2019) sets the basis study describing the sample and its main properties. A sample of jellyfish galaxy candidates is selected through visual inspection carried on the HST/F606W images of Hα emitting galaxies. Looking for ram pressure stripping morphological features we find the largest sample (N=73) of ram pressure stripping candidates in a single system to date. They show very high specific star formation rates and no apparent spatial distribution pattern. We also could not find a strong link between AGN activity and ram pressure stripping.

Chapter 3 – Galaxy cluster mergers as triggers for the formation of jellyfish galaxies

The work in Ruggiero et al. (2019) is a collaborative effort to understand the origin and spatial distribution of the OMEGA ram pressure stripping candidates. It describes a compared environmental analysis on the simulated Abell 901/2 multi-cluster system, considering the four main substructures merging, to the spatial distribution of the observed galaxies on the plane of the sky. We propose that regions of merging clusters can more easily trigger ram pressure stripping events as a result to the increased relative velocity. This might be a possible origin to the rich population found in the A901/2, suggesting that merging systems are the optimal laboratory for ram pressure stripping effects.

Chapter 4 – Morphometry as a probe to the evolution of jellyfish galaxies

A morphometric analysis of brightness profiles and sérsic indices with MORFOMETRYKA and IRAF/ELLIPSE on F606W HST images. Moreover,

we present a robust method for identifying trail vectors, which are vectors that indicate the apparent direction of motion of jellyfish galaxies. We identify a trend of low concentrated brightness profiles in part of the sample of ram pressure stripping candidates.

Chapter 5 – Conclusions and outlook

We summarise the main results and the conclusions of this thesis and the relevance of the previous chapters to the open debates in the literature regarding galaxy evolution. Likewise, we present possible future projects based on the open problems directly related to the results found in this thesis and taking into account the data available for the sample. Finally, we discuss the outlook of the field and the perspectives for the years to come.

Chapter 2

OMEGA V: The rich population of jellyfish galaxies in the multi-cluster system Abell 901/2

Published in Monthly Notices of the Royal Astronomical Society*

We present the results of a systematic search and characterisation of galaxies with morphological signatures of ram-pressure stripping, known as jellyfish galaxies, in the multi-cluster system A901/2, at $z \sim 0.165$, as part of the OMEGA survey. By visual inspecting ACS/HST F606W images looking for morphological signatures of ram-pressure stripping events in Hα-emitting galaxies, we identify a total of 70 jellyfish candidates. Out of these, 53 are clearly star-forming galaxies and 5 are highly probable AGN hosts, the classification of the remaining galaxies is more uncertain. They have late-type and irregular morphologies and most of them are part of the blue cloud with only 4 being previously classified as dusty reds. The AGN activity is not prominent in the sample and, of the few cases of galaxies hosting AGN, such activity does not seem to be correlated to the gas stripping phenomenon. Our jellyfish galaxy candidates do not have a preferential pattern of motion within the multi-cluster system, although the most compelling cases appear to inhabit the inner regions of the most massive sub-cluster centres. The specific star-formation rate of these galaxies indicates that their star formation activity is enhanced, in contrast with what is observed for the rest of the

*__Roman-Oliveira, F. V.__; Chies-Santos, A. L.; Rodríguez del Pino, B.; Aragón-Salamanca, A.; Gray, M. E. and Bamford, S. P.; 2019, MNRAS, 484, 892

star-forming galaxy population in the system. Half of the sample is forming stars at a higher rate than the main-sequence for field galaxies and this behaviour is more evident for the most compelling candidates. For some galaxies, the spatially resolved Hα emission appears to be as disturbed and extended as their continuum counterparts. Our findings point towards a scenario where the ram pressure stripping is triggering a period of intense and extended star formation throughout the galaxy while it is also disturbing the morphology. This is the largest sample of jellyfish galaxy candidates found in a single system suggesting that cluster mergers might be the ideal environment for studying ram pressure stripping effects.

2.1 Introduction

The environment in which galaxies inhabit influences their physical properties and evolution. As they interact with their surroundings, their morphologies and star formation properties can be severely changed. The low presence of early-type galaxies in the field and its dominance in denser regions of the Universe points towards a scenario in which environmental mechanisms play a major role in galaxy quenching and morphological evolution (Dressler, 1980).

Such transformations can be driven both by internal properties and processes, e.g. mass (Baldry et al., 2006), supernovae and AGN feedback (Booth & Schaye, 2009, Newton & Kay, 2013); and external ones, such as tidal interactions or mergers (Barnes, 1992), galaxy harassment (Moore et al., 1996) and ram pressure stripping (Gunn & Gott, 1972); the latter being more common in high density environments. Although there are several physical mechanisms competing, the dominance and extent of each one are not yet fully comprehended. For this reason, the morphological and physical changes that the environment induces in galaxies is crucial to the understanding of galaxy evolution as a whole.

Ram pressure stripping (RPS) is the interaction that occurs when a galaxy rich in gas falls toward a denser region, such as the core of a galaxy cluster, and it experiences the stripping of its cold gas as a result of a hydrodynamical friction with the hot and dense intracluster medium (ICM) (Gunn & Gott, 1972). It is cited as one of the most efficient mechanisms in quenching star formation in clusters (Boselli et al., 2016, Simpson et al., 2018), but it has also been suggested that, for a short period of time, it could enhance the star formation due to turbulences in the galaxy causing cold gas clouds to collapse (Bekki & Couch, 2003). Galaxies undergoing RPS also tend to display intense star formation in their outskirts, in the

shape of severely disturbed debris holding clumps of young stars (Cortese et al., 2007, Ebeling et al., 2014, Fumagalli et al., 2014, McPartland et al., 2016, Rawle et al., 2014, Yagi et al., 2010). The loss of the gas reservoir of a galaxy undergoing RPS can soon lead to a more passive existence, linking such process to the quenching of star formation in galaxies rich in gas in cluster environments (Jaffé et al., 2016, Vollmer et al., 2012). However, it is not always the case that the star formation is found to be enhanced. Some hydrodynamical simulations suggest that the quenching or enhancement could be a factor of galaxy properties, such as the inclination of the disk during the infalling on the cluster (Bekki, 2014, Steinhauser et al., 2016).

In the most extreme cases of galaxies undergoing RPS, the debris and gas trails can conglomerate unilaterally and extend to the opposite direction of motion. These cases can transform the morphology of the original galaxy in a way that resembles jellyfish-like creatures, hence their names. To our knowledge, the term jellyfish-like structure was first introduced by Bekki (2009). These galaxies have previously been found in low numbers in cluster environments (21 in Coma, Smith et al. (2010), Yagi et al. (2010), Gavazzi et al. (2018); 6 in Virgo, Abramson et al. (2016), Kenney et al. (2014), Kenney & Koopmann (1999), Boselli et al. (2016), Boselli et al. (2018), Fossati et al. (2018); 2 in A3627, Sun et al. (2006), Sun et al. (2007), Sun et al. (2010), Zhang et al. (2013); 1 in A1367, Yagi et al. (2017); 5 in A2744, Rawle et al. 2014). Systematic searches for jellyfish galaxies in several different systems have also been carried out, most notably in the MACS (The MAssive Cluster Survey) clusters (z= 0.30-0.43) by Ebeling et al. (2014) and McPartland et al. (2016) as well as in the OMEGAWINGS+WINGS clusters (z= 0.04-0.07) by Poggianti et al. (2016); the latter lead to the GASP (GAs Stripping Phenomena in galaxies with MUSE) survey, a large ESO/MUSE study on the ram pressure stripping phenomena (Poggianti et al., 2017b). Recently, jellyfish galaxies have been identified in the Illustris TNG simulations (Yun et al., 2019).

At first sight, the jellyfish morphology appears to resemble that of tadpole galaxies, objects first found in the higher redshift Universe probed by the Hubble Deep Field (HDF) (van den Bergh et al., 1996) and later studied in more detail in the Hubble Ultra Deep Field (HUDF) (Elmegreen & Elmegreen, 2010, Elmegreen et al., 2007, Straughn et al., 2015). These are galaxies with a diffuse tail attached to a head of a bright decentralised clumpy star-forming structure (Sánchez Almeida et al., 2013). However, the formation of tadpole galaxies cannot to be described entirely by the RPS phenomenon and there are numerous alternative proposed origins (see e.g. Sánchez Almeida et al. 2013). A striking difference between jellyfish and tadpole galaxies is that the former present enhanced star forma-

tion in the tails region (Poggianti et al., 2018), while in the latter, star formation is enhanced in the head region (Abraham et al., 1996, van den Bergh et al., 1996). It is also important to stress that the jellyfish phenomenon is associated with cluster environments, crucial to explain their origin, while that is not the case for tadpole galaxies.

The OMEGA survey was designed to generate deep, low-resolution spectra around the Hα (λ =6563 Å) and [NII] (λ =6548 Å, λ =6584 Å) emission-lines for all the galaxies in the Abell 901/2 multi-cluster system. This was accomplished with observations with the tunable-filter instrument OSIRIS located at the 10.4m Gran Telescopio Canarias (GTC). The main goal of the OMEGA survey is to provide a better understanding on star formation and AGN activity across the A901/2 system by targeting the emission lines Hα and [NII] in the whole area of the system (Chies-Santos et al., 2015, Rodríguez del Pino et al., 2017, Weinzirl et al., 2017, Wolf et al., 2018). The A901/2 system, at z $\sim$ 0.165, covers a 0.51 $\times$ 0.42 square degree area in the sky and its large range of different environments provides a great laboratory for galaxy evolution. It has been observed in many wavelengths and extensively studied by the STAGES (Gray et al., 2009) and COMBO-17 surveys (Wolf et al., 2003). Moreover, the system has been observed with XMM-Newton, GALEX, HST, Spitzer, VLT/VIMOS, PRIMUS, 2dF and GMRT.

Constraining the properties of jellyfish galaxies is crucial to understand the role of the RPS phenomena in the environmental quenching we observe in galaxies in dense environments. The combination of HST imaging (Gray et al., 2009) and Hα maps from the OMEGA survey is ideal to search for jellyfish galaxies and to study how this effect can alter the evolutionary path of galaxies in the environments probed in A901/2. This paper is organised as follows: in Section 2.2 we describe the data used throughout the study; in Section 2.3 we discuss the criteria used for selecting the sample of jellyfish galaxy candidates; in Section 2.4 we show and discuss the main results of our study by exploring their general properties, e.g. morphology, mass and SED types, as well as their star formation properties and spatial distribution as a function of environment; in Section 2.5 we present a summary of our findings and the conclusions.

Thorough the paper we adopt a $H_0 = 70 kms^{-1}Mpc^{-1}$, $\Omega_\Delta = 0.7$ and $\Omega_M = 0.3$ cosmology.

2.2 Data

2.2.1 The OMEGA Survey

In this work we have used the integrated star formation rates and AGN/SF emission-line diagnostics from Rodríguez del Pino et al. (2017). We have also used the Hα spatially resolved emission stamps from Rodríguez del Pino et al. in prep..

For a detailed description of the survey details, the data acquisition and reduction see Chies-Santos et al. (2015). The analysis of the integrated star formation and AGN properties of the whole survey can be found in Rodríguez del Pino et al. (2017). Weinzirl et al. (2017) performs the study of the phase-space properties of the OMEGA galaxies. The study of how inclination affects different star formation estimators was done in Wolf et al. (2018).

2.2.2 Additional data for the Abell901/2 multicluster system

In addition to the data from OMEGA, we have also used the ACS/WFC3 F606W Hubble Space Telescope (HST)/Advanced Camera for Surveys (ACS) images available from STAGES (Gray et al., 2009). We have used some of the galaxy properties available in the STAGES catalogue (Gray et al., 2009), such as stellar masses, the SED types classification, previously visually assigned morphologies and stellar environmental densities. The A901/2 galaxies were classified in three different SED types: blue cloud, old red and dusty red (Wolf et al., 2005). The blue cloud are blue normal star-forming galaxies while the old red are red passive galaxies. The dusty red have obscured star formation and have been shown to host active star formation on average four times lower than the blue cloud galaxies (Wolf et al., 2009). The term ”dusty” may be misleading, as these galaxies do not have more dust than the other star-forming galaxies. As they have relatively low star formation, the same amount of dust makes them look redder. Moreover, we have used the XMM-Newton X-ray image of the system for mapping the hot gas in the system (Gilmour et al., 2007). We have also used the stamps from the RGB COMBO-17 poster for display purposes. These images are illustrative and have the sole purpose to provide a better view of the galaxies.

2.3 The Sample

2.3.1 Sample Selection

In order to obtain a sample of jellyfish galaxy candidates in A901/2, we performed a search within the OMEGA sample of detected Hα-emitting sources from Chies-Santos et al. (2015), and Rodríguez del Pino et al. (2017). The OMEGA sample contains 439 Hα-emitting galaxies with masses ranging from 10^9 to $10^{11.5}$ $M_\odot$ that are classified as members of the A901/2 system (Gray et al., 2009). These galaxies can have active star formation and/or host AGN activity. Given that jellyfish galaxies have been found to strongly emit in Hα (Abramson et al., 2016, Bellhouse et al., 2017, Sheen et al., 2017, Smith et al., 2010, Vulcani et al., 2016) it is a reasonable starting point to search for them in OMEGA. Three of us (ACS, BRP and FRO) visually inspected the HST/F606W images searching for visual morphological features of gas stripping. Our classification scheme was based on the methods described in Ebeling et al. (2014) and Poggianti et al. (2016).

The visual inspection was first performed independently by each classifier who evaluated the presence of three main morphological features following Ebeling et al. (2014):

1. unilaterally disturbed morphology;
2. bright knots of star formation;
3. debris trails.

According to the level of visual evidence of morphological features of stripping, each classifier assigned a JClass for each galaxy ranging from 0 to 5, following the method described in Poggianti et al. (2016). Starting from JClass 1 for the weakest evidences, the stronger cases were classified with higher JClasses up to the most extreme JClass 5 events. Galaxies with no evidence of stripping were assigned JClass 0. The JClasses 1 and 2 are galaxies that may show some weak visual evidence of stripping, but the evidence is not strong enough for selecting them as secure candidates. The JClass 3 are galaxies with light visual evidences of stripping that are probable cases of galaxies undergoing a stripping event. Finally, JClass 4 and 5 cover the strongest candidates.

We leave the weakest cases (JClasses 1 and 2) out of the final sample of jellyfish candidates as their physical origin is difficult to evaluate based solely on the images observed.

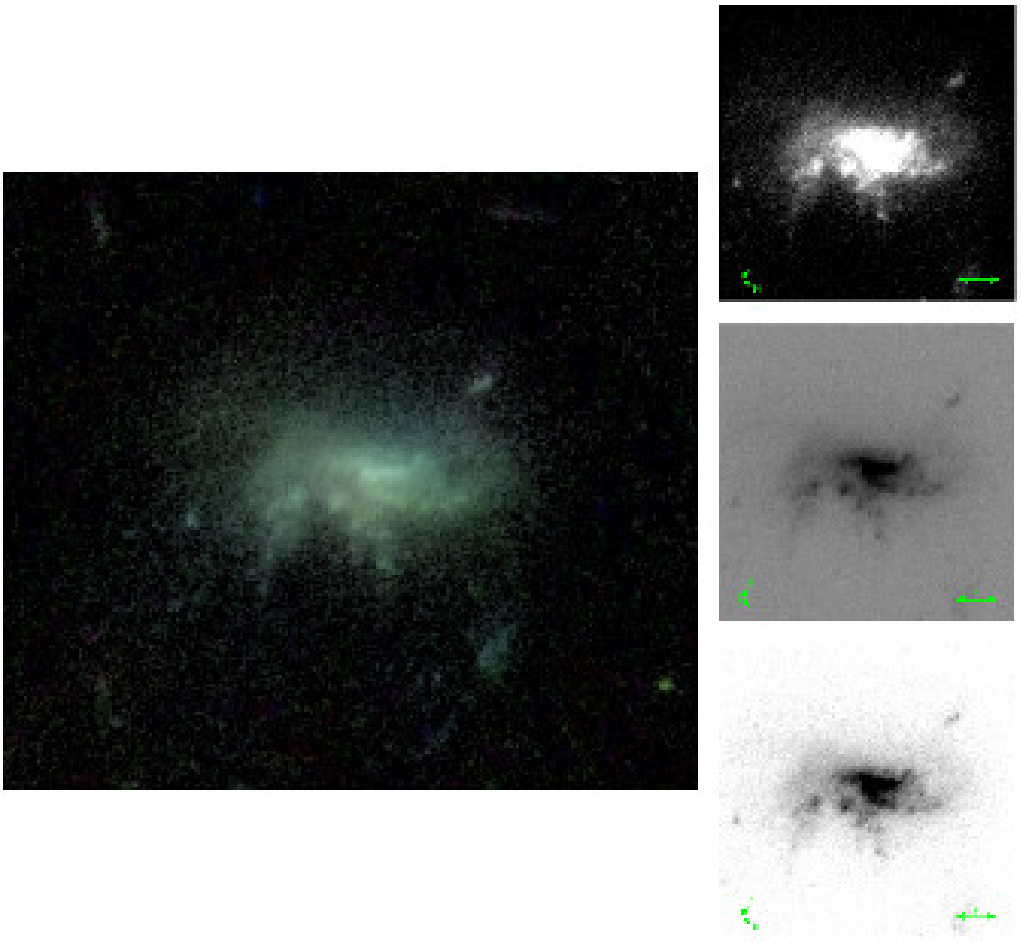

Our final sample of jellyfish candidates is selected by including those galaxies classified as JClass 3 or higher by at least two classifiers. We assign them a final JClass determined as the median of the three classifications. The final sample consists of 73 galaxies of which 11 galaxies are assigned a final JClass 5, 24 galaxies a final JClass 4 and the remaining 38 galaxies are assigned a final JClass 3. The whole sample of candidates is presented in the ATLAS that is available online as a supplementary material to this article. The Figure 2.1 shows one example of each of the JClass categories – top to bottom panels: JClass 5, 4, 3, 2 and 1.

To verify whether the sample selection is biased because of using only Hα-emitting galaxies, we applied the same selection method to a control sample. This control sample was composed by 200 random non-Hα-emitting galaxies that are confirmed cluster members and occupy the same range of mass. From the 200 galaxies, we found only one case of a JClass 4 and two cases of JClass 3. Therefore, there is little morphological evi-

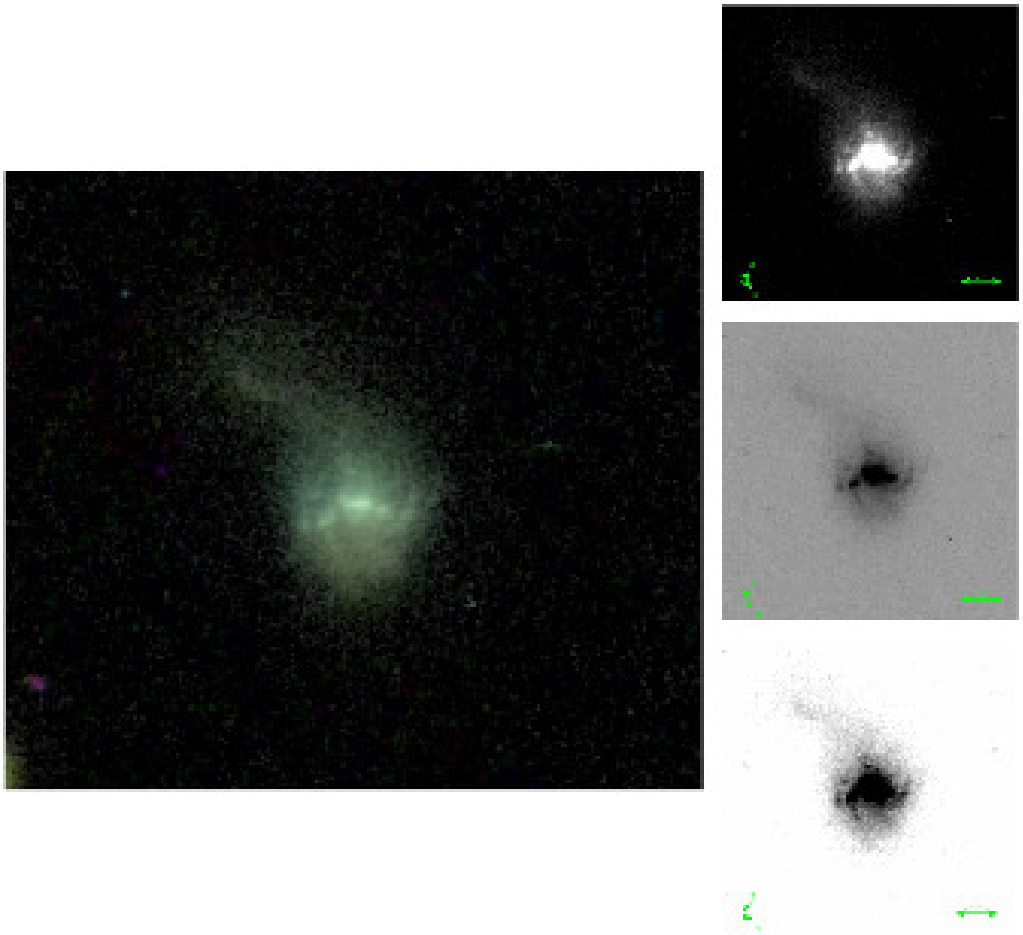

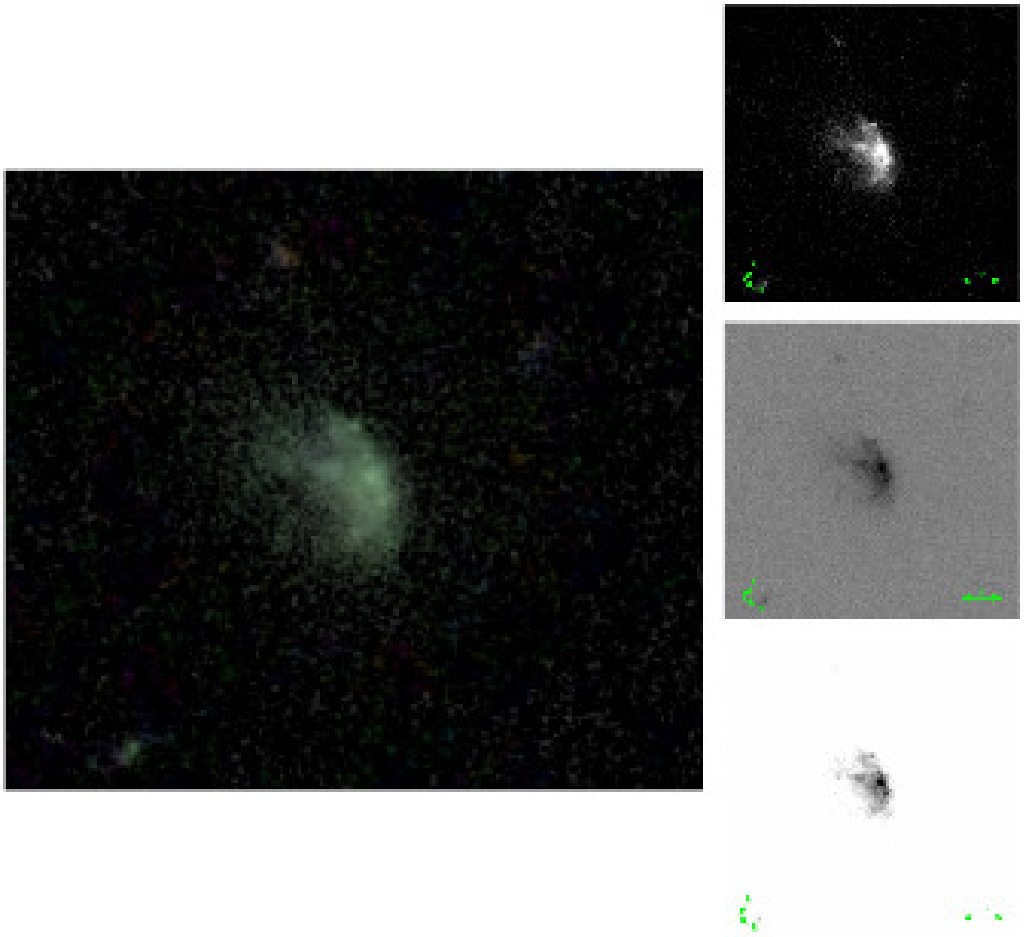

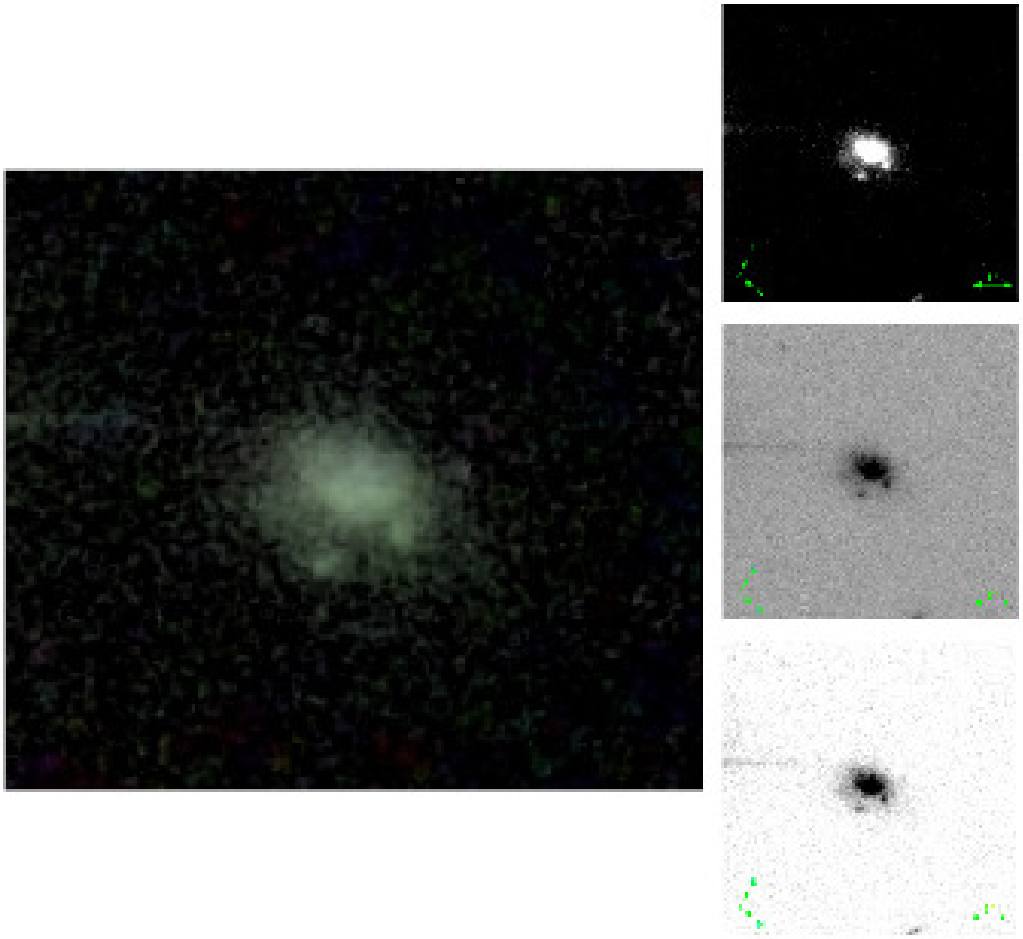

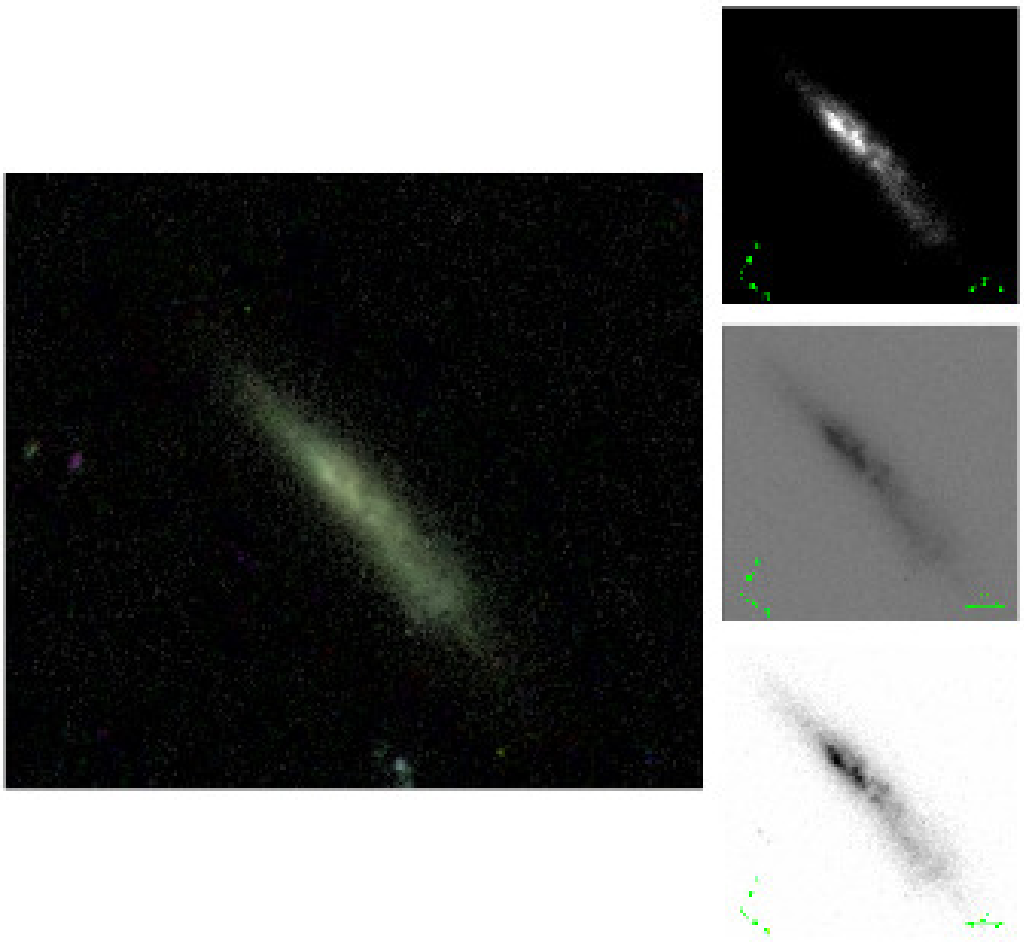

Figure 2.1: Examples of jellyfish galaxy candidates, the upper panel shows a JClass 5, the strongest case, and each following panel shows the next consecutive lower JClass until reaching JClass 1, the weakest case, at the bottom panel. For each galaxy: on the left the composed RGB image from the COMBO-17 poster. On the right three different contrasts of the HST image allowing the observer to recognise the debris trails and knots.

dence of RPS in the control sample. This indicates that we are selecting the majority of jellyfish candidates with very low incompleteness in our Hα detected sample. It also tightens the link between jellyfish galaxies and Hα emission which is an indicator of recent star formation.

The selected sample can also be contaminated by galaxies that have irregular jellyfish-like morphologies because of other mechanisms non-related to RPS. These contaminants should be mainly galaxies that went through tidal interactions with close companions or mergers. For testing our sample for such contaminants, we have checked if the jellyfish galaxy candidates appear to be systematically closer to their neighbours than the other galaxies in the system. Measuring the projected distance to the closest neighbour for both the final jellyfish candidates sample and for a control sample of 450 random cluster members in the same range of mass, through a Kolmogorov-Smirnov (KS) test we find no significant difference between both populations (p = 0.2). Therefore, the jellyfish galaxy candidates are not systematically closer to their neighbours than the rest of the galaxies. This result reassures that the mechanism responsible for the jellyfish signatures is most likely RPS rather than tidal interactions or mergers.

At the end of the selection process we reviewed each one of the candidates and applied a flag for possible tidal interactions and/or mergers for galaxies that appear to be too close to a companion. In total, three galaxies were flagged, IDs: 33058, 34033 and 34839. They remain in the ATLAS, but they are not included in the plots and analysis. Throughout the paper we may refer to different groups of JClasses by shortening the nomenclature, e.g. JClasses 3, 4 and 5 to JC345.

2.3.2 Trail Vectors

Galaxies undergoing RPS often leave trails of gas, dust and recently formed stars behind as they move around the system. Based on these morphological structures it is possible to infer the projected apparent infalling direction of the galaxies (McPartland et al., 2016, Smith et al., 2010). We call this the trail direction of the galaxy and we represent it with a trail vector, this vector should point towards the motion of the galaxy. In this section we describe the method we have followed for assigning the trail vectors as a second stage of the visual inspection.

Each one of the three classifiers independently assigned a trail vector to every jellyfish galaxy candidate as a first stage. The classification involved two steps: the identification of the most pronounced RPS signature

(e.g. tails) and then the recognition of the direction in which this feature is being stripped. After this stage, the three inspectors reviewed together the individually assigned vectors to yield a final vector with a unanimous agreement. Figure 2.8 shows some examples of the trail vectors assigned.

2.4 Results

2.4.1 Morphologies, stellar masses and SED types

In this subsection we explore the main properties of our sample of jellyfish galaxy candidates in comparison to the other Hα emitting galaxies in the OMEGA sample. We look at morphologies, stellar mass distribution and SED types to find whether the jellyfish phenomenon is associated to galaxies with distinct properties. In Figure 2.2 we show such comparisons.

In the left panel of Figure 2.2 we compare the morphological types assigned by the STAGES collaboration for the galaxies in the whole OMEGA sample and the jellyfish candidates sample. The sample of jellyfish galaxies (JC345) is composed mainly by late-type spirals and irregulars. In the middle panel of Figure 2.2, we show the distribution of SED types for both samples. Based on the SED types of the galaxies, out of the 70 jellyfish galaxy candidates analysed, 66 were found to be part of the blue cloud and 4 as being dusty reds (IDs: 11633, 17155, 19108, 30604). However, contrary to what could be expected, dusty red galaxies are only a small portion of our sample of jellyfish candidates. One reason why we may not detect many dusty reds as jellyfish galaxies might be due to the fact that these galaxies, despite having relatively high SFRs (only four times lower than that in blue spirals at fixed mass, Wolf et al. 2009), have significant levels of obscuration by dust which might hamper the identification of the jellyfish signatures. Another reason for that is that we selected jellyfish galaxy candidates within a parent sample of Hα emitting galaxies that had already a low fraction of dusty red galaxies ($\approx$ 15%). As these galaxies have low star formation it is harder to perceive the morphological features of RPS. Dusty red galaxies have been previously studied in this same system (Wolf et al., 2009) and RPS was suggested to be the main mechanism acting in these galaxies (Bösch et al., 2013). While in Bösch et al. (2013) one of the main evidences suggesting the action of enhanced RPS was the existence of disturbed kinematics without disturbed morphologies, in our study we strongly base our selection on such morphological distortions. Both our jellyfish galaxy candidates and the dusty red galaxies show different characteristics that can be correlated to the effect of RPS. Nevertheless, they

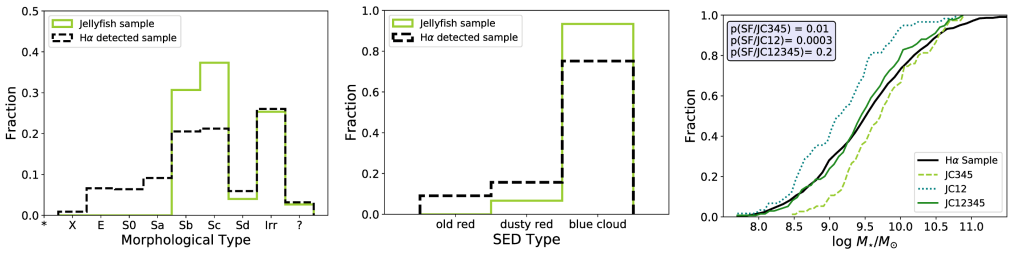

Figure 2.2: Left panel: the histogram of the STAGES morphological types of the jellyfish galaxies compared to the Hα sample. Middle panel: the SED types histogram determined by STAGES for both the jellyfish candidates sample and the Hα sample. Right panel: cumulative histogram of the stellar mass distributions for the OMEGA-Hα sample, the jellyfish candidates sample (JC345), the galaxies with weak RPS evidence (JC21) and all galaxies with JClass higher than 0 (134 galaxies).

might be tracing different stages of the same phenomenon, where dusty red galaxies have more regular morphologies, but disturbed kinematics. Our sample of morphologically disturbed jellyfish galaxy candidates may be showing the stage where the features of RPS are the most visible and the star formation rates are enhanced.

Finally, the right panel of Figure 2.2 shows the stellar mass distribution in a cumulative histogram for the different samples. We can see in the cumulative mass distribution that the jellyfish candidates (JC345) have higher masses than the other galaxies in the OMEGA sample (a KS test returns a pvalue of 0.01). Nevertheless, for less massive galaxies the visual evidence for gas stripping is less noticeable, specially in the continuum. In this way, RPS events in less massive galaxies may not be selected or may end up being assigned lower JClasses, as 1 or 2, which may cause a bias towards selecting more massive galaxies as jellyfish galaxy candidates. We check this hypothesis by adding the weaker cases JC12 to the plot, they appear to be less massive than the parent or the jellyfish sample. If we merge all JClasses together, we find that it follows very closely the mass distribution of the parent sample with no statistically significant difference (p = 0.2). Thus, we conclude that the apparent shift towards higher masses in this sample of jellyfish galaxy candidates is due to a selection bias.

2.4.2 Environmental Properties

To test effects due to environment we have compared the environments where jellyfish candidates and the star-forming galaxies in OMEGA re-

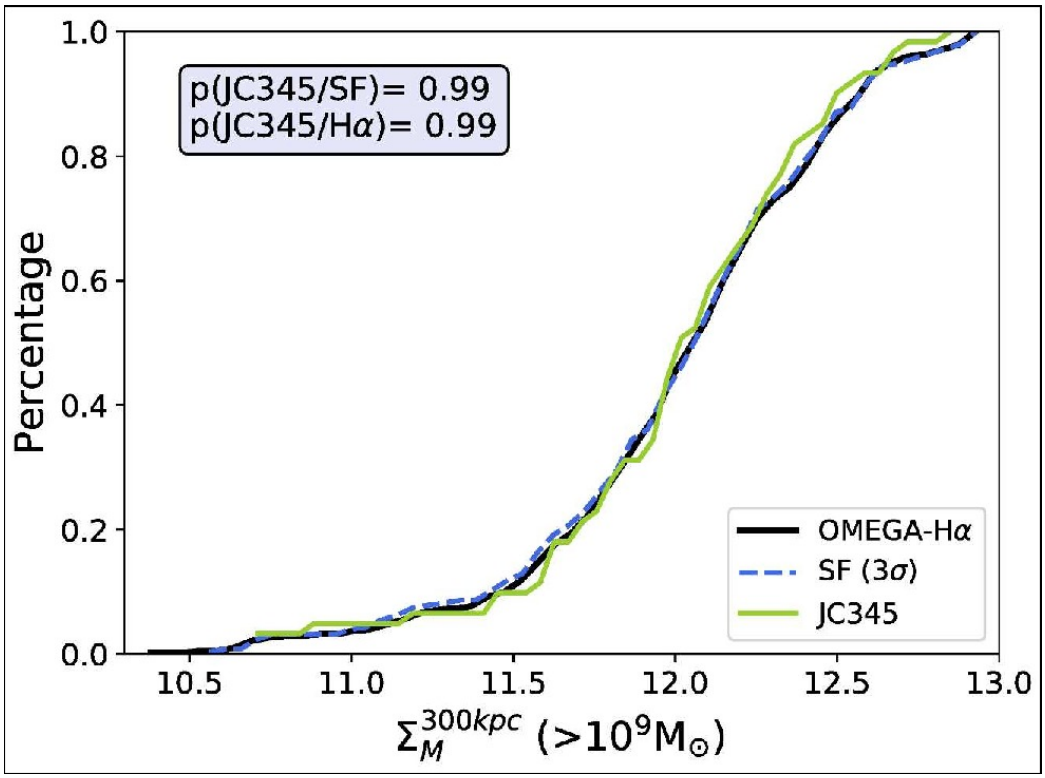

Figure 2.3: Cumulative histogram of the distribution of the galaxies by stellar matter density. We compare the jellyfish candidates (green solid line) to the OMEGA galaxies with active star formation (blue dashed line) and we plot the OMEGA-Hα sample (grey solid line) for reference.

side. We first compare the stellar mass density of both populations. This is calculated as described in Rodríguez del Pino et al. (2017) and by following the procedure of Wolf et al. (2009). We use the $\Sigma_M^{300kpc}(> 10^9 M_\odot)$ parameter. Figure 2.3 shows the cumulative histogram for the OMEGA-Hα sample, the OMEGA-SF and the jellyfish candidates (JC345). We find no significant difference among the samples. However, it is important to note that our range of environmental densities is not broad and there may exist some behaviour outside of this range that we might not be detecting.

We have also checked the relation between the sample and the environment as function of the projected radial distance between the galaxies and the positions of the sub-cluster centres. Here, in order to avoid the contamination by the galaxies in-between two sub-clusters, we are only analysing the galaxies enclosed in the inner regions of the virial radius R_{200} of each sub-cluster. In case of overlapping, which occurs with A901a and A901b, the galaxies are considered members of the sub-cluster they

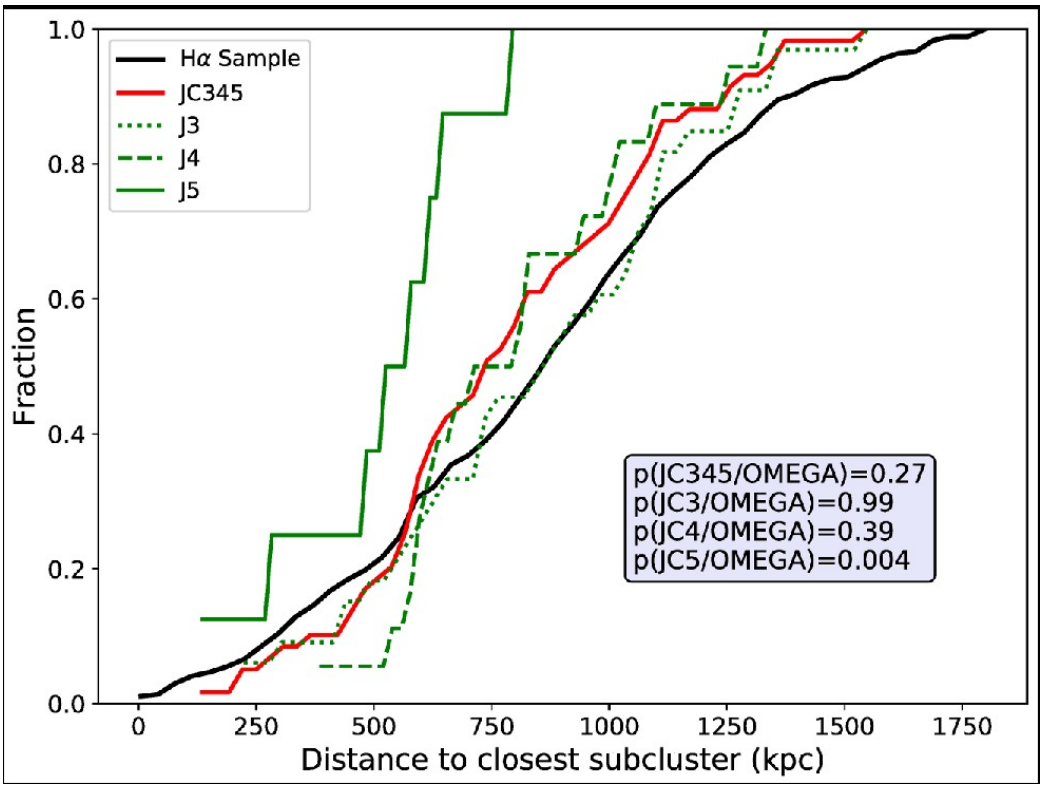

Figure 2.4: Cumulative histogram of the distribution of projected distances from the galaxies to the closest sub-cluster. We compare the jellyfish candidates by JClass to the OMEGA-Hα sample. The green lines show the jellyfish candidates distribution by JClass: 5 (solid line), 4 (dashed line) and 3 (dotted line). The OMEGA-Hα sample distribution is represented by the black solid line.

are closest to. We find that the whole distribution of jellyfish candidates (JC345) is not significantly different from the OMEGA sample (p=0.2). We have then divided the galaxies in subsamples of different JClasses, which is shown in Figure 2.4. We find that the higher the JClass, the closest they are to a sub-cluster centre. Performing KS tests in these three distributions we find the following values: p=0.004 for JC5, p=0.4 for JClass 4 and p=0.98 for JClass 3. Such behaviour is therefore only found to be highly significant for the strongest jellyfish candidates. However, these results are not entirely reliable given the small number of objects in the samples tested.

Spatial distribution of the ram pressure stripping events

In Figure 2.5 we explore the projected spatial distribution of the candidates on the system. We also show the contours of the X-ray emission divided into two different levels of significance: the black lines contour a 3σ level and the gray lines contour a 2σ level. The X-ray comes from the emission of the hot gas and traces its distribution. The highest level contour allows us to see where the majority of the hot gas is located and the second contour assists in establishing the extent of its distribution around the system. We find that approximately 40% of the galaxies are located outside the virial radius of the sub-clusters. However, for the most massive sub-clusters (A901a and A901b) the jellyfish galaxies are mostly located within the virial radius – only around 30% of the galaxies are outside the virial region. Whereas in less massive ones (A902 and SW group) their distribution is more extended – approximately half of the sample is located outside the virial radius of these sub-clusters. These galaxies are probably not yet attached to the gravitational potential of any of the sub-clusters. If we consider only the most compelling candidates (JC45), we see that half are located in the A902 system, however only two are found inside the virial radius of the SW group.

We also show in Figure 2.5 the respective trail vector of each galaxy. We can infer whether the galaxies appear to be falling towards or moving away from the sub-cluster centres. For quantifying that, we have calculated the angle between the trail vector and a vector pointing in the direction of the closest sub-cluster centre in projected distance. If the absolute value of this angular difference is smaller than 90° then we say the galaxy is moving towards the system and, if the difference is larger than 90°, then the galaxy is classified as moving away from the system.

Table 2.1 contains the number of galaxies either falling towards or outwards any of the systems divided by JClasses. The spatial analysis of these vectors altogether with the position of galaxies around the system suggests that they have no preferential sub-cluster centres to be falling towards or outwards. No sub-cluster shows a significant difference between the infalling towards/outwards numbers and as we restrict the analysis to each sub-cluster, however, on these circumstances we are prone to low number statistics. Our results are in contrast with those found by Smith et al. (2010) for jellyfish galaxies in the Coma cluster where they are mostly falling towards the cluster centre. An important note is that we are limiting our study to Hα emitting galaxies while in Smith et al. (2010) the sample is limited to UV emitting galaxies covered with GALEX, however, this should not drastically change our findings. Nevertheless, the differ-

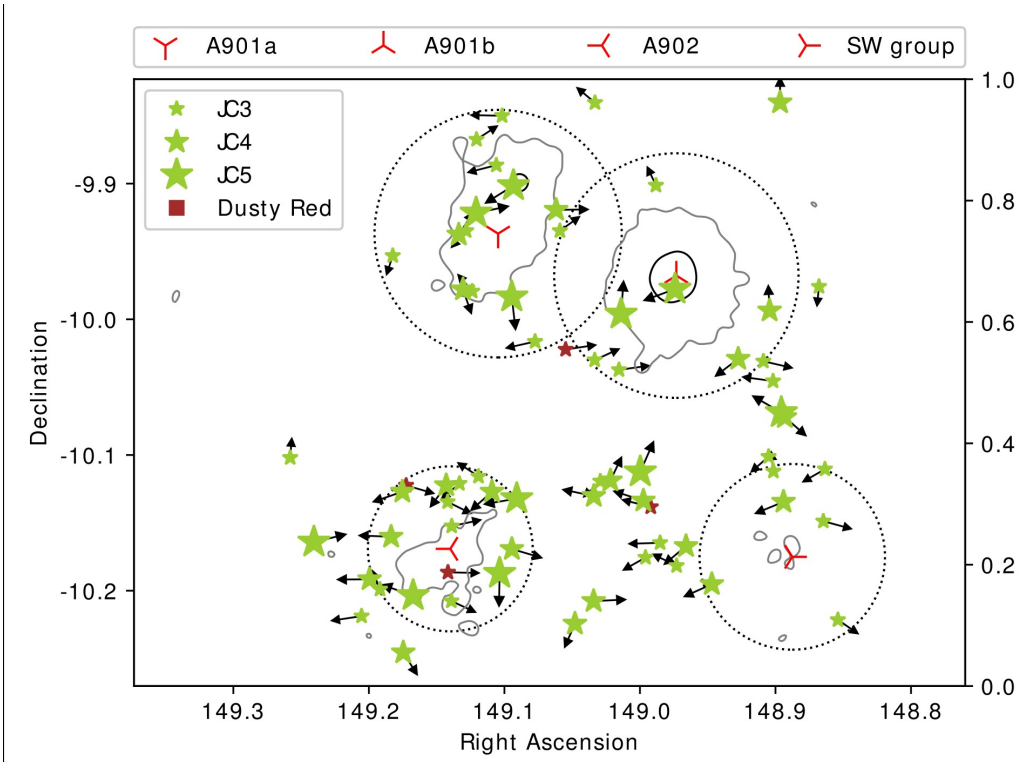

Figure 2.5: Spatial distribution of the jellyfish galaxies around the four sub-clusters in the A901/2 system. Each sub-cluster is labelled and have the circles showing their virial radius R_{200} (dash-dot black circles). The stars represent the jellyfish candidates according to the legend. The dusty red galaxies are marked in red. All of their respective trail vectors are shown as arrows. The grey contours show the gas density as measured from the x-ray emission, they are divided in three levels of significance: 3σ (solid dark line) and 2σ (solid gray line).

Cluster	Direction	JC5	JC4	JC3	Total
A901a	towards	2	1	2	5
	outwards	1	2	7	10
A901b	towards	1	1	4	6
	outwards	1	2	4	7
A902	towards	2	3	5	10
	outwards	2	8	5	15
SW group	towards	0	2	2	4
	outwards	2	3	7	12

Table 2.1: Distribution of the projected direction of motion of the candidates per sub-cluster and per JClass, as implied by the trail vectors assigned.

ences might be due to the fact that the dynamics of A901/2 are much more complex and is a still evolving system, whereas Coma is a more relaxed cluster.

Given that the effect of ram pressure depends strongly on the density of the hot gas (Gunn & Gott, 1972), in principle we would expect a correlation between the distribution of the hot gas and the jellyfish galaxies. In our case, this may explain why there are so few cases of evident jellyfish in the SW group since it is the region with the weakest x-ray emission, thus less hot gas. This also explains why the strongest candidates (JC45) tend to gather in the inner regions of the clusters. However, for the cases outside the inner regions of the sub-clusters, the influence of the merging system has to be taken into account as well. The effect of cluster mergers in the observation of RPS events has already been suggested in the Abell 2744 system by Owers et al. (2012). Three of the four jellyfish galaxies were found closely to the gradients in the X-ray emission, features of the cluster merging, suggesting that cluster mergers can trigger RPS events. This phenomenon has also been hinted in the work of McPartland et al. (2016), where their results suggest that extreme RPS events linked to cluster mergers. The fact that the Abell 901/2 multi-cluster system holds a rich jellyfish population is a compelling evidence that the unrelaxed nature of interacting systems may cause an enhancement of the fraction of jellyfish galaxy events.As well as increasing the number of cases, the distribution of RPS events in merging systems would not only follow the distribution of hot gas but also its dynamics. The RPS phenomenon has a square dependency on the relative velocity between the galaxy and the hot gas, while the dependency is linear with the density of the hot gas (Gunn & Gott, 1972). Interacting clusters provide much greater velocities than single re-

laxed systems on the frontiers of the interaction. For this reason, it is not unexpected that the jellyfish galaxies would not follow an even distribution around and towards the sub-cluster centres. These galaxies could be actually tracing the regions on where the relative velocity increases dramatically due to the interactions of the sub-clusters. A simulation work on the jellyfish galaxies in the A901/2 system shows the tendency of the galaxies gathering around the regions where the relative velocity of the ICM is higher (Ruggiero et al., 2019).

Projected Phase-Space Diagram

The phase-space analysis for the OMEGA-Hα sample has been performed in Weinzirl et al. (2017). Among other interesting results, it was found that there is no change in the sSFR of the star-forming galaxies at fixed mass throughout the cluster environment. This suggests that pre-processing of galaxies during the infall is a dominant mechanism in quenching the star formation.

In Figure 2.6 we show the most secure jellyfish candidates (JC45) and analyse their location in a projected phase-space diagram for each sub-cluster system. We separate the galaxies by sub-cluster according to the closest sub-cluster centres in projected angular distance. In this diagram we analyse two fiducial radii, the Boundary1 is defined as $R_p/R_{200} \leq 1.2, |\Delta V_{los}/\sigma_{scl}| \leq 1.5 - 1.5/1.2 \times R_p/R_{200}$ and comes from Jaffé et al. (2015) which was used for analysing the A963_1 system that lies at z$\sim$0.2 and is close in mass to Abell 901a. Boundary 2 is defined by $R_p/R_{200} \leq 0.5e|\Delta V_{los}/\sigma_{scl}| \leq 2.0 - 2.0/0.5 \times R_p/R_{200}$ and was taken from Weinzirl et al. (2017) that studies in detail the properties of the OMEGA galaxies in the phase-space diagram. The boundaries have the purpose to trace the frontier of the gravitational influence of the sub-clusters. However, it is important to note that the A901/2 multi-cluster is an unrelaxed system and the use of boundaries in the phase-space diagram analysis should be considered as a rough approximation. V_{los} represents the velocity in the line of sight of the galaxies and σ_{scl} represents the velocity dispersion of the sub-cluster.

The projected phase-space diagram divided by sub-centre complements the information provided in Figure 2.4. The strongest cases seem to gather closer to the centre and to the boundary of the virialised regions for the most massive clusters.

As for their velocities, we find that from JC345 sample, only 27 candidates are at high velocities ($\Delta V_{los}/\sigma_{cls}$ ¿ 1), in which three are JClass 5, eleven are JClass 4 and fourteen are JClass 3. We notice that our candidates

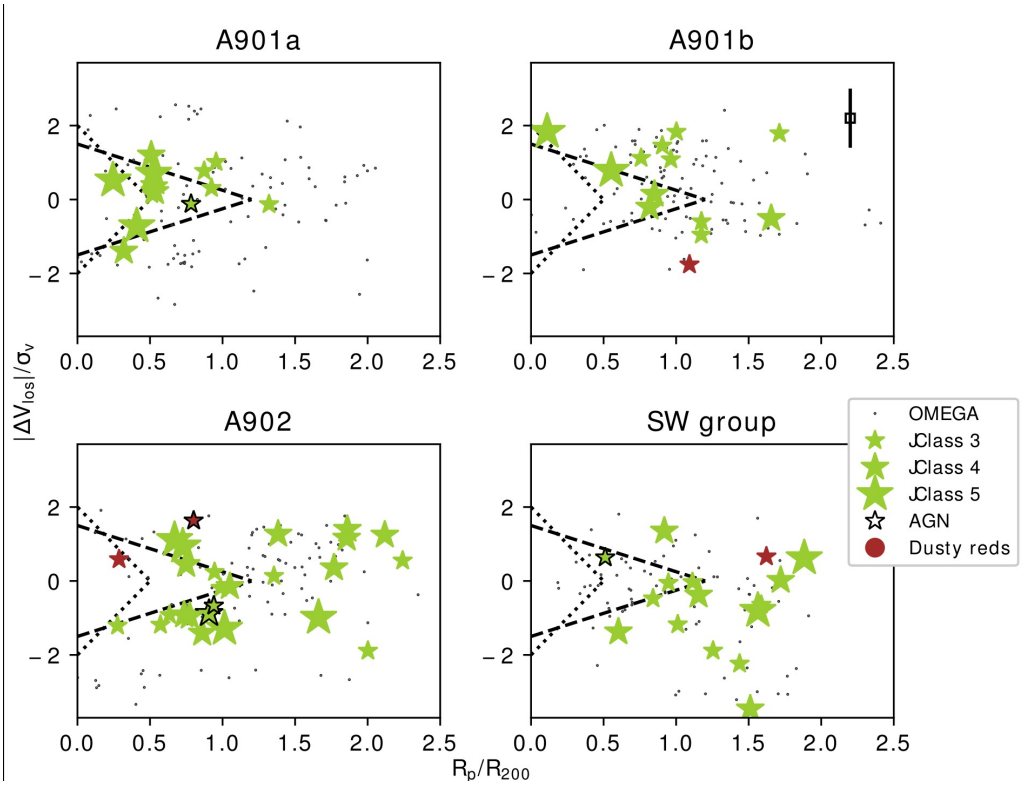

Figure 2.6: Phase space diagram for the jellyfish galaxy candidates divided by sub-cluster according to the legend. The sample is divided by JClass and represented by star symbols according to the legend. Galaxies within this sample that are hosts to an AGN are represented as a square and the dusty red galaxies are painted in red. The open gray circles in the background represents the OMEGA-Hα galaxies that show no morphological evidence of RPS. We analyse two fiducial boundaries: Boundary 1 (Jaffé et al., 2015) and Boundary 2 (Weinzirl et al., 2017).

do not show particularly high velocities, however, we are only probing the relative velocity on the line of sight to the sub-clusters. As discussed in Subsection 2.4.2, since the A901/2 system is in interaction, the dominant velocity would be in the hot gas motion as the system evolves and we can not estimate that from the projected velocity of the galaxies.

Missing AGN activity

We find that out of the 70 jellyfish galaxy candidates, 53 of them are star-forming galaxies and 5 are hosts to an AGN with high probability. The separation of AGN and star-forming galaxies was done in Rodríguez del Pino et al. (2017) through a WHAN diagram. We are considering as secure cases only galaxies with a high probability (higher than 3σ) of belonging to one of these two groups given their nuclear emission. Our findings suggest that AGN activity is not a strong feature in the sample. Extreme RPS cases have been proposed as a triggering mechanism for AGN activity (Poggianti et al., 2017a). However, the low fraction of AGN hosts in our sample, specially among the JClass 5 galaxies, and their position in the PPS diagram in Figure 2.6, points to the scenario that the RPS is not triggering AGN activity in the sample and that the few AGN cases we find do not seem to be correlated to RPS.

We find that no AGN is hosted by a JClass 5 galaxy, only one is hosted by JClass 4 galaxy and the remaining four AGNs are found in JClass 3 galaxies. If we lower the criteria to a 2σ probability, we find other 3 less probable cases of AGN activity: one in a JClass 5 galaxy, another in a JClass 4 and the remaining in a JClass 3 galaxy. Moreover, the most compelling jellyfish candidates (JC45) that are AGN do not seem to fall on the regions where the RPS is expected to be strongest - small radius and high velocities. Both of them are found at larger radii (r ¿ $0.5R_p/R_{200}$) and only one is in the high velocity region ($\Delta V_{los}/\sigma_{cls}$ ¿ 1).

Interestingly, even though the AGN activity does not seem related to the RPS, the AGN hosts seem to have relatively higher masses than the rest of the jellyfish candidates sample (4 of them are more massive than $10^{10.2} M_{\odot}$). It may be an evidence that the AGN found in the sample may be more related to the masses of the host galaxies and that the RPS signatures may be a coincidence instead of a trigger. However, the statistics is too low for a definite answer.

Finally, we have downloaded the publicly available GASP data for 42 jellyfish galaxies. For each MUSE data cube we have selected the integrated spectra in the 6×6 spaxels around the centre of the galaxies, fitted the emission lines and measured, in a similar way to the OMEGA

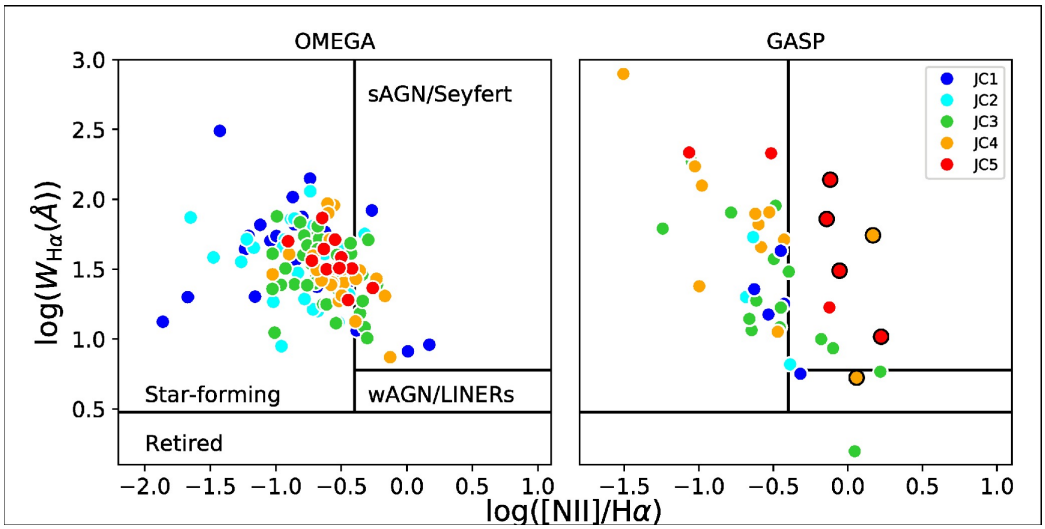

Figure 2.7: The WHAN diagram for jellyfish galaxies in the public GASP sample (left panel) and for the OMEGA jellyfish galaxy candidates (right panel). Different JClasses are shown in different colours according to the legend. The markers with a black edge are the galaxies present in Poggianti et al. (2017a).

data, EWs and line ratios. We show in Figure 2.7 the WHAN diagram (Cid Fernandes et al., 2010) comparison of our findings with that of the public GASP sample of jellyfish galaxies. As in Rodríguez del Pino et al. (2017) we employ the vertical line separation of [NII]/Hα=0.4 proposed by Stasińska et al. (2006). For the sake of comparison we add the JClasses 1 and 2 in this plot as the GASP sample keeps these objects. The trend we find in the OMEGA sample is consistent with what we find in the GASP sample. The majority of galaxies shows ongoing star formation not associated with nuclear activity. We have also generated the BPT diagrams for the GASP sample where this trend is perhaps even more visible. We chose, however, to only show the WHAN diagram as we can compare with the OMEGA jellyfish galaxy candidates sample as well.

2.4.3 Star Formation Properties

Spatially Resolved Star Formation

We have studied the Hα emission for the jellyfish candidates by analysing the Hα emission contours on top of the HST continuum images. The maps generated for the jellyfish candidates and for the other galaxies in the OMEGA sample will further be available and studied in detail in Rodríguez del Pino et al. in prep.. We show some examples in Figure 2.8 for jellyfish

galaxy candidates of JClasses 5, 4 and 3.

We show the Hα emission contours on top of the HST continuum images together with the final trail vector for all galaxies in the ATLAS. The contours are missing for some galaxies as there were not enough images in the OMEGA continuum and/or around the Hα line to build them accurately. The spatial distribution of the Hα emission, for part of the sample, is evidently disturbed and extended and, in some cases, the extension agrees with the trail vector previously assigned. This points towards a scenario that as well as stripping gas out of the galaxy, ram pressure may also enhance star formation activity, both inside and outside the galaxies. The fact that the Hα emission is disturbed and extended indicates that the star formation is also taking place where the gas is being stripped out of the galaxy and building the asymmetrical structures we observe.

Integrated Star Formation

As for the integrated star formation properties of the candidates, we generate a specific star formation rate (sSFR) versus mass diagram as in Rodríguez del Pino et al. (2017), shown in Figure 2.9. We compare the sSFR of the jellyfish galaxy candidates, divided by JClass, to the star-forming galaxies in the OMEGA sample. We also include in the figure the main sequence of star formation at the same redshift derived from the SDSS (Abazajian et al., 2009, DR7) field galaxies. We then draw two more lines with the same slope that goes through the median of each population of galaxies: the green solid line for jellyfish galaxies (JC345) and blue for the star-forming OMEGA galaxies. We find that our jellyfish galaxy candidates sample have higher sSFR than it would be expected for galaxies similar in mass in a field environment. Given that many galaxies in the parent sample have reduced their star formation activity, as seen in Rodríguez del Pino et al. (2017), it is striking that most of the jellyfish galaxies are going against this trend and are located above the field relation. In fact, 55% of the jellyfish galaxy candidates are above the main sequence line. The process that the jellyfish galaxies are undergoing is producing an enhancement in their star formation activity that places them above the field relation. This happens despite the environmental quenching that is reducing the star formation in the other star-forming galaxies in OMEGA (Rodríguez del Pino et al., 2017). To quantify the difference in specific star formation rates, we run a KS test in a cumulative histogram of the sSFR of both populations. The results show that none of the subsamples (JC345, JC45 and JC5) can be part of the same parent population. Whilst these galaxies have been selected only by visual evidence of RPS it suggests that such mechanism is indeed en-

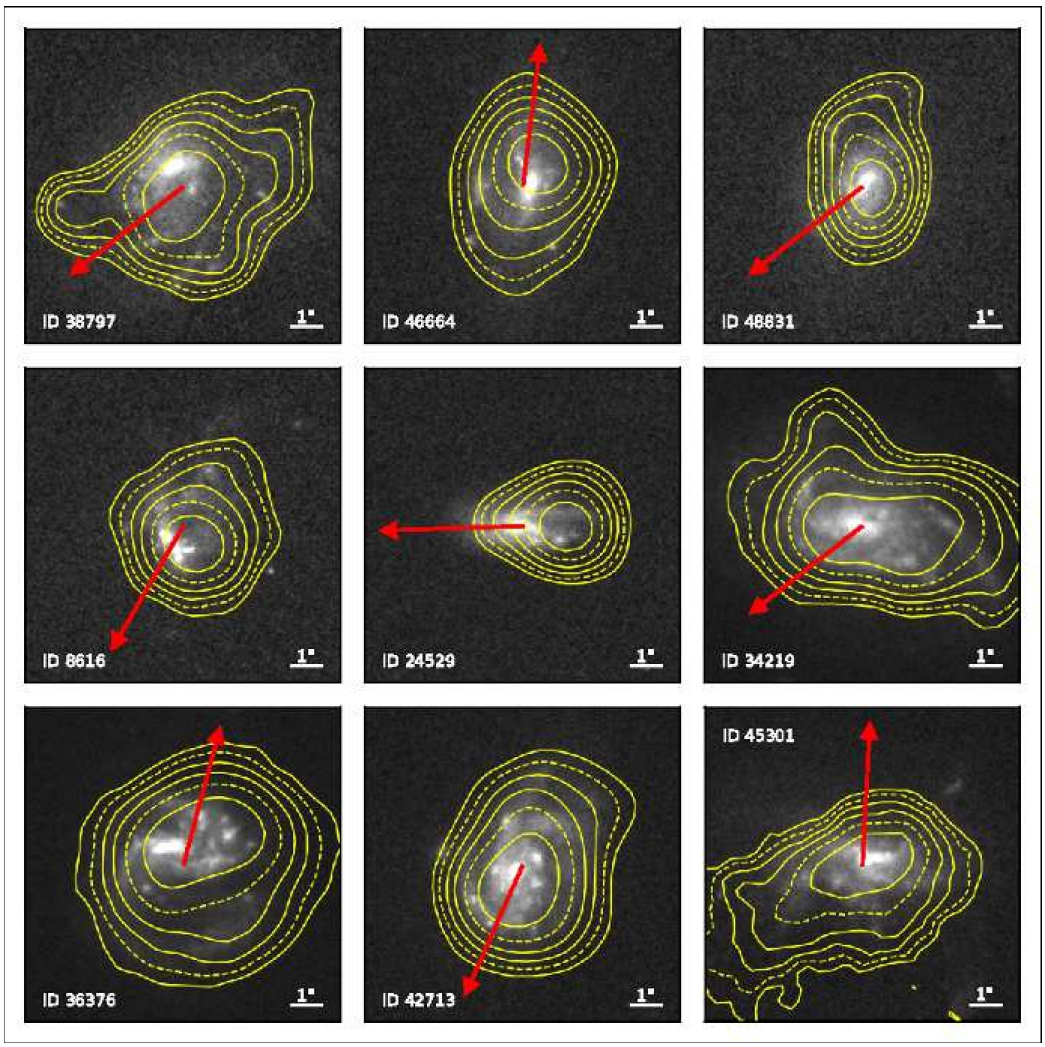

Figure 2.8: Examples of Hα contours and final trail vectors. Top row – JClass 3; middle row – JClass 4; bottom row – JClass 5.

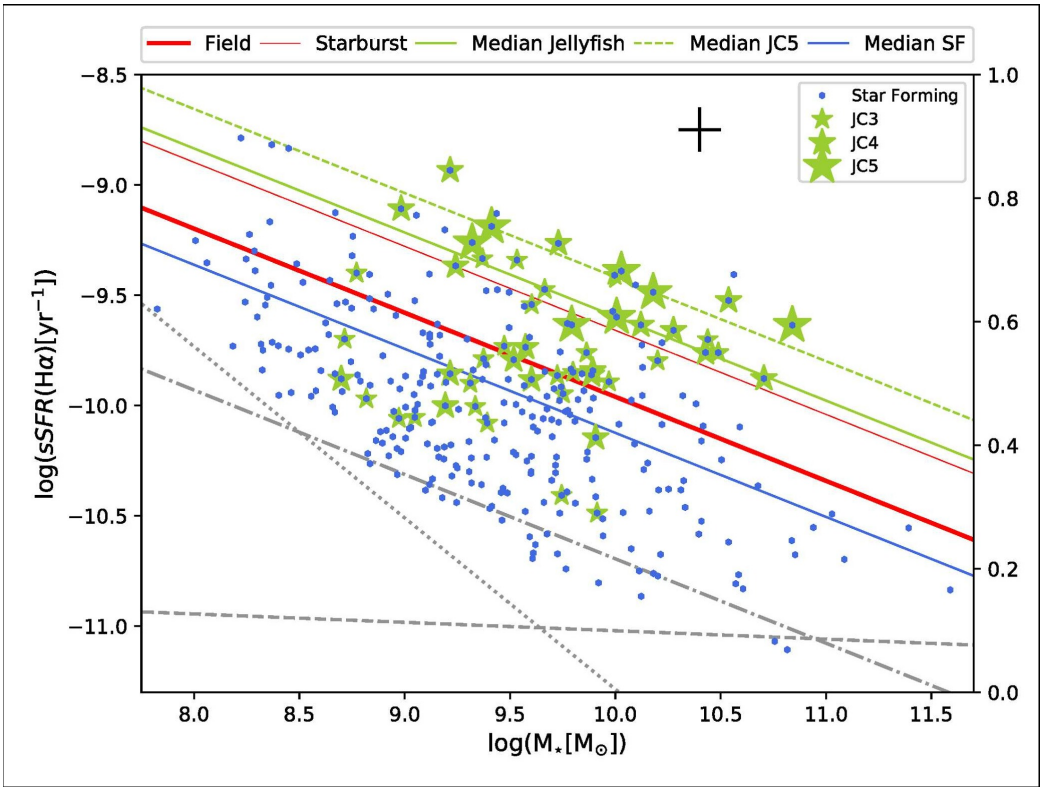

Figure 2.9: Specific star formation rate versus mass: jellyfish galaxies are separated by JClass and represented by the green star symbols, the larger the star the more evident the "jellyfish" morphology. The blue dots represent the OMEGA-SF. The main sequence sSFR-stellar mass relation for the SDSS field galaxies is represented by the red line. The green and blue lines are, respectively, lines that go through the median of the jellyfish (solid for JC345 and dashed for JC5) and star-forming populations with the same slope as the red line. The thinner red line marks a sSFR that is twice that of the main sequence, which has been used to outline starbursts (Elbaz et al., 2011). The grey lines show the detection limits of the OMEGA survey: Hα flux (dotted), equivalent width (dashed) and the lower boundary for the region free from incompleteness (dash-dot).

hancing the star formation of some of these galaxies. In Figure 2.9, we also draw a thinner second red line which stands for a sSFR of twice the value of the main sequence, we use it as a lower limit for what we can consider to be starburst galaxies (Elbaz et al., 2011). Using this line as reference, 19 of the 70 jellyfish candidates found seem to be undergoing a starburst period. This line has also been used in the work on the Abell 2744 system with 4 jellyfish galaxies where 1 of them showed to be starburst by this definition (Rawle et al., 2014). From these 19 starburst galaxies, when separating by JClasses, the starburst phenomenon seems to be correlated with how evident the jellyfish morphology is, where: 8 of the 11 JClass 5 galaxies, 6 of the 22 JClass 4 galaxies and only 5 of the 37 JClass 3 galaxies appear to be starbursts. An enhancement in the specific star formation rate in jellyfish galaxies has already been suggested by Rawle et al. (2014), for only 4 jellyfish galaxies in a merger system, and Poggianti et al. (2016), for 344 candidates scattered in several different clusters. Moreover, Vulcani et al. (2018) find that stripping galaxies show a systematic enhancement in the SFR-mass relation when compared to undisturbed galaxies. However, this is the first time that this effect is observed in a large number of objects in a single multi-cluster system. This could be explained by thinking about jellyfish galaxies as a quick transition morphology that links different stages of galaxy evolution. It may be that galaxies undergoing RPS suffer an enhancement in the star formation, specially in the outskirt regions, leading to a starburst episode. This stage soon runs out of available gas as it is being stripped away and then further leads to the quenching of the galaxy. This transformation could be strongly correlated with the visual features we observe and, as a consequence, correlated with the JClasses assigned: visually more evident phenomena could be marking the phase of the triggering of star-forming, whereas less evident phenomena could be either the pre-SF-trigger or the post-SF-trigger period.

2.5 Summary and Conclusions

In this work we have conducted a systematic search for galaxies that show morphological evidences of gas stripping in the Abell 901/2 system, at z $\sim$ 0.65, and a detailed analysis of their overall properties as part of the OMEGA survey. The search was conducted over the OMEGA parent sample of 439 Hα-emitting galaxies. The final sample is composed by 73 galaxies, classified in 5 different categories of visual magnitudes of the phenomenon named JClasses – 1 being the weakest evidence of RPS and 5 being the strongest. This is the largest sample of jellyfish galaxy candi-

dates in a single system to date. We flag down 3 galaxies as possible tidal interactions and run the analysis on the remaining 70, in which our main findings are:

1. The typical morphologies of the jellyfish galaxy candidates are late-type spirals or irregulars. The sample is dominated by blue cloud galaxies with only 4 being previously assigned a dusty red classification. We have found only 5 AGN host galaxies. Moreover, the jellyfish galaxy candidates appear to be slightly more massive than the other galaxies, which we associate to a visual selection bias.

2. The jellyfish galaxy candidates spatial distribution and apparent motion around the multi-cluster system does not show an obvious pattern. We find little correlation between the distribution of jellyfish galaxies and hot gas traced by X-ray emission. However, the most evident candidates (JC5) seem to be located closer to the centres of the sub-clusters when compared to the other less evident cases. The two most massive sub-clusters (A901a and A901b) have a larger and more concentrated population of jellyfish galaxies around them, While half of the compelling cases (JC45) are gathered around the intermediate mass system (A902). In fact, the sub-cluster with the lowest mass (SW group) has only two compelling jellyfish candidates (JC45) within its virialised region.

3. We find that the jellyfish galaxy candidates specific star formation rates are higher than the typical main sequence values, despite what happens to the other star-forming galaxies in the system that show significantly reduced star formation rates. In fact, the median trend for the sample shows higher sSFR than the lower limit of the starburst definition we have used from Elbaz et al. (2011). Furthermore, we also find evidence of extended and disturbed star formation for part of the sample.

Our interpretation is that the low fraction of dusty reds in the sample of jellyfish galaxy candidates – 4 out of 70 – suggests that the galaxies selected through visual evidence are at a later stage of the RPS event than those that only show disturbed kinematics. At first only the gas is affected and the RPS does not significantly impact the morphology of the galaxy. However, the disturbed gas triggers extended star formation that leads to a disturbed jellyfish morphology. We also find no link between our most compelling jellyfish candidates and AGN activity. Due to the low fraction of AGN within our sample – 5 out of 70 – and the fact that the few ones we

find are not located in the region of the phase-space diagram where RPS is at its peak, we are not able to link both of these phenomena in A901/2.

The large number of jellyfish galaxy candidates found is a compelling evidence that RPS events might be enhanced in interacting systems, making multi-cluster systems ideal environments to search for other jellyfish galaxy candidates. Also, the apparent lack of pattern in the motion and spatial distribution of the sample of candidates around A901/2 might be evidence of how the RPS phenomenon occurs in multi-cluster systems. Since there is added dynamics to the ICM due to the motion of the subclusters, the relative velocity between the galaxy and the hot gas dominates over the factor of the ICM density. Therefore, the distribution and motion of the galaxies do not necessarily follow the hot gas traced by the X-rays.

Our findings also point to the enhancement of star formation as consequence of the RPS phenomenon. In our sample of jellyfish galaxy candidates we found a strong correlation between the morphological asymmetry, traced by the JClasses, and high specific star formation rates. This result supports the evolutionary scenario proposed that: at first, the disturbances are only dominant in the gas and star formation is not enhanced; at a later stage, the perturbations work as a trigger of star formation on the outskirt regions of the galaxy creating the morphological features that we identified in this work. The extended star formation enhances the overall sSFR of the galaxy and can cause a starburst period that is probably short lived as the gas continues to be stripped to further cause a quenching in the star formation.

Acknowledgements

This work is based on observations acquired through ESO large Programme ESO188.A-2002 at the *Gran Telescopio Canarias*, installed at the *Observatorio del Roque de los Muchachos* of the *Instituto de Astrofísica de Canarias*, on the island of La Palma. We also use observations collected at the European Organization for Astronomical Research in the Southern Hemisphere under ESO program 196.B-0578. This study was financed in part by the *Coordenação de Aperfeiçoamento de Pessoal de Nível Superior - Brasil* (CAPES) - Finance Code 001. ACS and FRO acknowledge funding from the brazilian agencies *Conselho Nacional de Desenvolvimento Científico e Tecnológico* (CNPq) and the Rio Grande do Sul Research Foundation (FAPERGS) through grants PIBIC-CNPq, CNPq-403580/2016-1, CNPq-310845/2015-7, PqG/FAPERGS-17/2551-0001, PROBIC/FAPERGS and L'Oréal UNESCO ABC *Para Mul-*

heres na Ciência. BRP acknowledges financial support from the Spanish Ministry of Economy and Competitiveness through grants ESP2015-68964 and ESP2017-83197. At last, we are grateful for the valuable comments from the anonymous referee.

Chapter 3

Galaxy cluster mergers as triggers for the formation of jellyfish galaxies: case study of the A901/2 system

Published in Monthly Notices of the Royal Astronomical Society*

The A901/2 system is a rare case of galaxy cluster interaction, in which two galaxy clusters and two smaller groups are seen in route of collision with each other simultaneously. Within each of the four substructures, several galaxies with features indicative of jellyfish morphologies have been observed. In this paper, we propose a hydrodynamic model for the merger as a whole, compatible with its diffuse X-ray emission, and correlate the gas properties in this model with the locations of the jellyfish galaxy candidates in the real system. We find that jellyfish galaxies seem to be preferentially located near a boundary inside each subcluster where diffuse gas moving along with the subcluster and diffuse gas from the remainder of the system meet. The velocity change in those boundaries is such that a factor of up to ∼1000 increase in the ram pressure takes place within a few hundred kpc, which could trigger the high rate of gas loss necessary for a jellyfish morphology to emerge. A theoretical treatment of ram pressure

*Ruggiero, R.; Machado, R. E. G.; **Roman-Oliveira, F. V.**; Chies-Santos, A. L.; Lima Neto, G. B.; Doubrawa, L. and Rodríguez del Pino, B.; MNRAS, 484, 906

stripping in the environment of galaxy cluster mergers has not been presented in the literature so far; we propose that this could be a common scenario for the formation of jellyfish morphologies in such systems.

3.1 Introduction

In a ΛCDM cosmology, primordial inhomogeneities in the density field of the Universe are expected to act as seeds for the later formation of structures. On small scales, gravity tends to make initially small inhomogeneities evolve into collapsed structures, most notably dark matter haloes, which later become the hosts of objects such as galaxies and galaxy clusters. In accordance with ΛCDM, such haloes often interact with each other through mergers; galaxy cluster mergers are the most extreme version of such interactions, and are the most energetic events in the universe since the Big Bang (Sarazin, 2002).

One prominent example of a system in interaction is the A901/2 multi-cluster, at $z \sim 0.165$. This is an unrelaxed system that contains four main cores – A901a, A901b, A902 and the SW group – and provides an ideal laboratory for probing galaxy evolution along different scales of environment and galaxy masses (Gray et al., 2004, 2009). All four subclusters are at similar redshifts (see e.g. Weinzirl et al., 2017), and the two most massive cores (A901a and A901b) have overlapping virial radii, which indicates that the system is likely a multi-cluster merger in its early stages. This is reinforced by the fact that a system with the mass of A901/2 ($\sim 3.5 \times 10^{14}$ $M_\odot$) is expected to collapse if its spacial extent is smaller than about 5 Mpc (Busha et al., 2003), while most of the mass in A901/2 is within a spacial scale of a few Mpc.

Numerical simulations have often been employed to study mergers of galaxy clusters, both from a more general, theoretical point of view, and also in order to model specific objects. Binary cluster collisions are particularly well suited for this purpose, because the numerical resolution can be entirely focused on the objects of interest, as opposed to fully cosmological simulations of structure formation. For example, the Bullet Cluster has been studied in this way (Lage & Farrar, 2014, Mastropietro & Burkert, 2008, Springel & Farrar, 2007), as have other so-called dissociative clusters (e.g. Donnert, 2014, Machado et al., 2015, Molnar & Broadhurst, 2015), in which gas and dark matter are offset as a result of the collision. Numerous other observed clusters have been modelled by dedicated simulations that aim to reconstruct their dynamical histories. Simulations have been used to study several phenomena related to collisions of galaxy clusters,

such as radio relics (e.g. van Weeren et al., 2011), sloshing cold fronts (e.g. Machado & Lima Neto, 2015, Walker et al., 2018, ZuHone et al., 2010), turbulence (e.g. Vazza et al., 2012, ZuHone et al., 2013b), thermal conduction (e.g. ZuHone et al., 2013a), etc. Tailored simulations involving more than two initial objects are more uncommon. For example, a triple merger has been simulated by Brüggen et al. (2012) in order to model 1RXS J0603.3+4214.

Gas-rich galaxies which move within the environment of galaxy clusters are expected to have their evolution affected by the interaction with the intracluster medium (ICM). The ram pressure exerted by the ICM can lead to gas loss by ram pressure stripping (Gunn & Gott, 1972), which, in more extreme cases, leads to the formation of "jellyfish morphologies", in which the galaxy is observed featuring a filamentary tail of stripped gas and stars. The phenomenon of ram pressure stripping of cluster galaxies has been extensively modelled through numerical simulations, which have explored e.g. the role of inclination angle in the rate of gas loss (Roediger & Brüggen, 2006), the changes in star formation rate which take place within the disks of affected galaxies (Kronberger et al., 2008, Ruggiero & Lima Neto, 2017, Steinhauser et al., 2012), and the predicted emission features within their tails (Kapferer et al., 2009, Tonnesen & Bryan, 2010). Although most of the numerical work on ram pressure stripping has been based on idealised setups, cosmological simulations of galaxy formation have also been used to explore the phenomenon, as e.g. in Tonnesen et al. (2007) and more recently in Yun et al. (2019).

Jellyfish galaxies have been found in large numbers in different cluster systems (see e.g. Ebeling et al. (2014), Poggianti et al. (2016)). However, the number of jellyfish galaxies found in single systems is usually small. The numbers range from 21 in Coma (Smith et al., 2010, Yagi et al., 2010), 3 in Virgo (Abramson et al., 2016, Kenney & Koopmann, 1999, Kenney et al., 2014), 1 in A3627 (Sun et al., 2006) and 5 in A2744 (Rawle et al., 2014). Nevertheless, the rich population of $\sim$70 jellyfish galaxy candidates found in the A901/2 system (Roman-Oliveira et al., 2019) indicates that clusters in interaction may be an ideal environment to search for these galaxies. Moreover, McPartland et al. (2016) performs a large systematic search for such jellyfish morphologies and suggests that galaxy cluster mergers are more likely to be triggering extreme ram pressure stripping events. This scenario has also been suggested in Owers et al. (2012), where four jellyfish galaxies were found near merger signatures of the gas. It is not surprising that such relation could exist: in galaxy cluster mergers, higher ICM velocities are found than in isolated clusters, making those environments favourable for the formation of jellyfish structures.

In this work, we attempt to probe the physical mechanism behind the formation of jellyfish galaxies in galaxy cluster mergers. For that, we model the diffuse gas in the A901/2 system with a galaxy cluster merger simulation, and then compare the gas conditions in this model to the location of a sample of jellyfish galaxies found in this system, allowing us to infer a scenario for the triggering of jellyfish morphologies both in the A901/2 system and in galaxy cluster mergers in general. Such theoretical treatment of ram pressure stripping in galaxy cluster mergers has not been given so far in the literature.

This paper is structured as follows. In Section 3.2, we describe the sample of jellyfish galaxy candidates we use and comment on how they were selected. Then we proceed to describe the setup and the results of our galaxy cluster merger simulation in Section 3.3. The gas conditions in this simulation are correlated with the locations of the jellyfish galaxies in our sample in Section 3.4, where we tentatively propose a physical mechanism for the generation of many of those jellyfishes. Finally, our results are discussed and summarised in Section 3.5, where possible extensions of our work are also presented.

3.2 Sample of galaxies

The galaxies used in this study come from an extensive search for galaxies with jellyfish morphological signatures in the A901/2 system (Roman-Oliveira et al., 2019). This sample was selected through visual inspection of HST/ACS F606W images of galaxies in the parent sample of Hα emitting galaxies in the OMEGA survey (Chies-Santos et al., 2015, Rodríguez del Pino et al., 2017, Weinzirl et al., 2017, Wolf et al., 2018). The visual inspection method applied follows the work of Ebeling et al. (2014) and Poggianti et al. (2016). A classification in JClasses was also employed, in which a number from 1 to 5 is assigned to a galaxy to evaluate its degree of asymmetry – larger values are correlated with a greater likelihood of the galaxy being an actual jellyfish.

The final sample is restricted to the most reliable cases of jellyfish candidates, which we take as those classified as JClass 3 to 5. This sample contains the 73 galaxies that we use in this work. The image stamps are available at the OMEGA jellyfish candidates ATLAS[†].

[†]OMEGA jellyfish candidates ATLAS: `http://lief.if.ufrgs.br/~fernandavro/atlas.pdf`

3.3 Simulations

This work is based on a galaxy cluster merger simulation including the dark matter haloes and intracluster gas of the 4 subclusters in the A901/2 system, which was used to reproduce their positions on the plane of the sky, along with their observed X-ray properties. The simulations were run with the code GADGET-2 (Springel, 2005); in Appendix 3.6, we also briefly compare the gas conditions in the main simulation with its results when it is run in RAMSES (Teyssier, 2002), in order to assess its robustness against a change in numerical methodology.

3.3.1 Simulating the system as a whole

Here we describe the simulation setup, in which the four subclusters were included with the goal of obtaining a suitable model of the system as a whole. Our aim here was chiefly to recover the relative distances between four subclusters having the known virial masses and also having plausible gas content. The main observational constraints are the virial masses of the subclusters, derived from gravitational weak lensing (Heymans et al., 2008).

The redshifts of the subclusters are close to each other (e.g. Weinzirl et al., 2017), so we assume that they are on the same plane. We further assume, for simplicity, that the trajectories of the four subclusters are on the plane of the sky. Virial equilibrium would require velocity dispersions of roughly 1000 km/s; we drew random velocities but choosing the signs of the Cartesian coordinates such that the subclusters are all incoming, i.e. falling towards the centre of mass. It should be noted that our explicit assumption here is that the subclusters are currently infalling towards their first approach, i.e. they have not previously collided.

As a preliminary step, we represent each cluster as a point mass having the M_{200} from Heymans et al. (2008). They are assigned velocities as described above, and position coordinates are known straightforwardly from observations. With this information we perform a simple gravitational N-body simulation (via direct summation) inverting the sign of time; i.e. we simply calculate the orbits backwards in time, for 5 Gyr. This exercise provides a good approximation for the $t = 0$ of the actual hydrodynamical simulation.

In the next step, we set up four actual subclusters including dark matter and gas. The method for generating initial conditions is similar to those used in Machado & Lima Neto (2015) or Ruggiero & Lima Neto (2017), for

Table 3.1: Initial conditions of the simulated subclusters. The first column gives the names of the models and the objects they are meant to represent. The second and third columns give the virial mass and virial radius. The fourth column gives the overall gas fraction.

	M_{200} ($M_\odot$)	r_{200} (kpc)	$f_{\rm gas}$
subcluster A (A901a)	1.3×10^{14}	1034	0.08
subcluster B (A901b)	1.3×10^{14}	1036	0.15
subcluster C (A902)	0.4×10^{14}	688	0.08
subcluster D (SW Group)	0.6×10^{14}	788	0.06

example. The dark matter haloes follow a Hernquist (1990) profile:

$$\rho_{\rm h}(r) = \frac{M_{\rm h}}{2\pi} \frac{r_{\rm h}}{r\,(r+r_{\rm h})^3}\,, \tag{3.1}$$

where $M_{\rm h}$ is the total dark matter mass, and $r_{\rm h}$ is a scale length. The gas is represented by a Dehnen (1993) density profile (with gas mass $M_{\rm g}$ and scale lenght $r_{\rm g}$), adopting $\gamma = 0$:

$$\rho_{\rm g}(r) = \frac{(3-\gamma)\,M_{\rm g}}{4\pi} \frac{r_{\rm g}}{r^\gamma (r+r_{\rm g})^{4-\gamma}}\,. \tag{3.2}$$

The requirement of hydrostatic equilibrium determines the gas temperatures. Realisations of these initial conditions are created according to the procedures described in Machado & Lima Neto (2013). The virial masses, virial radii and gas fractions of the initial conditions are given in Table 3.1.

Each of the four subclusters has 10^6 gas particles and 10^5 dark matter particles. Tests of the present simulations indicated convergence across three orders of magnitude in particle numbers, as far as the orbits are concerned. Moreover, since the subclusters are not interpenetrating, their gravitational potentials remain sufficiently spherical in the current stage of the approach. In this specific configuration, one could even attempt to model them by rigid analytic spherical potentials without much loss of detail. We opted to represent them as N-body particles. Here we employ the smoothed particle hydrodynamics (SPH) N-body code GADGET-2 (Springel, 2005), and the evolution is followed for 5 Gyr.

The four subclusters, created in the manner described above, are then placed at the locations that were reached by the end of the backwards

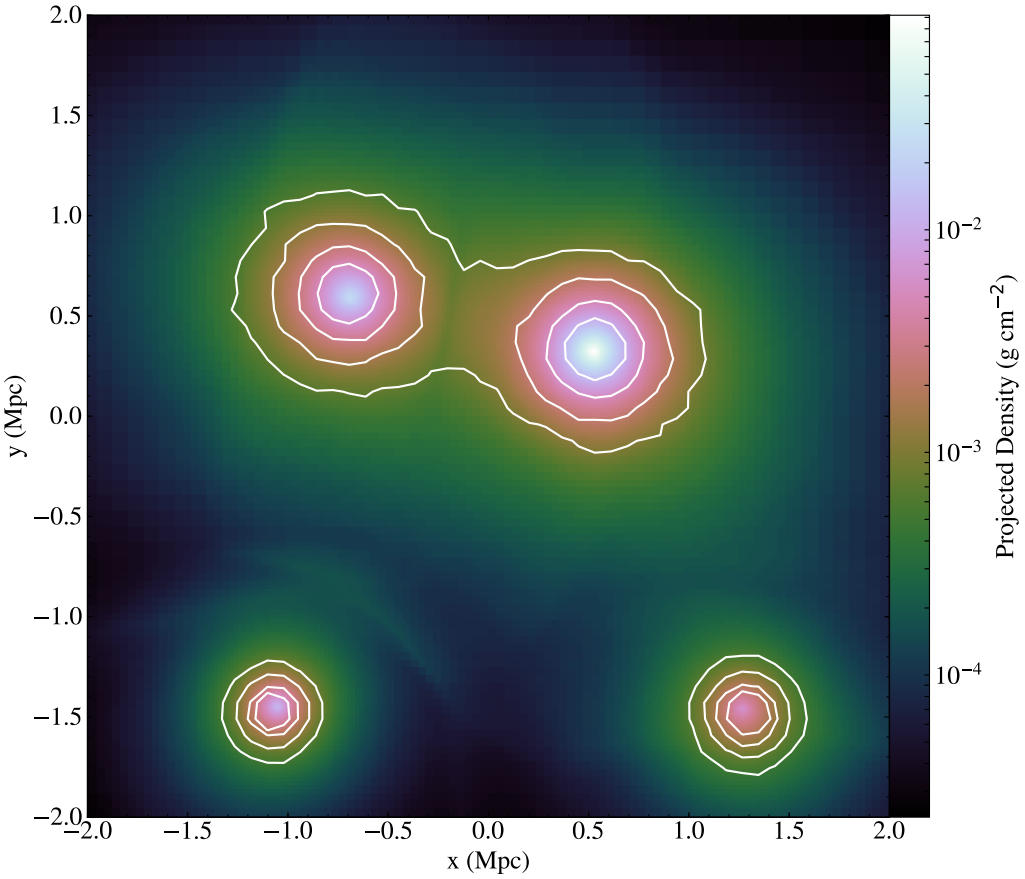

Figure 3.1: This is the snapshot that best reproduces the observed relative separations between the subclusters ($t = 4.3\,\mathrm{Gyr}$). Colours represent the projected gas density. Total projected mass is shown as contours.

point-mass integration. And then the subclusters are allowed to evolve forward in time for 5 Gyr. They fall towards the centre of mass until the current observed separations are reached. However, they do not reach exactly the desired coordinates by the end, because the orbits of four point masses are not identical to the orbits of four extended objects. Some fine tuning of their initial positions and velocities was performed by trial and error until an acceptable agreement was reached. In the resulting preferred model, the instant when the coordinates best matched the observations was $t = 4.3\,\mathrm{Gyr}$.

3.3.2 X-ray mock image

Observations indicate that A901b is the only one of the four with significant X-ray diffuse emission. A901a hosts a very bright AGN, so its extended emission is unclear. A902 is barely above the background noise, and the SW Group is essentially undetectable in X-rays (Gilmour et al., 2007). To ensure a higher X-ray emission, subcluster B in Table 3.1 has the highest gas content of the four. In the absence of detailed observational constraints, the other simulated subclusters were chosen to have a low gas fraction of approximately 8 per cent (or 6 per cent in the case of the SW group), towards the lower limit of what is expected for their masses (Laganá et al., 2013). The simulated gas densities of the best-matching instant are shown in Fig. 3.1. In this figure, one may also notice that the centroids of the projected total mass distributions of the four subhaloes reproduce the observed relative separations in a good approximation.

We performed a more quantitative test to ensure that the simulated gas densities were not excessive. Using the $t = 4.3\,\mathrm{Gyr}$ snapshot of the simulation, we produced a mock X-ray image with the following procedure, assuming thermal emission from a hot plasma. We used `pyXSIM`[‡], a Python package for simulating X-ray observations from astrophysical sources. It is based on an algorithm of Biffi et al. (2012, 2013), but see also ZuHone et al. (2014). In brief, it takes as input the simulated densities and temperatures of the gas, assumes a constant metallicity of $0.3\,\mathrm{Z}_\odot$, and generates a photon sample assuming a spectral model (APEC from the AtomDB database[§]). The photon sample is then projected along the line of sight (the z axis of the simulation). Given the coordinates of the cluster, a foreground Galactic absorption model is also applied, assuming a neutral hydrogen column of $N_\mathrm{H} = 4 \times 10^{20}\,\mathrm{cm}^{-2}$. The photon list is exported to be used by the SIXTE[¶] (Simulation of X-ray Telescopes) package, to be convolved with the *XMM* instrument response (the EPIC MOS camera, in this case). The effective exposure time was 67 ks and the energy range was 0.2–7.0 keV. Poissonian noise was added to the resulting 600×600-pixel mock image, shown in Fig. 3.2. Note that the X-ray emission of the SW group is present in the first frame, albeit very faint. Once noise is added, it is lost in the background.

Our resulting model is approximate, and it cannot be expected to account for all details of the observed systems. Furthermore, there are no assurances that the solution we have found for the orbits is unique, as is

[‡] `http://hea-www.cfa.harvard.edu/~jzuhone/pyxsim/`

[§] `http://www.atomdb.org/`

[¶] `http://www.sternwarte.uni-erlangen.de/research/sixte/`

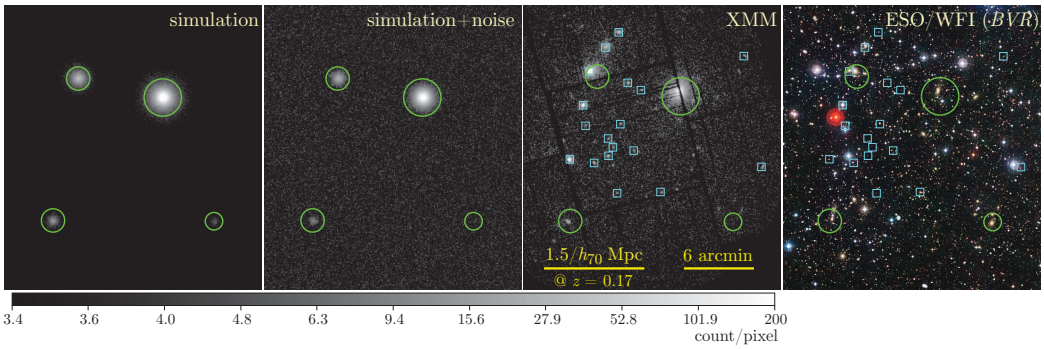

Figure 3.2: Comparison between the the mock X-ray image and the observations. First frame: mock X-ray image produced from the simulation. Second frame: same as before, but with added noise. Third frame: *XMM* observation. Fourth frame: Optical image from ESO/WFI.

always the case in such reconstructions. However, the gas properties in the model are physically well-motivated, and compatible with the observational expectation of X-ray detections – two subclusters with significant emission are obtained, plus two near the threshold of detection (bearing in mind that the diffuse emission of A901a is somewhat inconclusive due to the very bright point source). Therefore, the resulting snapshot of the simulation should offer a sufficiently realistic environment in which to study ram pressure effects.

3.4 Local conditions of the jellyfish galaxies

Now we turn to the analysis of the gas properties in the merger model presented in the previous section, with the goal of answering the question: what explains the presence of jellyfish galaxies at the locations where they are found in A901/2? Naturally, the two most important quantities to be analysed should be the diffuse gas density and the diffuse gas velocity across the system, since jellyfish morphologies are caused by ram pressure stripping events, while the ram pressure $P_{\rm ram}$ depends on those two quantities (Gunn & Gott, 1972):

$$P_{\rm ram} = \rho_{\rm ICM} v_{\rm ICM}^2, \tag{3.3}$$

where $v_{\rm ICM}$ is the ICM velocity relative to a galaxy under consideration. In generating plots involving those quantities, we have used the Python package YT (Turk et al., 2011) to deposit the simulation particles into a space-filling grid with a "cell-in-cloud" approach.

In our analysis, we focus on the ram pressure calculated in the reference frame of each subcluster, as a first approximation for the ram pressure experienced by its member galaxies. The effect of peculiar velocities of member galaxies relative to their parent cluster will be discussed later. These reference frames are defined by the average speed of the dark matter particles within $r_{200}/3$ of the centre of a given subcluster, with the centre location defined as that of the density peak of this cluster's ICM. We have verified that the results that follow are not sensitive to the choice of the inner radius in the velocity calculation – using the velocities within radii closer to r_{200} yield similar results, but we find it more meaningful to restrict ourselves to the inner region of each subcluster since that region is in principle less disturbed by tidal effects.

With those four reference frames defined, we are then able to calculate the ram pressure of the system as a whole in each of them. This is shown in Fig. 3.3, where the ram pressure is shown in slices along the plane of the four subclusters in our model, overlaid with streamlines of diffuse gas velocity. At the centre of each subcluster the ram pressure is low, since in that region the diffuse gas is on average moving along with the cluster halo. On the other hand, the ram pressure is intense far from the cluster centre, since the diffuse gas from other clusters is moving in the opposite direction at high speed. It turns out that a reasonably narrow ($\sim$100 kpc) boundary exists between those two regions, where a significant increase in the ram pressure takes place. The dashed contours in Fig. 3.3 are the approximate locations of those boundaries, which were obtained using ram pressure isocontours, and in each subplot the positions of the galaxies in our sample closest (in projected space) to the subcluster considered in that plot than to any of the other three are shown.

Figure 3.8 shows a gas density slice of the simulation, in which all the ram pressure boundaries are shown simultaneously, along with the locations of all our jellyfish candidates and some examples of HST images for those galaxies. This plot shows that the density in the system does not feature any pronounced structure at the locations of the boundaries, which implies that they emerge exclusively due to the velocity structure of the diffuse gas around their locations. It is not surprising that this should be the case, since the clusters are approaching each other (and thus their diffuse gas is moving at opposing directions), while the ram pressure depends very strongly on the diffuse gas speed, more so than on its density (see Eq. 3.3). In this way, the ram pressure boundaries can be identified as regions where gas moving along each subcluster and gas from the remainder of the system meet.

It can be visually noted in Fig. 3.3 that many galaxies are located in the

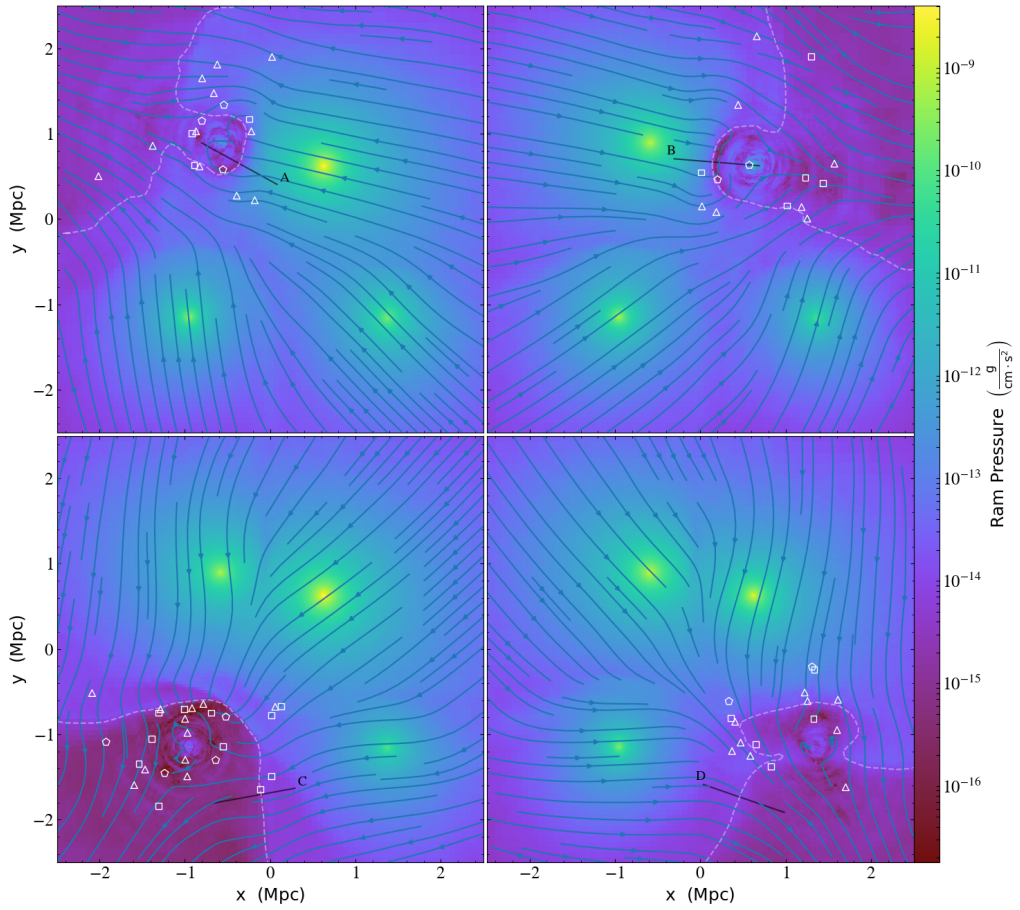

Figure 3.3: Ram pressure intensities in the reference frames of each of the four subclusters. Each subplot is a midplane slice. The dashed lines show the approximate locations of the ram pressure boundaries in each subcluster, and triangles, squares and pentagons represent the locations of jellyfish galaxies classified as JClass 3, 4 and 5, respectively. Ram pressure profiles along the four black lines are shown in Fig. 3.6.

vicinities of the ram pressure boundaries. This is not always the case – for instance, many galaxies in the A902 subcluster are found in a region without an apparent connection to the boundary we find for that subcluster. Still, a correlation seems to exist. We quantify this effect in the following manner. First, we measure the projected distance from each jellyfish galaxy to its respective nearest boundary. Then, we generate a random cloud of points occupying the same area as those galaxies and also measure their distances to the nearest boundaries. The comparison between these two distributions of distances is shown in Fig. 3.4, which makes it evident that the jellyfishes are systematically closer to a boundary than what would be expected from a random distribution. The Kolmogorov-Smirnov test applied to cumulative, normalised histograms for both samples indicates that the chance of the two distributions being equivalent is very small, of 1 in $\sim$85 million (p-value of 10^{-6} per cent). We also make the same comparison using the STAGES sample (Gray et al., 2009) of galaxies in the A901/2 cluster instead of a random sample, filtered for member galaxies with stellar mass between $10^8\,M_\odot$ and $10^{12}\,M_\odot$. The upper quartile, lower quartile and median for the jellyfish distribution are all lower than for the STAGES distribution, with a chance of 1 in 757 (p-value of 0.13 per cent) of the two distributions being equivalent, further reinforcing our thesis that the jellyfishes are systematically closer to the ram pressure boundaries we report.

The distribution of distances to the nearest boundary can also be analysed as a function of JClass. This is shown in Fig. 3.5. The three distributions are overall quite similar, but an interesting feature is that the median distance to the nearest boundary decreases systematically with JClass. This could be an indication that jellyfish morphologies are more pronounced when a galaxy has just encountered a boundary, and then on a short timespan after that, they become less intense. The median distance for JClass 5 galaxies is 53 kpc smaller than for JClass 3 galaxies; assuming that the galaxies move at 1000 km/s, this would imply that the transition from JClass 5 to 3 happens on a timescale of 53 Myr in this scenario. Despite this being a tantalising hypothesis, Kolmogorov-Smirnov tests applied to the distributions for JClass 3 and 4, 3 and 5 and 4 and 5 galaxies yield p-values of 6.75, 13.5 and 7.06 per cent respectively, meaning we have a low confidence that a difference actually exists between the three distributions.

As a more quantitative illustration of the ram pressure variations along the ram pressure boundaries we report, we show in Fig. 3.6 ram pressure profiles along the four black lines in Fig. 3.3, which were chosen arbitrarily for the sake of illustration. Before the boundaries are crossed, the ram

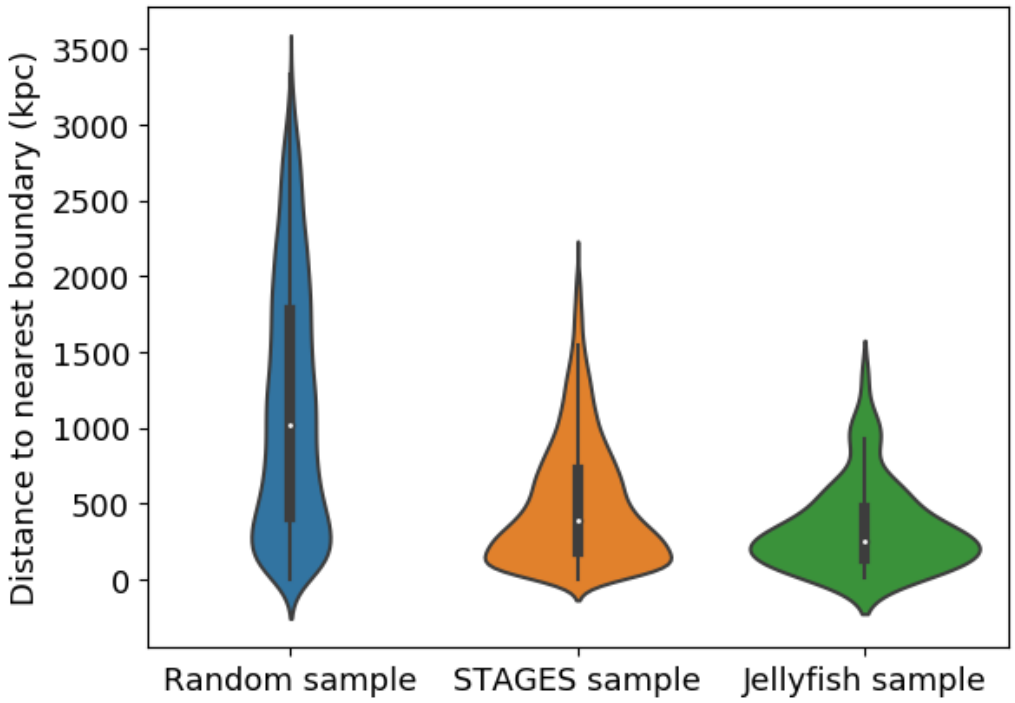

Figure 3.4: Violin plot showing the distributions of distances to the nearest ram pressure boundary for a random set of points, the STAGES sample of galaxies in the A901/2 cluster, and our sample of jellyfishes. The jellyfishes are systematically closer to the boundaries than it would be expected if their locations were random, and they are also systematically closer than the non-jellyfish galaxies in the system.

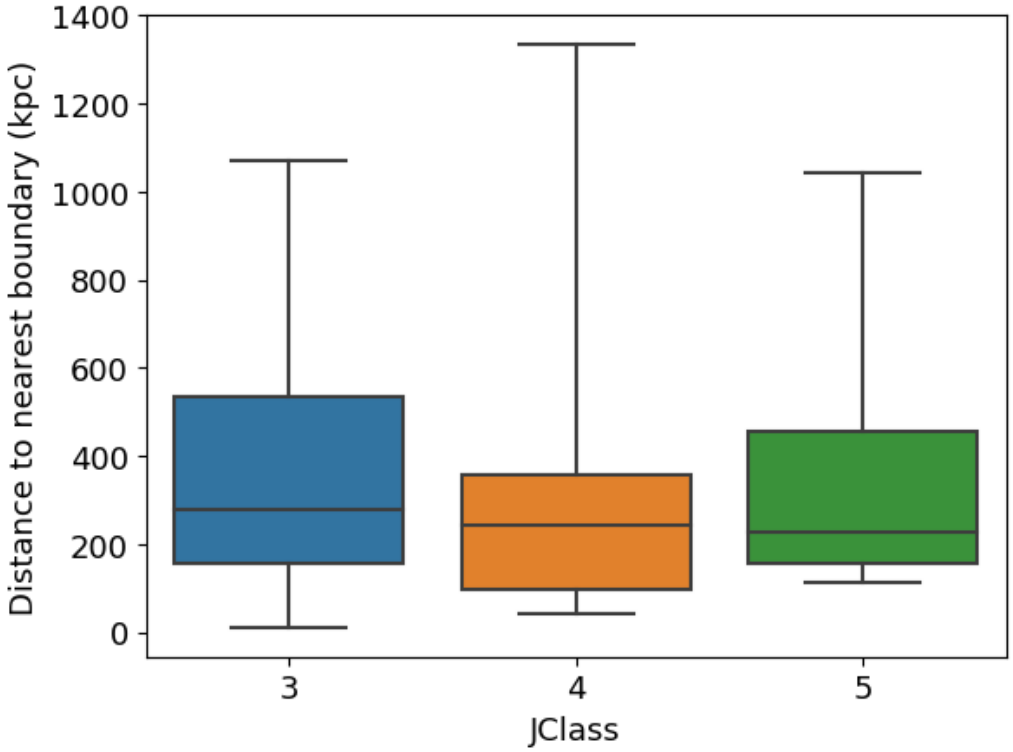

Figure 3.5: Box plot showing the distances between the jellyfish galaxies and the nearest ram pressure boundaries as a function of JClass. The median distances decrease with JClass: they are 279 kpc, 245 kpc and 226 kpc for JClass 3, 4 and 5 galaxies, but a Kolmogorov-Smirnov test applied to the pairs of distributions lead us to conclude that this is not a statistically significant result.

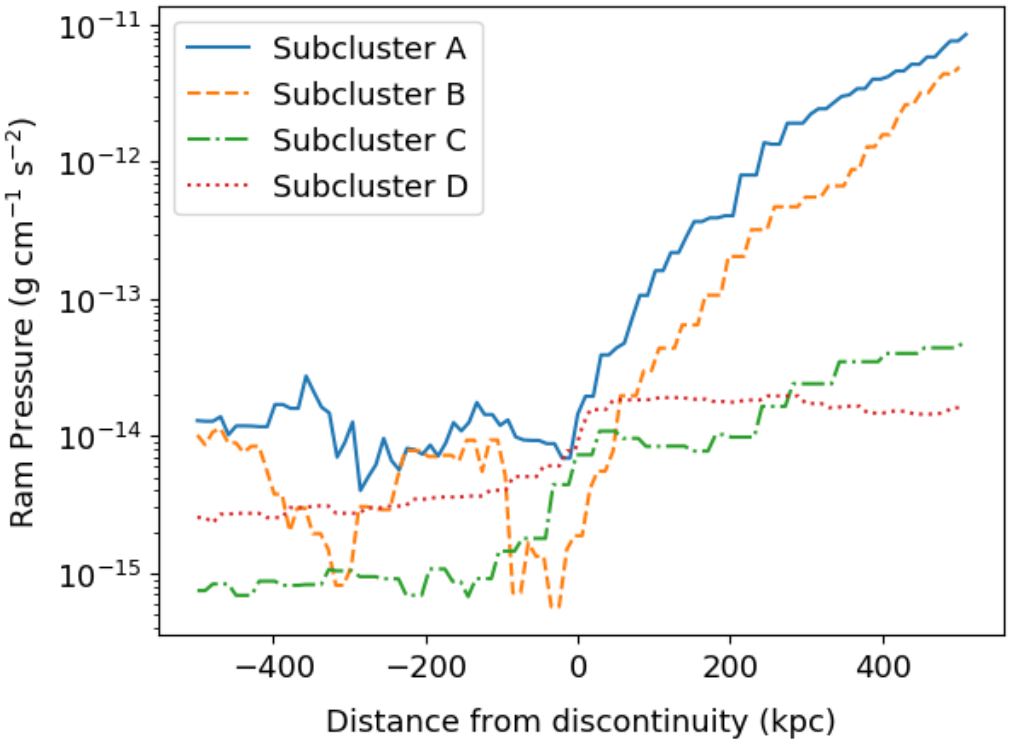

Figure 3.6: Ram pressure variation along the four black lines shown in Fig. 3.3, which are all perpendicular to their respective ram pressure boundaries. This illustrates the ram pressure increase which takes place in those boundaries, which can be of a factor of up to 1000.

pressure profiles feature some noise, but overall they remain somewhat constant. After the boundary is crossed, an increase of a factor of 10 – 1000 (depending on the cluster) takes place in the ram pressure within a few hundred kpc. The two largest subclusters (A and B) feature ram pressure increments larger than that of the remaining two (C and D), mainly due to their proximity to each other.

An initial hypothesis of the analysis so far was to calculate ram pressure in the reference frames of each subcluster, as an approximation for the velocities of its member galaxies. But the galaxies in reality feature peculiar velocities relative to their parent clusters. In Fig. 3.7 we show the same map as in Fig. 3.3 for subcluster C for reference frames with different velocities added in the same direction as that of the cluster average. We have chosen this subcluster for the sake of illustration because it is the one with the simplest ram pressure boundary. We find that the ram pressure boundary is only pronounced for velocities within roughly 100 km/s of

the average cluster velocity; beyond that, the boundary fades away and the ram pressure intensity becomes correlated with the gas density at each location. This adds up to our picture so far in the following manner: our scenario should involve galaxies moving at relatively low speed relative to their parent subcluster, perhaps close to their apocentric passage. Those galaxies are still moving at high speed in the reference frame of the system as a whole, allowing them to cross the ram pressure boundary within a short timescale, of $\sim$100 Myr, and then become jellyfishes after that.

One could also wonder whether our results would be different for off-plane ram pressure slices, i.e. planes parallel to the plane of the centres of the 4 subclusters, but at a certain height – so far we have limited ourselves to a mid-plane slice. We have verified that the locations of the ram pressure boundaries are very close to that in the mid-plane slice for heights of up to $\sim$500 kpc; the main difference is that the off-plane densities are lower, making the off-plane ram pressure increments also smaller.

3.5 Discussion and summary

We have employed in our analyses a tailored simulation of the A901/2 system. Even though it consists of four subclusters, we were able to reach a satisfactory model. Dedicated simulations of galaxy cluster mergers involving three or more objects have not often been attempted – an example is Brüggen et al. (2012). In a general situation, the large number of degrees of freedom in the initial conditions would render the exploration of the parameter space nearly impracticable. However, in the particular case of A901/2, this approach was feasible due to some simplifying assumptions that were adopted – apart from the usual setup of such idealised simulations (initially spherical objects, hydrostatic equilibrium, absence of small-scale substructures, etc). Regarding the dynamics of the system, our assumption was that the four objects are incoming for their first approach. This seems to be justifiable, given that they currently display no noticeable large-scale disturbances in their morphologies. Furthermore, we assumed for simplicity that the orbits are all on the plane of the sky. In our best model, the relative separations between the four subclusters are recovered. More importantly, the diffuse X-ray emissions are also quite well reproduced. This suggests that, in spite of the simplifying assumptions adopted, the gas properties in the simulation must be realistic within a good approximation.

From comparing the gas conditions in this model to the locations of the jellyfish galaxies in our adopted sample, we have inferred a possible

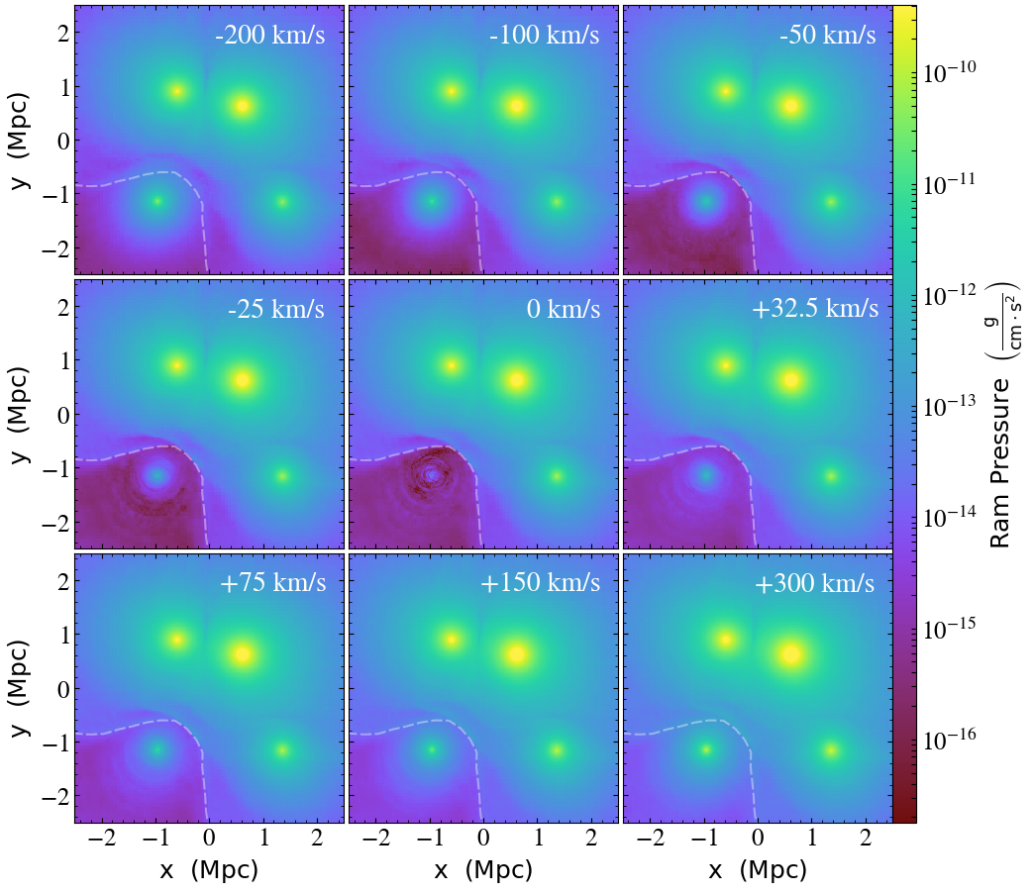

Figure 3.7: Effect of peculiar velocities relative to the parent galaxy cluster. Each panel is a midplane ram pressure slice in a reference frame defined by the average velocity of the A902 subcluster plus the indicated velocity, added in the same direction. A ram pressure increase in the boundary we report is pronounced for velocities within 100 km/s of the average cluster velocity.

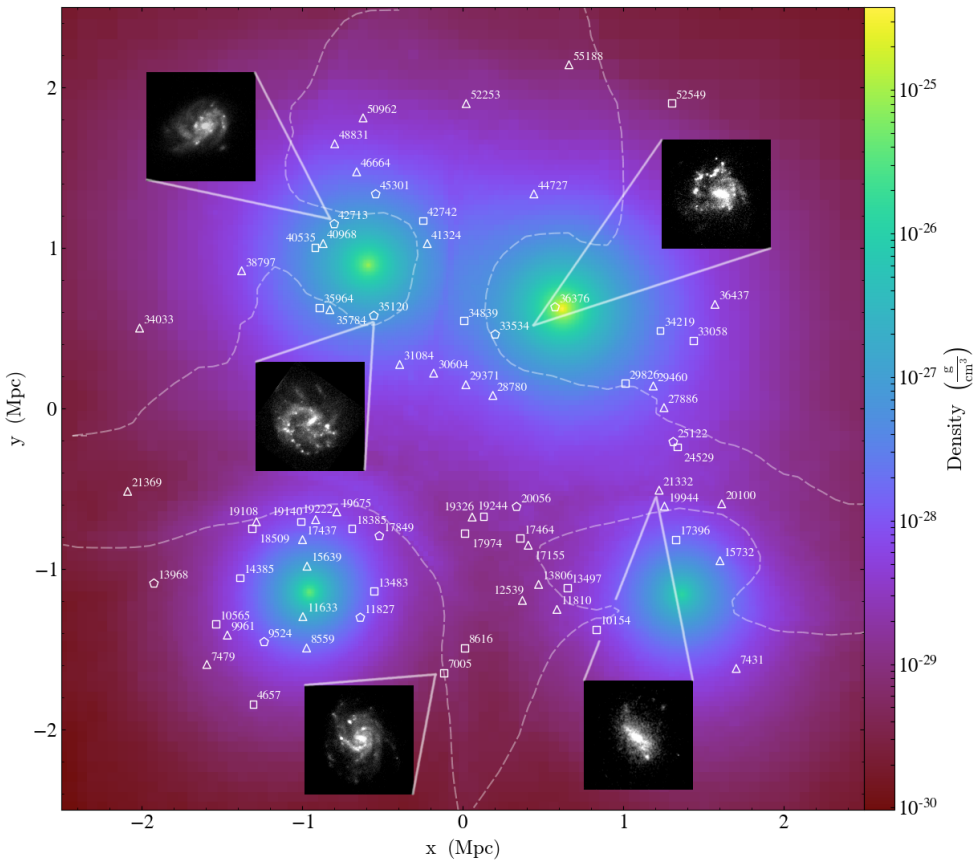

Figure 3.8: Identification of our sample of galaxies over a midplane density slice of our simulation. The dashed lines are the locations of the ram pressure boundaries shown in Fig. 3.3. Some HST thumbs in arbitrary scale are shown for the sake of illustration, and, also as in Fig. 3.3, triangles, squares and pentagons are used for JClass 3, 4 and 5 galaxies respectively.

mechanism for the triggering of jellyfish morphologies in this interaction environment, which is that the galaxies become jellyfishes when they cross a boundary within its parent subcluster where a significant increase in the ram pressure takes place, due to gas originally from the subcluster and gas from the remainder of the system meeting. A ram pressure increment of a factor of up to 1000 takes place on a scale of $\sim$100 kpc, while the galaxies are expected to be moving at speeds greater than 1000 km/s, implying a timescale of $\sim$100 Myr to cross the boundaries. We believe that this combination of a large increment in the ram pressure and a relatively short timescale to cross the boundaries makes it reasonable to conjecture that those boundaries could markedly affect the evolution of the gas content within the galaxies and turn them into jellyfish. One caveat which should be pointed out is that this mechanism does not necessarily apply to all of the jellyfishes in the system. Indeed, in each subcluster a subset of galaxies far away from the respective boundary exists, which could have had their jellyfish morphologies triggered by a mechanism unassociated to the merger altogether. Still, we find significant differences in the distributions of distance to nearest boundary between the jellyfish sample and both a random sample and the STAGES sample of member galaxies in the system. This suggests that it is reasonable to assume that a significant fraction of the jellyfishes are indeed being generated by the aforementioned mechanism.

Another caveat is that the exact locations of the ram pressure boundaries in the real system could be different from the ones we report due to a variety of factors – for instance, the exact positioning of clusters in the line of sight, deviations from our adopted initial density profiles and deviations from hydrostatic equilibrium in the clusters prior to the merger are all factors which could lead to different ram pressure distributions. Indeed, regarding deviations from hydrostatic equilibrium, cosmological simulations have pointed out that random bulk motions are relevant in the ram pressure stripping of galaxies in isolated galaxy clusters (Tonnesen & Bryan, 2008). One illustrative implication of this is the following: if, for some reason, the boundary for subcluster C shown in Fig. 3.3 is in reality located some 100 kpc lower than what we find, then it would be located right on top of a concentration of about 8 jellyfish galaxies, which are all behind the boundary in our model.

Although this entire work is devoted to the particular case of the A901/2 system, we expect the ram pressure boundaries we report inside each subcluster to be present in all galaxy cluster mergers which are still in the early stages of the collision, before their centres have crossed each other. In this way, a similar analysis to the one presented here could be carried

out for other observed galaxy clusters, in order to probe the universality of the mechanism. Perhaps the biggest difficulty in this is finding jellyfish galaxies in clusters in the first place – they are rare and their identification is very dependent on visual inspection. Previous observational work on jellyfish galaxies, such as McPartland et al. (2016) and Owers et al. (2012), have hinted that such galaxies could actually be preferentially found in galaxy cluster merger systems; our findings are consistent with interacting galaxy clusters being a favourable environment for searching for such galaxies.

The summary of this paper is as follows. We have developed a hydrodynamic model for the A901/2 system using a multi-cluster merger simulation, consistent with their positions relative to each other, their masses and their X-ray emissions. This model was used to correlate the gas conditions in the system with the locations of the jellyfish galaxy candidates in it identified by Roman-Oliveira et al. (2019). We have found that at each subcluster, a boundary exists where gas moving along the cluster and gas from the remainder of the system meet; in those boundaries, an increment of a factor of 10 – 1000 in the ram pressure takes place within a few hundred kpc, due to a large increment in the diffuse gas velocity. More importantly, we have found that jellyfish galaxies in the system seem to be preferentially located near those boundaries, which could mean that the crossing of those boundaries is the mechanism behind the formation of jellyfishes at those locations. We propose that this mechanism could be common in galaxy cluster mergers which are at the beginning stages of their encounter, possibly making those environments particularly favourable for searching for jellyfish galaxies. This is the first theoretical treatment of ram pressure stripping in the environment of galaxy cluster mergers which has been presented in the literature.

Acknowledgements

RR thanks the São Paulo Research Foundation, FAPESP, for the financial support (grant 15/13141-7). This work has made use of the computing facilities of the Laboratory of Astroinformatics (IAG/USP, NAT/Unicsul), whose purchase was made possible by the Brazilian agency FAPESP (grant 2009/54006-4) and the INCT-A. Simulations were carried out in part at the Centro de Computação Científica e Tecnológica (UTFPR). This study was financed in part by the *Coordenação de Aperfeiçoamento de Pessoal de Nível Superior - Brasil* (CAPES) - Finance Code 001. ACS and FRO acknowledge funding from the Brazilian agencies *Conselho Nacional de Desenvolvi-*

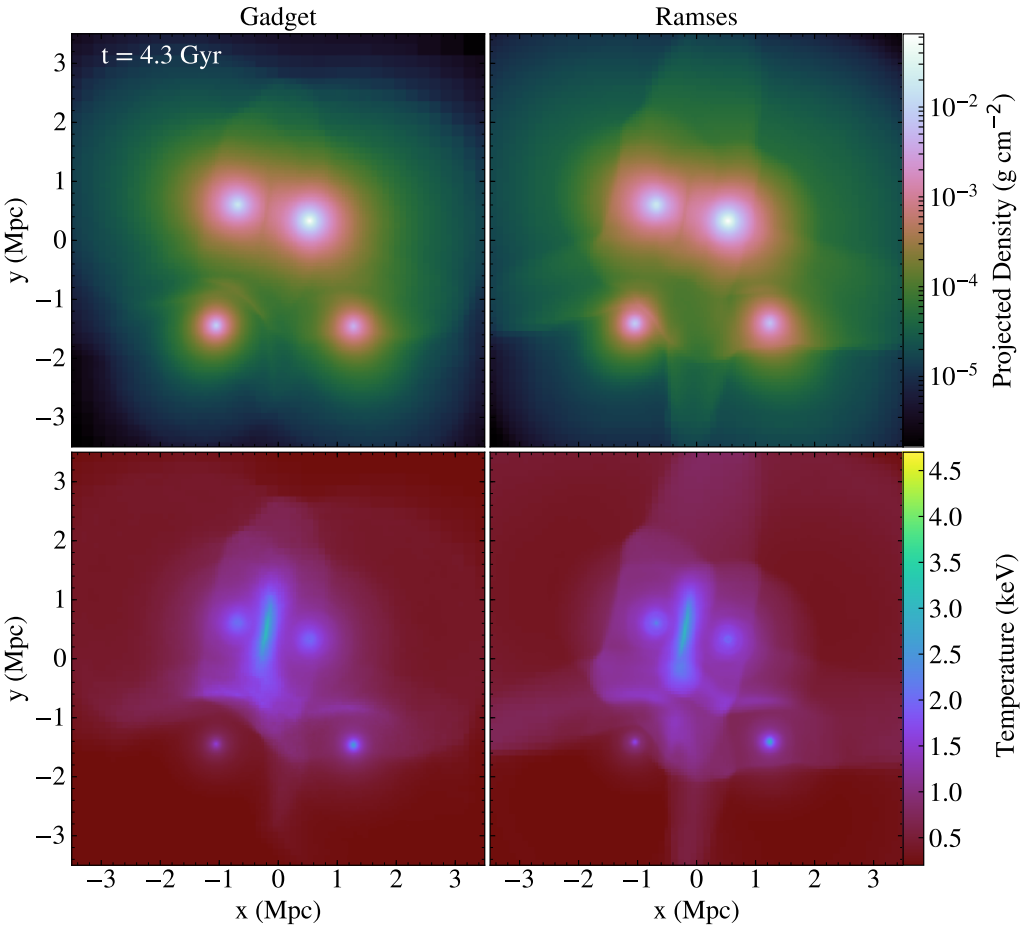

Figure 3.9: Comparison between GADGET-2 (left) and RAMSES (right) results, showing gas density maps (upper panels) and temperature maps (lower panels), for $t = 4.3\,\mathrm{Gyr}$.

mento Científico e Tecnológico (CNPq) and the Rio Grande do Sul Research Foundation (FAPERGS) through grants PIBIC-CNPq, CNPq-403580/2016-1, CNPq-310845/2015-7, PqG/FAPERGS-17/2551-0001, PROBIC/FAPERGS and L'Oréal UNESCO ABC *Para Mulheres na Ciência*. GBLN thank financial support from CNPq and FAPESP (2018/17543-0).

3.6 Code comparison

To compare the hydrodynamic evolution results obtained from the simulation using the code GADGET-2, new simulations were performed with the RAMSES code. Both methods attempt to solve the fluid equations, but in

very different ways: GADGET-2 is a cosmological simulation code based on smoothed particle hydrodynamics (SPH) technique that computes gravitational forces with a hierarchical tree algorithm (Springel, 2005), whereas RAMSES is based on an Adaptive Mesh Refinement (AMR) technique, with a tree based data structure allowing recursive grid refinements on a cell-by-cell basis (Teyssier, 2002). Both runs used the same initial conditions, and with comparable resolution (the minimum and maximum refinement levels defined on RAMSES were 6 and 12 respectively). A mass-based refinement criterion was employed on the RAMSES run, in order to ensure that the discretisation was equivalent to that of a particle-based code like GADGET-2.

The analysis and of the output was done using the YT analysis code (Turk et al., 2011), so it was possible to create Fig. 3.9, showing the projected density and temperature maps for the instant of time $t = 4.3\,\mathrm{Gyr}$. When comparing the two codes, it can be noted that the final coordinates of the objects are in good agreement, that is, the global morphology is quite similar (with the possible exception of small-scale details). Similarly, the ranges of temperature are comparable, even in regions of intense variations. This overall agreement is consistent with other studies on the comparison between AMR and SPH simulations as shown in O'Shea et al. (2005), Hubber et al. (2013) and Kim et al. (2014).

Chapter 4

Morphometry as a probe of the evolution of jellyfish galaxies: evidence of broadening in the surface brightness profiles of A901/A902 ram pressure stripping candidates

Submitted to Monthly Notices of the Royal Astronomical Society*

We explore the morphometric properties of a group of 73 ram pressure stripping candidates in the A901/A902 multi-cluster system, at z∼0.165, to characterise the morphologies and structural evolution of jellyfish galaxies. By employing a quantitative measurement of morphometric indicators with the algorithm MORFOMETRYKA *on Hubble Space Telescope (F606W) images of the galaxies, we present a novel morphology-based method for determining trail vectors. We study the surface brightness profiles and curvature of the candidates and compare* MORFOMETRYKA *and* ELLIPSE *on retrieving information of the irregular structures present in the galaxies. Our morphometric analysis shows that the*

*__Roman-Oliveira, F. V.__; Chies-Santos, A. L.; Ferrari, F.; Lucatelli, G. and Rodríguez del Pino, B.

ram pressure stripping candidates have peculiar concave regions in their surface brightness profiles. Therefore, these profiles are less concentrated (lower Sérsic indices) than other star forming galaxies that do not show morphological features of ram pressure stripping.

4.1 Introduction

Previous research shows that dense environments influence the evolution of galaxies (Butcher & Oemler, 1984, Dressler, 1980). Passive elliptical galaxies are more frequently found in the centre of galaxy clusters and star forming disc galaxies are more common as satellite galaxies (Bamford et al., 2009). This is linked to transformations in both morphology and galaxy properties, such as colours and star formation rates. What is yet not clear is the impact of the several external galaxy evolution drivers concurrently at play in such environments, e.g. stripping through tidal (Barnes, 1992) and ram pressure interactions (Gunn & Gott, 1972), galaxy harassment (Moore et al., 1996), mergers (Barnes, 1992, Bekki, 1999), starvation or strangulation (Larson et al., 1980). In this work, we explore the relationship between the ram pressure stripping effect in galaxies and their evolution in galaxy clusters.

Ram pressure stripping is an efficient mechanism in removing gas from orbiting galaxies in clusters. It occurs when there is a hydrodynamic friction between the interstellar medium (ISM) in a galaxy and the intracluster medium (ICM) as the galaxy falls into a galaxy cluster. Jellyfish galaxies are the most representative example of galaxies undergoing ram pressure stripping, these are rare and extreme cases of galaxies with extensive tails that can be identified throughout many wavelengths (Poggianti et al., 2019). Many studies over the past decade provide important information on the origins, distribution and physical properties of ram pressure stripped galaxies (Ebeling et al., 2014, Poggianti et al., 2016, Smith et al., 2010). Recently, there have been new statistically significant studies on the properties of large samples of jellyfish galaxies such as the GaSP collaboration (Poggianti et al., 2017b), the McPartland et al. (2016) sample in massive clusters and the rich population of ram pressure stripping candidates found in the Abell 901/2 system as part of the OMEGA survey (Roman-Oliveira et al., 2019) that are the targets of this study.

The efficiency of the stripping is linearly dependent on the density of the ICM and quadratically on the relative velocity between the galaxy and the environment (Gunn & Gott, 1972). There are two triggering mecha-

nisms, that can act simultaneously, in the stripping of an infalling galaxy: a significant increase in the ICM density (e.g. approaching the centre of a cluster) and/or a high relative velocity between the galaxy and the surrounding medium (e.g. the region between merging clusters). The latter has been thoroughly investigated for the case of Abell 901/2 system in Ruggiero et al. (2019) where they find regions in the system where ram pressure stripping could be enhanced due to a possible merger between the substructures, explaining the spatial distribution and the large number of candidates of the observed sample of ram pressure stripping candidates. This would confirm previous tentative results that suggest that jellyfish galaxies can be more commonly found in galaxy cluster interactions (McPartland et al., 2016, Owers et al., 2012).

Recent research also finds that although the star formation quenching and the morphological transformation both happen to galaxies as part of their evolution, there is a time delay between these processes (Cortese et al., 2019, Kelkar et al., 2019). Investigating morphological characteristics of galaxies that are currently going through a major change both in their star formation rates and overall structure can provide insight on whether both changes are linked and how they take place.

So far, very little attention has been paid to the morphological analysis of galaxies with irregular properties, such as jellyfish galaxies. One study by McPartland et al. (2016) analyses a set of jellyfish galaxies from a morphometric point of view with the main goal of finding a larger sample of ram pressure stripping candidates. Nonetheless, this analysis can be extremely useful to assess the physical changes that these galaxies are undergoing.

In this paper, we set out to investigate the morphological features of candidate galaxies undergoing ram pressure stripping in a sample of 73 ram pressure stripping candidates in A901/A902 at z$\sim$0.165. We direct the reader to find more information on the sample in Roman-Oliveira et al. (2019), where we describe the selection and its main properties, and in Ruggiero et al. (2019) that further explores the origin of the possible ram pressure stripping events. Our goal is to understand how the ram pressure stripping mechanism is modifying their structure and its contribution to the scenario of quenching and morphological evolution in dense environments. We perform the morphometric analysis using the MORFOMETRYKA algorithm (Ferrari et al., 2015) to measure trail vectors, surface brightness profiles and other morphometric quantities.

This work is organised as follows: in Section 4.2 we detail the data, sample and methods used; in Section 4.3 we show the results of the morphometric analysis for trail vectors, surface brightness profiles and cur-

vature; and in Section 4.4 we summarise our conclusions. We adopt a $H_0 = 70 \mathrm{kms}^{-1}\mathrm{Mpc}^{-1}, \Omega_\Delta = 0.7$ and $\Omega_M = 0.3$ cosmology through this study.

4.2 Data and Methods

4.2.1 Abell 901/2

Abell 901/2 is a multi-cluster system at z$\sim$0.165 composed of four main sub-cluster structures and filaments. It has been intensely studied by the STAGES collaboration (Gray et al., 2009) and, more recently, by the OMEGA survey (Chies-Santos et al., 2015, Rodríguez del Pino et al., 2017, Roman-Oliveira et al., 2019, Weinzirl et al., 2017, Wolf et al., 2018) in many different wavelengths. It is a particularly interesting system because of its large galaxy population and diverse environments, making it suitable for detailed studies of galaxy evolution through a vast range of stellar masses and environments.

Sample

In this study we make use of Hubble Space Telescope (HST) observations in the ACS/F606W passband of the Abell 901/2 multi-cluster system where a sample of 73 ram pressure stripping candidates has been previously selected through visual inspection as part of the OMEGA survey. Along with the HST imaging, we use a model PSF (point spread function) obtained with Tiny Tim (Krist, 1993).

Although the jellyfish galaxy tails are not as visible in optical bands, the stellar disc shows a disturbed morphology that can be evidence of more extreme disturbances in other wavelengths (Poggianti et al., 2019). This can be used to select samples of ram pressure stripping candidates, like the ones used in this paper. Searching for ram pressure stripping features on optical images is an efficient and economic method of finding ram pressure stripping candidates that has been employed on many works through visual inspection (Ebeling et al., 2014, Owers et al., 2012, Poggianti et al., 2016, Rawle et al., 2014). The disturbed morphologies of these candidates can be due to ram pressure stripping, however samples selected this way also have some degree of contamination by minor mergers or tidal interactions. Therefore, only follow-up studies in other passbands could rightly confirm the origin of the stellar disc disturbance.

The F606W passband has an effective wavelength midpoint (λ_{eff}) around 5777Å; at $z \sim 0.165$ we are thus covering the rest-frame R-band around 6730Å. This interval covers intermediate/old stellar populations that contribute to the continuum emission in this red part of the spectrum and to some extent young stellar populations by encompassing the Hα emission. In this range of wavelengths, the presence of dust can significantly obscure star formation in nearly edge-on galaxies (Wolf et al., 2018), which composes a minority of the sample. Besides, the morphometric measurements of the stellar disc should be mostly unaffected.

The sample was selected in Roman-Oliveira et al. (2019) and the selection method was conducted mirroring the works of Poggianti et al. (2016) and Ebeling et al. (2014). This is the largest sample up to date for a single system containing galaxies with morphological signatures linked to ram pressure stripping effects, such as tails and bright knots of star formation. The galaxies are selected in different categories according to the prominence of the ram pressure stripping features in their morphologies. The strongest candidates are grouped in JClass 5, the weakest candidates in this sample are grouped in JClass 3 and the intermediate candidates are grouped in JClass 4. For further details on the the selection and eligibility criteria and basic physical properties of the sample refer to Roman-Oliveira et al. (2019).

4.2.2 Morphometric analysis

Several techniques have been developed to quantify the physical structures of galaxies in measurable ways. One example is the CASGM non-parametric system that measures concentration, asymmetry, smoothness, Gini coefficient and M20 parameters (Abraham et al., 1994, Conselice et al., 2000, Lotz et al., 2004).

Our work is based on the MORFOMETRYKA algorithm that establishes a new method dedicated to morphology classification from a physical standpoint. It includes the parameters cited above as well as entropy (H) and spirality (σ_ψ) as new parameters (Ferrari et al., 2015). The most recent version of MORFOMETRYKA also provides the curvature of the brightness profile with KURVATURE (Lucatelli & Ferrari, 2019), which is a powerful tool for probing the presence of multiple components in galaxies. An example of the performance of MORFOMETRYKA for one of our galaxies displaying signatures of ongoing ram pressure stripping can be seen in Figure 4.1.

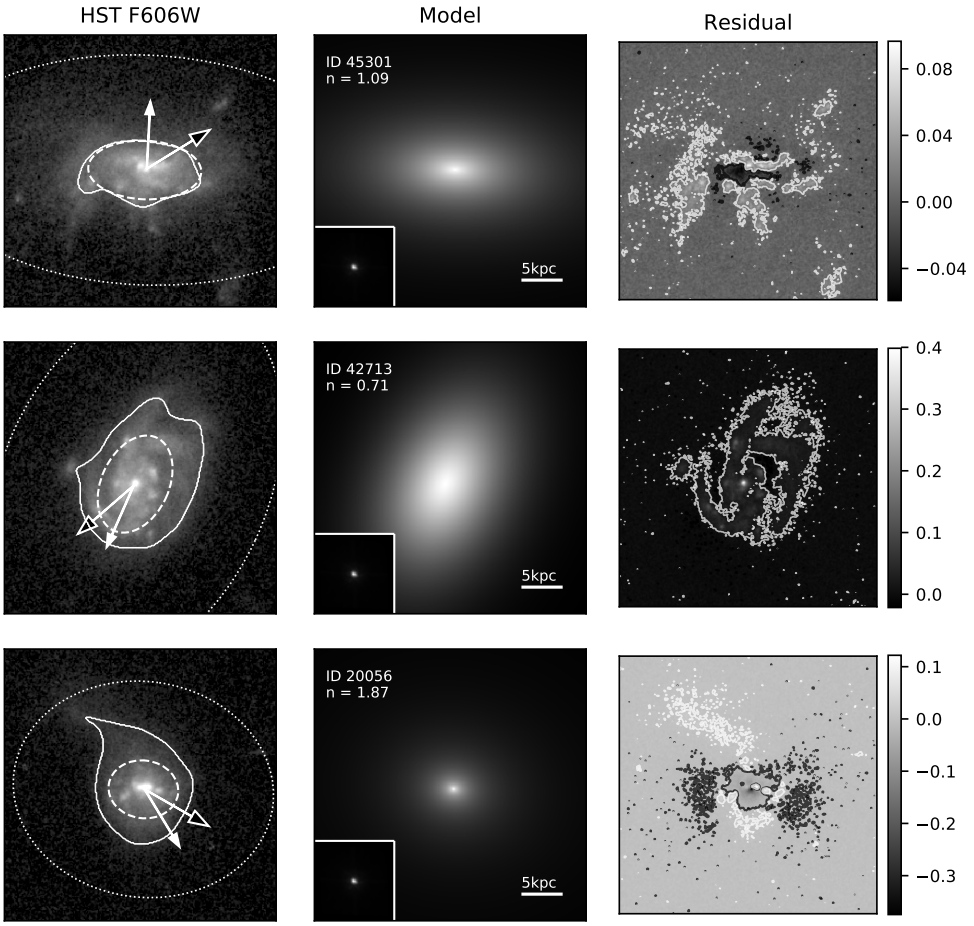

Figure 4.1: MORFOMETRYKA analysis of three galaxies with the strongest ram pressure stripping features in A901/A902. Left column: original HST image. The outer dotted ellipse represents twice the Petrosian region, the dashed inner ellipse represents twice the effective radius of the Sérsic model. The solid line is the segmented region. The black headed arrow shows the morphometric trail vector and the white headed arrow shows the visually assigned trail vector. Middle column: two-dimensional Sérsic model. The bottom-left square shows the HST/F606W PSF modelled with Tiny Tim. The galaxy ID and Sérsic index are noted in the top-left corner. Right column: Residual image with its respective colourbar. The contours show regions that have values 3 σ above the sky background, for negative value the contours are represented in black and for positive values the contours are represented in white.

4.3 Results

4.3.1 Morphometric Trail Vectors

Definition and use as an asymmetry measurement

Within MORFOMETRYKA, we implement an automatic way to define the direction of motion. As jellyfish galaxies fall into the galaxy cluster they leave a trail of material behind. This trail hints at the projected motion around the system. This method has been adopted so far mainly through visual inspection in a number of works (Ebeling et al., 2014, Roman-Oliveira et al., 2019, Smith et al., 2010), but most recently Yun et al. (2019) measured trail vectors for 800 ram pressure stripping candidates in the Illustris TNG by defining the direction of a vector between the density-weighted mean to the galaxy centre positions. Here, we perform something similar to Yun et al. (2019) from the standpoint of observations in which we measure a trail vector ($\mathbf{x}$) from the position of the centre of light to the peak of light. The peak of light is correlated to the centre of the galaxy and should remain the same before and after undergoing ram pressure stripping. The centre of light is a density-weighted mean of the light distribution that is highly affected by perturbations in the morphology. We measure the morphometric trail vector with MORFOMETRYKA following: $\mathbf{x} = (x_0, y_0)_{\rm peak} - (x_0, y_0)_{\rm CoL}$. For more details on how these components are measured we refer the reader to Ferrari et al. (2015).

Not only this method gives a quantifiable measurement of the orientation of the projected motion of the galaxies, but it is also more sensitive to slight perturbations in the structure that visual inspection cannot account for. The offset between the two points can also be considered a proxy for asymmetry, since the peak of light and centre of light coincide in an axisymmetric structure with a surface brightness profile that decays with increasing radius, such as a pure disc component. In Figure 4.2 we show a comparison between the trail vector length (TVL) to two morphometric asymmetry parameters, A1 and A2. We test this both for the trail vectors measured for the ram pressure stripping candidates and for a control sample of star forming galaxies that do not show morphological features of ram pressure stripping as for our selection. The galaxies that form this control sample were selected as star forming galaxies based on their Hα emission as detailed in Rodríguez del Pino et al. (2017). A1 and A2 are determined by accounting the residual of an image with its rotated counterpart the details for how they are calculated can be found in Ferrari et al. (2015). The main difference between A1 and A2 is that A1 is sensitive

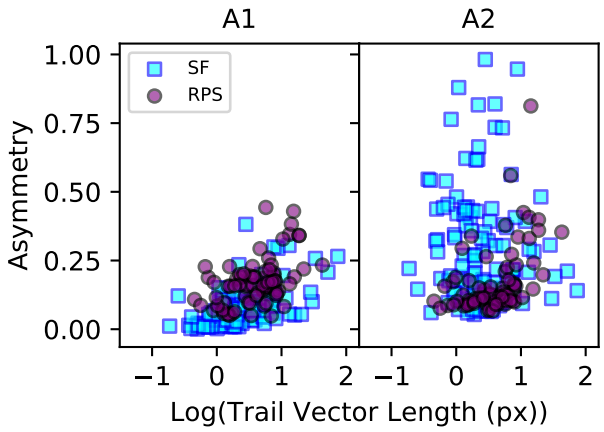

Figure 4.2: Asymmetry versus trail vector length in ram pressure stripping candidates and star forming galaxies in A901/A902. In the left panel we show the asymmetry parameter A1, defined in Abraham et al. (1996), and in the right panel we show the parameter A2, defined in Ferrari et al. (2015) that is less sensitive to the sky.

to the sky background while A2 is unaffected by it. We measure a Pearson correlation for the TVL with A1 and A2. In Table 4.1 we show the resulting Pearson coefficients and respective p-values. We find that for the ram pressure stripping candidates they are related with great certainty (p-values of 2e-05 and 2e-06). However, for the other star forming galaxies we find a correlation of the TVL with A1, but no correlation between TVL and A2. Many star forming galaxies have low A1 values and high A2 values. This can be due to the fact that although A2 is unaffected by the sky background, it tends to be more sensitive than A1 to small perturbations inside a galaxy, for example spiral arms or a clumpy disk. Therefore, galaxies that do not have a very asymmetric morphology, but have this perturbations will not follow a correlation with TVL. Another important scenario is that some galaxies may have large A1 or A2 values but not be unilaterally asymmetric, in which case the TVL will be relatively small for the asymmetry parameters measured, breaking up the correlation between each other. The correlation between TVL and both the asymmetry parameters probed suggests that the morphometric trail vectors are a good parameter for measuring unilateral asymmetries. This method vectors can be applied to large datasets and aid the analysis and identification of new ram pressure stripping candidates, which is a large improvement over visually assigned trail vectors.

	Pearson coefficient	p-value
RPS, TVL and A1	0.478	2e-05
RPS, TVL and A2	0.505	5e-06
SF, TVL and A1	0.564	3e-11
SF, TVL and A2	-0.05	0.6

Table 4.1: Statistics of the Pearson correlation between trail vector length (TVL) and asymmetry parameters A1 and A2 for ram pressures stripping candidates (RPS) and star forming galaxies (SF).

Comparison to the visually assigned trail vectors

In Figure 4.3 we compare the visually assigned trail vectors from Roman-Oliveira et al. (2019) with the morphometric trail vectors presented in this work by calculating the angular difference between both vectors. We are considering 45 degrees as the threshold to which we consider as a good agreement between the vectors since it would still point towards the same general direction and it is comparable to the disagreement between the vectors suggested by different inspectors during the visual assignment. Similarly, we consider an angular difference of 135 degrees or more to be a good agreement in direction although it is suggesting an opposite pointing. We find that about half of the galaxies can be considered in good agreement by these standards. However, if we restrict this comparison to only the galaxies that have a TVL of at least 5 pixels, which at z$\sim$0.165 is around $0.6kpc$, about three quarters of the galaxies considered are in good agreement. This suggests that the direction of the morphometric trail vectors are more reliable for higher TVLs and should be considered carefully for galaxies with less prominent morphological disturbances. In Figure 4.4 we show the spatial distribution of the ram pressure stripping candidates with the new morphometric trail vectors. Similarly to what was found with the visually assigned trail vectors, we see no correlation between the direction of the projected motion of the candidates in the system.

Besides, there is an intrinsic bias on measuring the coordinates of the peak of light, in the case of galaxies that do not have a definitive centre or when the peak is found in a bright star forming region outside the centre. As for measuring the centre of light, the coordinates are most sensitive to the shape selected to represent the morphology of the galaxy. In the case of MORFOMETRYKA we are calculating the centre of light inside the segmented region – this region is shown in Figure 4.1. The MORFOMETRYKA segmentation selects a region that has a significant intensity above the background sky – the region is selected through applying histogram

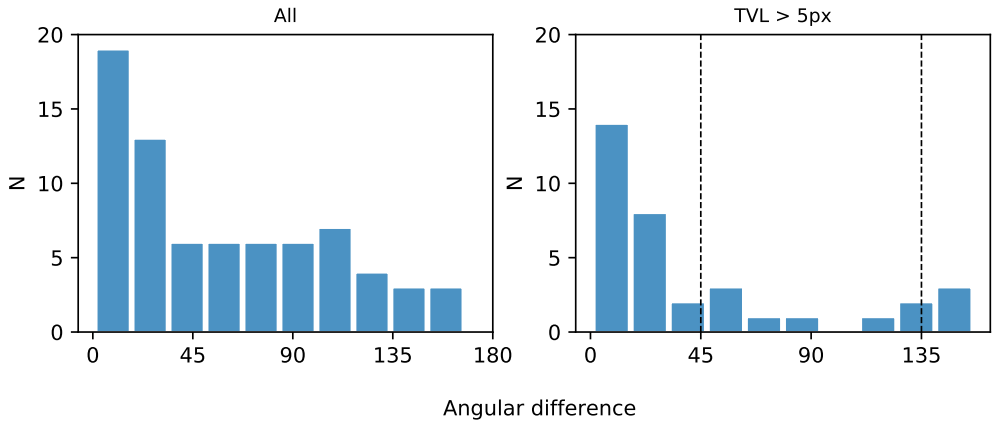

Figure 4.3: Histogram of the angular difference between morphometric and visually assigned trail vectors. Left panel: for all the ram pressure stripping candidates. Right panel: for ram pressure stripping candidates with a trail vector length of at least 5px (∼0.6kpc at z∼0.165). The vertical dashed lines mark angular differences of 45 and 135 degrees.

thresholding on a filtered image to avoid sharp edges (see Ferrari et al. (2015) for more details). This segmentation is sensitive to the size of the image analysed, which is why it is important to have an image stamp large enough to cover the structures of interest, but small enough that it will not introduce contamination from nearby sources.

Lastly, besides the scenarios we commented, in some cases, the disagreement between the morphometric and the visually assigned trail vectors can be due to the morphometry being more sensitive to disturbances that are too small for the inspectors to correctly assign a vector, in which case the morphometric trail vector is superior to the visually assigned one. We emphasise that this method has its limitations regarding projection effects and it works best for edge-on/inclined galaxies. In the case of face-on galaxies it may still be able to provide an accurate orientation of the trail vector but it might underestimate the TVL. This discrepancy can be better seen in Yun et al. (2019), where trail vectors were estimated in a similar way for jellyfish galaxies in the Illustris TNG simulations. Some galaxies show clear extended jellyfish tails when seen edge-on, but do not look as disturbed when face-on. Additionally, the reader can visualise all the results in the online material we provide: an ATLAS with all the galaxy stamps, segmented areas, morphometric and visually assigned trail vectors.

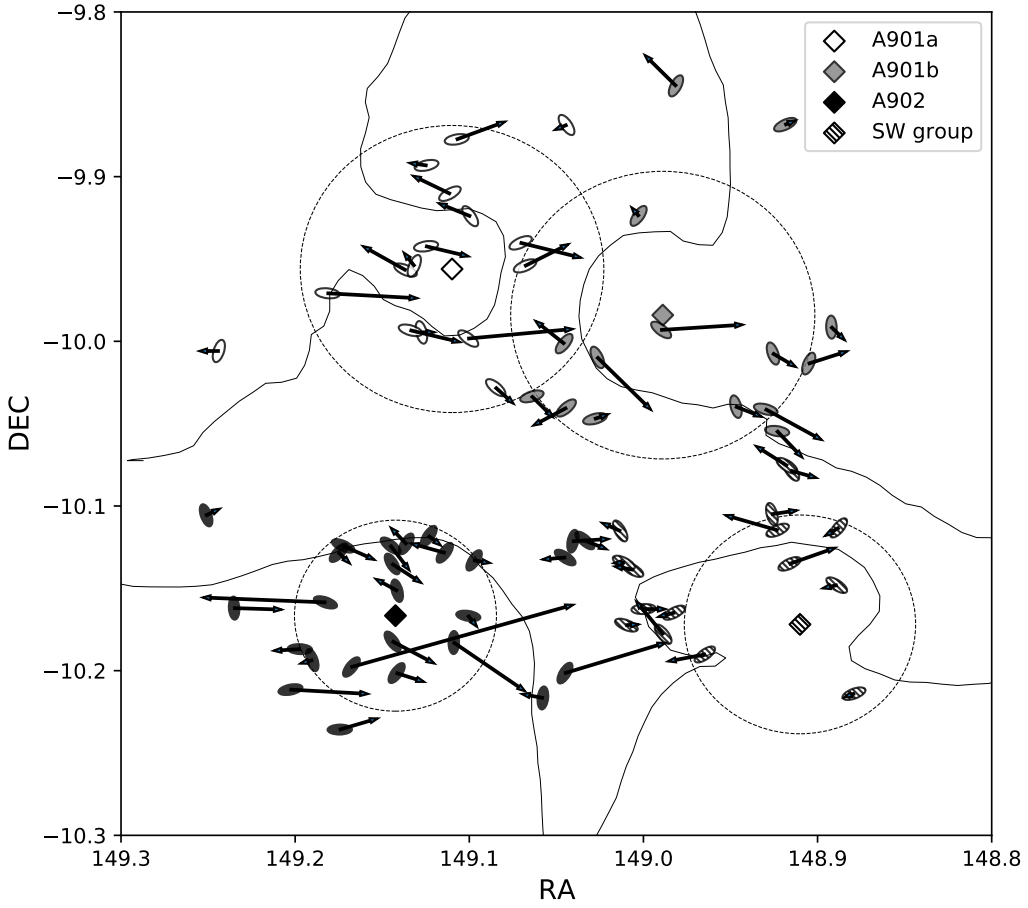

Figure 4.4: The spatial distribution of the ram pressure stripping candidates and their morphometric trail vectors tracing their projected motion on the sky. The centres of each subcluster is marked with a diamond symbol according to the legend. The ram pressure stripping candidates are represented with ellipses with the measured position angles and their colours match the subcentre that they are closest to in projected distance. The arrows represent the measured trail vectors and the length is proportional to the distance between the centre and the peak of the light distribution. The continuous lines show the expected region where ram pressure stripping would be triggered in response to the merging clusters as detailed in Ruggiero et al. (2019). The dotted circles represent the virial radius (R_{200}) of each subcluster used in Ruggiero et al. (2019).

4.3.2 Surface Brightness Profiles

MORFOMETRYKA and Sérsic indices distribution

With MORFOMETRYKA, we model the surface brightness profiles of the ram pressure stripping candidates with a single two-dimensional Sérsic Law (Sersic, 1968) to investigate the light distribution properties. It is important to note that this does not model the distorted tails, but it does give an overall assessment of the light concentration in the galaxies. In Figure 4.1, we showcase the MORFOMETRYKA models and residuals for three example galaxies with Sérsic indices that represent three groups of surface brightness: disc-like (n$\sim$1), more concentrated than a disc (n$>$1) and less concentrated than a disc (n$<$1). The galaxies chosen (IDs 45301, 42713 and 20056) were classified in Roman-Oliveira et al. (2019) as JClass 5, which means they have the strongest features of ram pressure stripping among the sample.

We first analyse the distribution of Sérsic indices of the modelled profiles of the ram pressure stripping candidates and compare it to the other star forming galaxies in the system. In this, we find that the Sérsic indices distribution for the ram pressure stripping is centred around n$\sim$1, with a median $\tilde{n} = 1.06$. We account also for the dependency of stellar mass with Sérsic index by considering two separate bins of mass below and above $M_* = 10^{9.5}\ M_\odot$. We chose this threshold as it lies in between the median mass of both the candidates and the control sample. In Table 4.2 we show the parameters measured for the distribution of Sérsic indices for both samples and bins. Both distributions are similar, the main difference seems to be that the ram pressure stripping candidates are more tightly distributed around the mean and that the division in stellar mass bins does not affect the distribution.

ELLIPSE and surface brightness curvature profiles

We find from the Sérsic distribution that the overall surface brightness profile of the ram pressure stripping candidates can be approximated to discs. However, MORFOMETRYKA cannot fit most of the details that stem from the irregular structure. For further investigating the light distribution of the sample, we use IRAF/ELLIPSE task (Jedrzejewski, 1987). ELLIPSE achieves a more accurate measurement of the brightness profile by fitting several ellipses of increasing semi-major axes and different position angles, being more sensitive to irregular structures of galaxies. In Figure 4.5 we show the results from ELLIPSE for the same galaxies we analyse in Figure 4.1. We maintain the same contrast used in the previous figure

	N	$\tilde{n}$	$\overline{n}$	σ_n
RPS	73	1.06	1.18	0.61
$RPS_{low\ mass}$	22	1.03	1.04	0.35
$RPS_{high\ mass}$	51	1.08	1.24	0.69
SF	112	1.03	1.48	2.14
$SF_{low\ mass}$	89	0.98	1.51	2.37
$SF_{high\ mass}$	23	1.12	1.34	0.73

Table 4.2: Distribution of Sérsic indices for the ram pressure stripping candidates (RPS) and star forming galaxies (SF) in A901/A902. We show the values for the full samples and for bins of stellar mass above and below $M_* = 10^{9.5}\ M_\odot$. The columns show the number of galaxies (N), median ($\tilde{n}$), mean ($\overline{n}$) and stardard deviation (σ_n) of the Sérsic indices.

to allow the reader to visually compare the results obtained from the two algorithms.

We assess the quality of both models by evaluating the residuals from the contours shown in the right panels of Figure 4.1 and Figure 4.5. The contours highlight the regions 3 standard deviations below (black contours) or above (white contours) the sky background. Therefore, the black contours show regions that are being overfitted by the model and the white contours show clumpy star forming regions, arms or irregular structures not represented in the model. We calculate ratios of residual to the original image and we found that neither codes tend to overfit the galaxies, as the ratios of the black contoured regions to the original are around 0.03 for all galaxies – except for MORFOMETRYKA fitting the galaxy 20056 with a ratio of 0.2. As for white contours, ELLIPSE has a much better performance with ratios or residual to original of 0.06 for all three galaxies, effectively covering most of the emission of the galaxy even for the irregular components. In that aspect, MORFOMETRYKA ranges in ratios of 0.08 (ID 20056), 0.14 (ID 45301) to 0.35 (ID 42713).

In Figure 4.6 we show the surface brightness profiles measured with MORFOMETRYKA and ELLIPSE for the three galaxies as well as the best fit Sérsic models. In all the three cases we see a large scale structure that has a concave shape in the surface brightness profile. However, even though ELLIPSE retrieves the light distribution of the galaxy, a single Sérsic fit does not represent well all the features we see in the surface brightness profile, this is especially true for the case of ID 20056 that has extended emission in comparison to its effective radius. These galaxies seem to have multiple structural components and a single Sérsic fit can only fit one of these

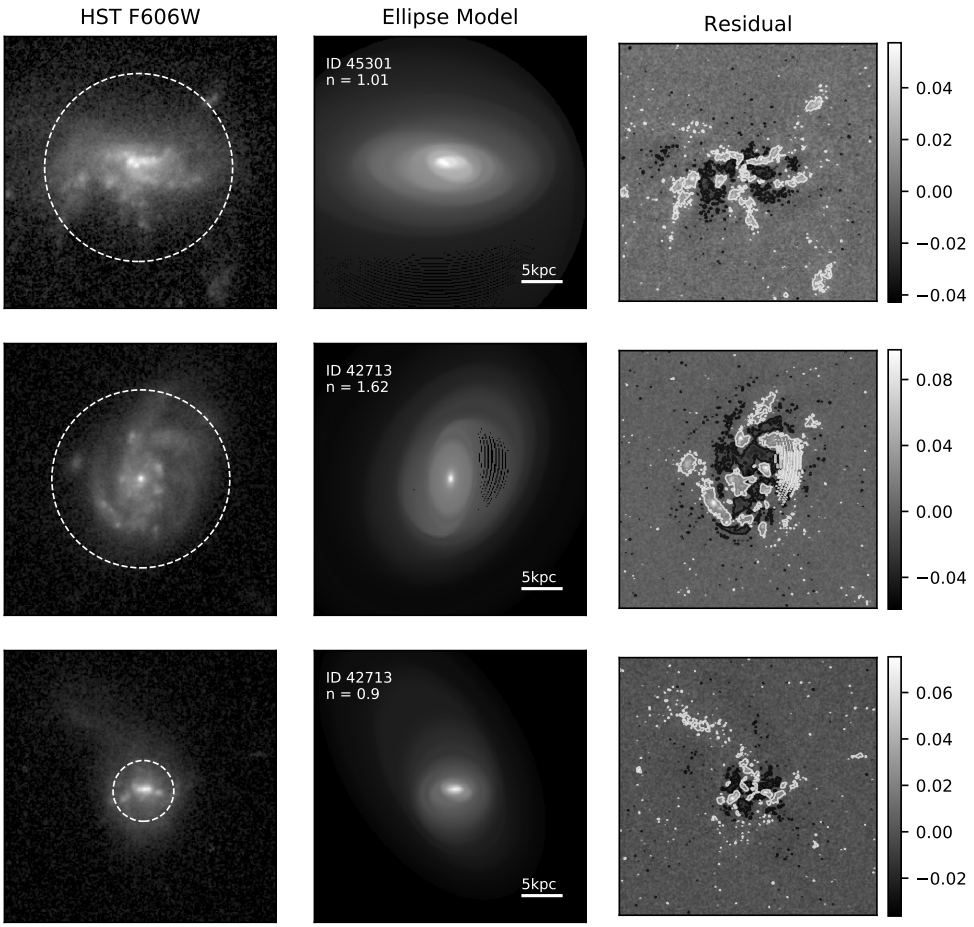

Figure 4.5: ELLIPSE analysis of the same three galaxies from Figure 4.1. Left column: original HST image. The dashed circle represents twice the effective radius of the model. Middle column: ELLIPSE model. The ID and Sérsic index fitted are noted in the top-left corner. Right column: residual image and its respective colourbar. The contours and contrast are the same as those in Figure 4.1.

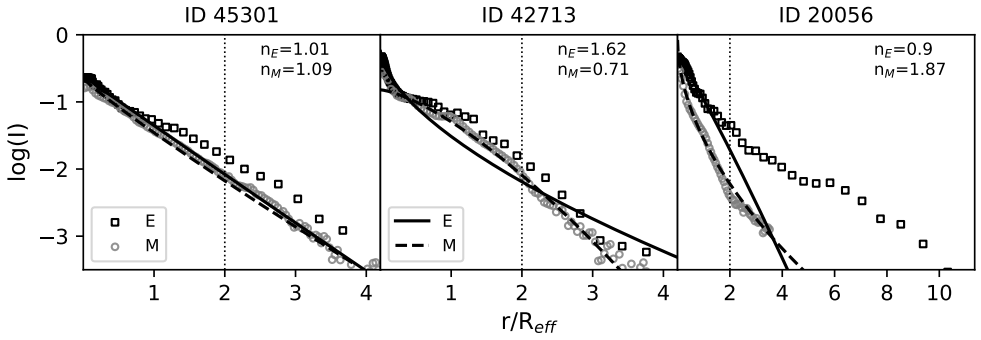

Figure 4.6: Surface brightness profiles for the three galaxies show in Figure 4.1 and Figure 4.5. The vertical dotted lines mark twice the effective radius, this relates to the dashed circles in Figure 4.5. The black square and gray circle markers show the ELLIPSE (E) and MORFOMETRYKA (M) surface brightness profile, respectively. The black solid and dashed lines are the best single Sérsic fit for ELLIPSE and morfometryka, respectively. The Sérsic indices for both fits are noted in each panel.

components. In the case of ID 20056, the Sérsic fit best represents the inner region, but not the more extended concave profile. A similar situation occurs for the other two galaxies in both MORFOMETRYKA and ELLIPSE measured profiles. For evaluating these structures we take advantage of the tool KURVATURE (Lucatelli & Ferrari, 2019), it measures the curvature of a surface brightness profiles by calculating its concavity. The concave shapes we find are related to a negative curvature which is related to low concentrated of light in surface brightness profiles, such as Sérsic fits with n ¡ 1.

To better understand curvature measurements, in Figure 4.7 we show the relation between Sérsic indices and the curvature of surface brightness profiles. Sérsic profiles with high Sérsic indices (n $>$ 1) have positive curvature profiles, while low Sérsic indices (n $<$1) have negative curvature profiles and pure discs (n=0) have null curvature. This is a powerful tool to assess the concentration of light distribution and discriminate different structural components in a galaxy without depending on a parametric model. Therefore, a negative curvature profile is directly related to a region of low concentration of light in the surface brightness profile, the area of the curvature profile also correlates to Sérsic index. It is important to note that the negative areas should not be related to noise. Curvature measurement is sensitive to transitions between two regions with different brightness profiles. Hence, the transition between a decreasing brightness profile of a galaxy meeting the constant background noise would be in-

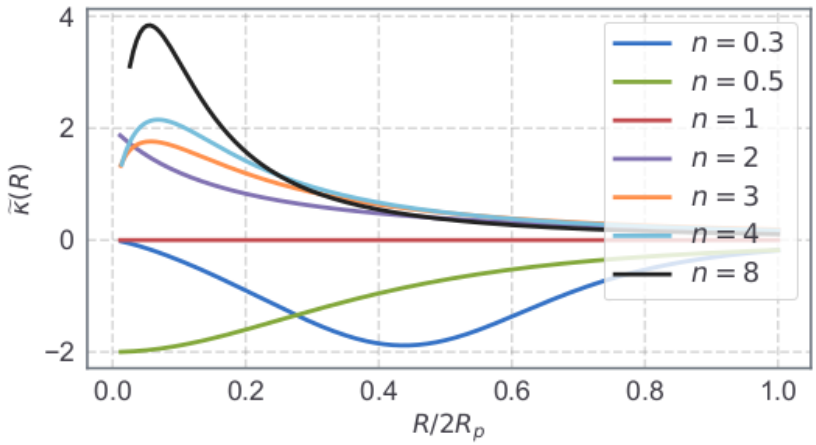

Figure 4.7: Curvature ($\tilde{k}(R)$) for Sérsic profiles of different Sérsic indices. Negative curvature profiles are associated with structures of low Sérsic indices, a null curvature profile represents a pure disc and positive curvature profiles are associated with high Sérsic indices that follow light distributions more concentrated than a pure disc.

terpreted by KURVATURE with a positive curvature. In the cases where the curvature diverges in outer regions, most are in the positive direction. Following this same reasoning, concave regions could be associated with regions that lack light in respect to their surroundings, such as in ring or bar structures. Perhaps regions with high dust extinctions can also contribute to the phenomenon. However, the ram pressure stripping candidates we are probing do not necessarily contain more dust than the star forming galaxies in the control sample, therefore, the presence of dust affects both samples in similar ways.

We quantify the presence of the concave features by measuring the cumulative negative area in the surface brightness profiles of the ram pressure stripping candidates and the control sample of star forming galaxies. To avoid contamination from galaxies with weak signatures of ram pressure stripping, we are considering only the JClass 4 and JClass 5 ram pressure stripping candidates. We show the cumulative histograms in Figure 4.8 where we compare both groups of galaxies with a KS test across 2 Petrosian radii (R_p) and in four different radial bins. We neglect the central values in $r \leq 0.1\ R_p$ due to the curvature profile being unstable in the inner regions. We find that both samples are significantly different when looking at the full radius range and the outer radial bins ($r \geq 0.5\ R_p$), with the ram pressure stripping candidates always having more negative area than the star forming galaxies. This is more prominent for the radial bins above

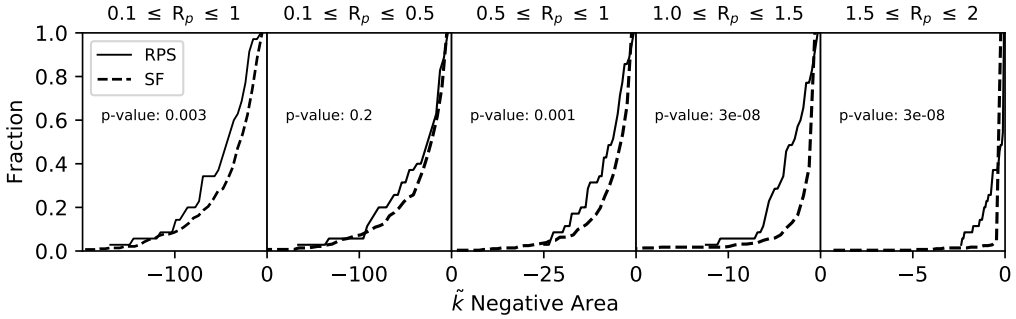

Figure 4.8: Cumulative distribution of the total negative area in the curvature profiles, within a given radius, measured with MORFOMETRYKA tool KURVATURE for the ELLIPSE brightness profiles for JClass 4 and 5 ram pressure stripping candidates (solid line) and star forming galaxies (dashed line) in the A901/A902 system. The left panel accounts the surface brightness up to 2 R$_p$, the following panels are divided into radial bins of 0.5 R$_p$. The p-values shown are calculated with a KS test.

1.0 R$_p$. These results suggest that ram pressure stripping may systematically alter the galaxy morphology by broadening the surface brightness profiles effectively creating galaxies that have the stellar component less concentrated than a pure disc in the outer regions (0.5 R$_p$ $\geq$ r $\leq$ 2.0 R$_p$).

Concave features in surface brightness profiles are not unique to the ram pressure stripping candidates analysed here, but seem to be present more often in our ram pressure stripping candidates than in normal star forming galaxies. These concave features, when seen in normal disc galaxies, are usually associated with structural components such as rings or bars, which are not prominent in our sample. However, these features can also be associated with an overall low concentrated light distribution, such as seen in the surface brightness profiles of some dwarf galaxies (Ludwig et al., 2012) or ultra diffuse galaxies (Liao et al., 2019).

4.4 Conclusions

Following the studies on the star formation rates and spatial distribution of the ram pressure stripping candidates at the A901/A902 multi-cluster system (Roman-Oliveira et al., 2019, Ruggiero et al., 2019), we attempt to use their morphological structure as a probe to expand our understanding of their evolution. We perform a morphometric analysis using the MORFOMETRYKA algorithm (Ferrari et al., 2015) and the IRAF task ELLIPSE (Jedrzejewski, 1987) for independent surface brightness profiles measure-

ments. Our two main results are:

- We define a robust morphometric method for measuring trail vectors in jellyfish galaxies based on the spatial difference between the peak and centre of the light distribution in galaxies. This can also be used as a proxy of morphological asymmetry.
- Our analysis of the surface brightness profiles finds a significant presence of low concentration regions that can be seen as concavities in the surface brightness profiles, we quantify these regions by measuring the curvature (Lucatelli & Ferrari, 2019). When these are compared to the normal star forming galaxies in the same system, the ram pressure candidates show larger areas of negative curvature in the outer regions of their surface brightness profiles. This suggests that the extreme ram pressure that produces jellyfish features also serves to broaden the surface brightness profiles creating regions that are less concentrated than pure discs.

The findings reported here shed new light on the possible next steps in the morphological evolution of galaxies undergoing ram pressure stripping in dense environments. We suggest that, at least temporarily, extreme events of ram pressure stripping may affect the morphology by broadening the surface brightness profiles of galaxies. Additionally, the implementation of morphometric trail vectors is an important step towards systematic selection and analysis of projected motions of new ram pressure stripping candidates, as well as another useful tool to quantify asymmetry.

These are preliminary findings on the morphological transformation of ram pressure stripping candidates. The details on how ram pressure stripping could alter the morphology of the stellar disc are still largely unknown. A further investigation of the morphometric properties of these galaxies in a different passband can retrieve information on how the morphology of different physical tracers is being affected. Particularly, applying the same morphometric analysis on the OMEGA Hα emission and building Hα morphology profiles Koopmann & Kenney (2004) can unveil the extent and concentration of the star formation spatially, whether it is being enhanced or suppressed in different regions of the galaxies and if it is related to the concave regions we see in the F606W passband.

Acknowledgements

This work was conducted as part of an M.Sc. thesis in a Federal University despite the hard current policies of Brazil's far-right government

against education and science. We thank the referee for the constructive comments which substantially helped to improve the quality of this work. We also thank Alfonso Aragón-Salamanca for comments in the original manuscript. This study was financed in part by the *Coordenaçao de Aperfeiçoamento de Pessoal de Nível Superior* - Brasil (CAPES) Finance Code 001, the *Programa de Pós Graduação em Física* of *Universidade Federal do Rio Grande do Sul* and PROPESQ/UFRGS. ACS acknowledges funding from the Brazilian agencies *Conselho Nacional de Desenvolvimento Científico e Tecnológico* (CNPq) and the *Fundação de Amparo à Pesquisa do Estado do Rio Grande do Sul* (FAPERGS) through grants PIBIC-CNPq, CNPq-403580/2016-1, CNPq-310845/2015-7, PqG/FAPERGS-17/2551-0001, PROBIC/FAPERGS and L'Oréal UNESCO ABC *Para Mulheres na Ciência*. STSDAS and PyRAF are products of the Space Telescope Science Institute, which is operated by AURA for NASA.

Chapter 5

Conclusions and Outlook

The results shown in this thesis provide important insights to understand the role of ram pressure stripping in the accelerated evolution of galaxies in dense environment – most notably in the context of the morphology-density relation and in the quenching of galaxies.

Firstly, we present the largest sample, to date, of ram pressure stripping candidates in a single system. We have found a systematic enhancement of the specific star formation rates in the candidates. This corroborates what was found for other samples in other works such as Rawle et al. (2014), Poggianti et al. (2016) and Vulcani et al. (2018). We also did not find a correlation between ram pressure stripping and AGN activity, opposed to what was suggested in Poggianti et al. (2017a). We suggest that the relation with the AGN found for some of the most extreme jellyfish galaxies in the GASP sample might be due to stellar mass bias or environment instead of the ram pressure stripping event.

We also find evidence that merging clusters and other multi-cluster systems may be the optimal environment to search for jellyfish candidates as they host regions with enhanced relative velocities that act as a trigger to new ram pressure stripping events. This is in line with tentative results presented in previous works such as Owers et al. (2012) and McPartland et al. (2016).

Finally, our morphometric analysis allowed the rapid and robust identification of trail vectors, previously only possible via visual inspection (Ebeling & Kalita, 2019, Ebeling et al., 2014, Roman-Oliveira et al., 2019, Smith et al., 2010). We also find tentative results suggesting that ram pressure stripping might broaden the surface brightness profile of galaxies.

In summary, these findings contributed to better understand how the ram pressure stripping affects star formation rates and AGN activity; in

which environments it is more prevalent and most efficient; and how it ultimately alters the morphology of galaxies.

The search and analysis of ram pressure stripping events has been on the rise in the past decade and is still a very promising field as there are still many open questions to be investigated. Particularly as a direct consequence of this work, we still need to verify the tentative results regarding the brightness profile trends seen in the Abell 901/2 ram pressure stripping candidates and provide a physical meaning to this behaviour if it proves to be relevant. This can guide the understanding of what exactly happens in the galaxy morphology as it undergoes ram pressure stripping. For that, a thorough analysis of the curvature of the brightness profiles (Lucatelli & Ferrari, 2019) can be employed as a more accurate way of measuring the light diffuse structures in the external regions of the galaxies.

Another follow-up possibility is the compared morphometric analysis different bands. In the case of the sample presented in this thesis, we can analyse the continuum emission from the HST data to the Hα emission and define Hα morphologies (Koopmann & Kenney, 2004). Analysing the extent and morphometric quantities of the Hα emission compared to the continuum can help our understanding of how ram pressure stripping is affecting the different elements in the galaxies (e.g. star formation regions, intermediate age stellar populations). Besides, having spatial information of the star formation regions of the galaxies can provide insight in which regions are undergoing enhanced star formation and if there might be regions with truncated or anaemic star formation.

Besides the context of the Abell 901/2 ram pressure stripping candidates and the data available for them, there are still ongoing debate in the community regarding the relation of jellyfish galaxies with other extreme objects, such as Ultra Diffuse galaxies, Ultra Compact Dwarf galaxies and Post-starburst galaxies. The connection between these peculiar objects can support to trace a consistent framework of how dense environments drive galaxy evolution. In addition to this, it is yet poorly understood how the jellyfish galaxy tails evolve what results from the star clusters formed within them.

Agradecimentos

Este trabalho não seria possível sem o apoio financeiro e estrutura do PPGFIS/UFRGS e da CAPES.

Antes de tudo gostaria de agradecera todas as pessoas em que tiver o prazer de trabalhar. Em especial meus orientadores Ana e FabrÃcio, meus colaboradores Alfonso, Bruno e o grupo do OMEGA e Rafael e Geferson.

Um agradecimento especial aos meu pais, Carla e Rodrigo, por me ensinarem a importância do saber e da curiosidade. Também por nunca aceitarem pouco de mim.

A toda a minha família pelo carinho e por todas as vezes que os ouço falando de mim com orgulho. Por me apoiarem mesmo que muitas vezes não entendessem exatamente o que eu estou fazendo – e mesmo assim sempre continuarem animados e perguntando mais. Principalmente a tia Lisa por ter sido meu segundo lar.

Ao Ben por ter sido um amor, um amigo, mas acima de tudo um companheiro.

À Capitu pelo suporte emocional e companhia incondicional.

Ao pessoal da M201 pela convivência por dois anos. Em especial a Carol por ter sido minha amiga, minha vizinha de sala e ter lido todas as versões de tudo o que escrevi.

À Larissa e Marina por serem tão bons exemplos do que amizade significa e por todo o vinho compartilhado.

Ao Emílio e Rodrigo pelo suporte e resiliência.

Thiago, João, Nícolas, Vítor e tantos outros, obrigada pela amizade e por tantos bons momentos nos últimos vários anos. Porto Alegre não seria minha casa se não fosse por todos vocês.

Bibliography

Abazajian K. N., et al., 2009, , 182, 543

Abraham R. G., Valdes F., Yee H. K. C., van den Bergh S., 1994, , 432, 75

Abraham R. G., van den Bergh S., Glazebrook K., Ellis R. S., Santiago B. X., Surma P., Griffiths R. E., 1996, , 107, 1

Abramson A., Kenney J., Crowl H., Tal T., 2016, , 152, 32

Baldry I. K., 2008, Astronomy and Geophysics, 49, 5.25

Baldry I. K., Glazebrook K., Brinkmann J., Ivezić Ž., Lupton R. H., Nichol R. C., Szalay A. S., 2004, , 600, 681

Baldry I. K., Balogh M. L., Bower R. G., Glazebrook K., Nichol R. C., Bamford S. P., Budavari T., 2006, , 373, 469

Bamford S. P., et al., 2009, , 393, 1324

Barnes J. E., 1992, , 393, 484

Bekki K., 1998, , 502, L133

Bekki K., 1999, , 510, L15

Bekki K., 2009, , 399, 2221

Bekki K., 2014, , 438, 444

Bekki K., Couch W. J., 2003, , 596, L13

Bellhouse C., et al., 2017, , 844, 49

Biffi V., Dolag K., Böhringer H., Lemson G., 2012, , 420, 3545

Biffi V., Dolag K., Böhringer H., 2013, , 428, 1395

Booth C. M., Schaye J., 2009, , 398, 53

Bösch B., et al., 2013, , 549, A142

Boselli A., et al., 2016, , 596, A11

Boselli A., et al., 2018, , 620, A164

Bournaud F., Duc P. A., Amram P., Combes F., Gach J. L., 2004, , 425, 813

Brüggen M., van Weeren R. J., Röttgering H. J. A., 2012, , 425, L76

Bundy K., et al., 2006, , 651, 120

Busha M. T., Adams F. C., Wechsler R. H., Evrard A. E., 2003, , 596, 713

Buta R., Mitra S., de Vaucouleurs G., Corwin H. G. J., 1994, , 107, 118

Butcher H., Oemler Jr. A., 1984, , 285, 426

Chies-Santos A. L., et al., 2015, , 450, 4458

Cid Fernandes R., Stasińska G., Schlickmann M. S., Mateus A., Vale Asari N., Schoenell W., Sodré L., 2010, , 403, 1036

Conselice C. J., Bershady M. A., Jangren A., 2000, , 529, 886

Cortese L., et al., 2007.

Cortese L., et al., 2019, , 485, 2656

Dehnen W., 1993, , 265, 250

Donnert J. M. F., 2014, , 438, 1971

Dressler A., 1980, , 236, 351

Ebeling H., Kalita B. S., 2019, , 882, 127

Ebeling H., Stephenson L. N., Edge A. C., 2014, , 781, L40

Elbaz D., et al., 2011, , 533, A119

Elmegreen B. G., Elmegreen D. M., 2010, , 722, 1895

Elmegreen D. M., Elmegreen B. G., Ravindranath S., Coe D. A., 2007, , 658, 763

Eneev T. M., Kozlov N. N., Sunyaev R. A., 1973, , 22, 41

Ferrari F., de Carvalho R. R., Trevisan M., 2015, , 814, 55

Fossati M., et al., 2018, , 614, A57

Fumagalli M., Fossati M., Hau G. K. T., Gavazzi G., Bower R., Sun M., Boselli A., 2014, , 445, 4335

Gavazzi G., Consolandi G., Gutierrez M. L., Boselli A., Yoshida M., 2018, , 618, A130

Gilmour R., Gray M. E., Almaini O., Best P., Wolf C., Meisenheimer K., Papovich C., Bell E., 2007, , 380, 1467

Gray M. E., Wolf C., Meisenheimer K., Taylor A., Dye S., Borch A., Kleinheinrich M., 2004, , 347, L73

Gray M. E., et al., 2009, , 393, 1275

Gunn J. E., Gott III J. R., 1972, , 176, 1

Haines C. P., La Barbera F., Mercurio A., Merluzzi P., Busarello G., 2006, , 647, L21

Hernquist L., 1990, , 356, 359

Heymans C., et al., 2008, , 385, 1431

Hopkins P. F., Cox T. J., Hernquist L., 2008, , 689, 17

Hubber D. A., Falle S. A. E. G., Goodwin S. P., 2013, , 432, 711

Hubble E. P., 1926, , 64, 321

Jaffé Y. L., Smith R., Candlish G. N., Poggianti B. M., Sheen Y.-K., Verheijen M. A. W., 2015, , 448, 1715

Jaffé Y. L., et al., 2016, , 461, 1202

Jedrzejewski R. I., 1987, , 226, 747

Kapferer W., Sluka C., Schindler S., Ferrari C., Ziegler B., 2009, , 499, 87

Kaviraj S., 2014, , 440, 2944

Kelkar K., Gray M. E., Aragón-Salamanca A., Rudnick G., Jaffé Y. L., Jablonka P., Moustakas J., Milvang-Jensen B., 2019, , 486, 868

Kenney J. D. P., Koopmann R. A., 1999, , 117, 181

Kenney J. D. P., Geha M., Jáchym P., Crowl H. H., Dague W., Chung A., van Gorkom J., Vollmer B., 2014, , 780, 119

Kim J.-h., et al., 2014, , 210, 14

Koopmann R. A., Kenney J. D. P., 2004, , 613, 866

Krist J., 1993, in Hanisch R. J., Brissenden R. J. V., Barnes J., eds, Astronomical Society of the Pacific Conference Series Vol. 52, Astronomical Data Analysis Software and Systems II. p. 536

Kronberger T., Kapferer W., Ferrari C., Unterguggenberger S., Schindler S., 2008, , 481, 337

Laganá T. F., Martinet N., Durret F., Lima Neto G. B., Maughan B., Zhang Y.-Y., 2013, , 555, A66

Lage C., Farrar G., 2014, , 787, 144

Larson R. B., Tinsley B. M., Caldwell C. N., 1980, , 237, 692

Liao S., et al., 2019, , 490, 5182

Lotz J. M., Primack J., Madau P., 2004, , 128, 163

Lucatelli G., Ferrari F., 2019, , 489, 1161

Ludwig J., Pasquali A., Grebel E. K., Gallagher John S. I., 2012, , 144, 190

Machado R. E. G., Lima Neto G. B., 2013, , 430, 3249

Machado R. E. G., Lima Neto G. B., 2015, , 447, 2915

Machado R. E. G., Monteiro-Oliveira R., Lima Neto G. B., Cypriano E. S., 2015, , 451, 3309

Mastropietro C., Burkert A., 2008, , 389, 967

McPartland C., Ebeling H., Roediger E., Blumenthal K., 2016, , 455, 2994

Molnar S. M., Broadhurst T., 2015, , 800, 37

Moore B., Katz N., Lake G., Dressler A., Oemler A., 1996, , 379, 613

Newton R. D. A., Kay S. T., 2013, , 434, 3606

O'Shea B. W., Nagamine K., Springel V., Hernquist L., Norman M. L., 2005, , 160, 1

Owers M. S., Couch W. J., Nulsen P. E. J., Randall S. W., 2012, , 750, L23

Peng C. Y., Ho L. C., Impey C. D., Rix H.-W., 2002, , 124, 266

Pettitt A. R., Wadsley J. W., 2018, , 474, 5645

Poggianti B. M., et al., 2016, , 151, 78

Poggianti B. M., et al., 2017a, , 548, 304

Poggianti B. M., et al., 2017b, , 844, 48

Poggianti B. M., et al., 2018, ,

Poggianti B. M., et al., 2019, , 887, 155

Rawle T. D., et al., 2014, , 442, 196

Rodríguez del Pino B., et al., 2017, , 467, 4200

Roediger E., Brüggen M., 2006, , 369, 567

Roediger E., Brüggen M., Owers M. S., Ebeling H., Sun M., 2014, , 443, L114

Roman-Oliveira F. V., Chies-Santos A. L., Rodríguez del Pino B., Aragón-Salamanca A., Gray M. E., Bamford S. P., 2019, , 484, 892

Ruggiero R., Lima Neto G. B., 2017, , 468, 4107

Ruggiero R., Machado R. E. G., Roman-Oliveira F. V., Chies-Santos A. L., Lima Neto G. B., Doubrawa L., Rodríguez del Pino B., 2019, , 484, 906

Sánchez Almeida J., Muñoz-Tuñón C., Elmegreen D. M., Elmegreen B. G., Méndez-Abreu J., 2013, , 767, 74

Sarazin C. L., 2002, in Feretti L., Gioia I. M., Giovannini G., eds, Astrophysics and Space Science Library Vol. 272, Merging Processes in Galaxy Clusters. pp 1–38 (arXiv:astro-ph/0105418), doi:10.1007/0-306-48096-4˙1

Schawinski K., et al., 2014, , 440, 889

Sersic J. L., 1968, Atlas de Galaxias Australes

Sheen Y.-K., et al., 2017, , 840, L7

Simard L., et al., 2002, , 142, 1

Simpson C. M., Grand R. J. J., Gómez F. A., Marinacci F., Pakmor R., Springel V., Campbell D. J. R., Frenk C. S., 2018, ,

Smith R. J., et al., 2010, , 408, 1417

Sparke L. S., Gallagher J. S., 2000

Springel V., 2005, , 364, 1105

Springel V., Farrar G. R., 2007, , 380, 911

Stasińska G., Cid Fernandes R., Mateus A., Sodré L., Asari N. V., 2006, , 371, 972

Steinhauser D., Haider M., Kapferer W., Schindler S., 2012, , 544, A54

Steinhauser D., Schindler S., Springel V., 2016, , 591, A51

Straughn A. N., et al., 2015, , 814, 97

Sun M., Jones C., Forman W., Nulsen P. E. J., Donahue M., Voit G. M., 2006, , 637, L81

Sun M., Donahue M., Voit G. M., 2007, , 671, 190

Sun M., Donahue M., Roediger E., Nulsen P. E. J., Voit G. M., Sarazin C., Forman W., Jones C., 2010, , 708, 946

Tapia T., et al., 2014, , 565, A31

Teyssier R., 2002, , 385, 337

Tonnesen S., Bryan G. L., 2008, , 684, L9

Tonnesen S., Bryan G. L., 2010, , 709, 1203

Tonnesen S., Bryan G. L., van Gorkom J. H., 2007, , 671, 1434

Toomre A., 1977. p. 401

Turk M. J., Smith B. D., Oishi J. S., Skory S., Skillman S. W., Abel T., Norman M. L., 2011, , 192, 9

Vazza F., Roediger E., Brüggen M., 2012, , 544, A103

Vollmer B., et al., 2012, , 537, A143

Vulcani B., et al., 2016, , 833, 178

Vulcani B., et al., 2018, , 866, L25

Walker S. A., ZuHone J., Fabian A., Sanders J., 2018, Nature Astronomy, 2, 292

Weinzirl T., et al., 2017, , 471, 182

Wolf C., Meisenheimer K., Rix H.-W., Borch A., Dye S., Kleinheinrich M., 2003, , 401, 73

Wolf C., Gray M. E., Meisenheimer K., 2005, , 443, 435

Wolf C., et al., 2009, , 393, 1302

Wolf C., et al., 2018, , 480, 3788

Wyder T. K., et al., 2007, , 173, 293

Yagi M., et al., 2010, , 140, 1814

Yagi M., Yoshida M., Gavazzi G., Komiyama Y., Kashikawa N., Okamura S., 2017, , 839, 65

Yun K., et al., 2019, , 483, 1042

Zhang B., et al., 2013, , 777, 122

ZuHone J. A., Markevitch M., Johnson R. E., 2010, , 717, 908

ZuHone J. A., Markevitch M., Ruszkowski M., Lee D., 2013a, , 762, 69

ZuHone J. A., Markevitch M., Brunetti G., Giacintucci S., 2013b, , 762, 78

ZuHone J. A., Biffi V., Hallman E. J., Randall S. W., Foster A. R., Schmid C., 2014, arXiv:1407.1783,

van Weeren R. J., Brüggen M., Röttgering H. J. A., Hoeft M., 2011, , 418, 230

van den Bergh S., Abraham R. G., Ellis R. S., Tanvir N. R., Santiago B. X., Glazebrook K. G., 1996, , 112, 359